Faculty of Science and Technology

University of Canberra

Australia

Bio-inspired Design and Non-linear Model Predictive Control of a Self-Aligning Gait Rehabilitation Robot

Yinan Jin

Primary Supervisor: Assoc. Prof. Shahid Hussain

Co-Supervisor: Prof. Roland Goecke

Advisors: Assoc. Prof. Prashant K. Jamwal, Assoc. Prof. Wayne Spratford and Dr Mergen H. Ghayesh

A thesis submitted for the degree of

Doctor of Philosophy at the University of Canberra

17th October 2023

Abstract

The field of robot-assisted rehabilitation has seen significant development in recent years. With the development of compliant robots that can be safely used in proximity to people, the use of robots to assist rehabilitation has increased rapidly. The need for gait rehabilitation robots arises from the increasing number of people who are affected by conditions that impair their ability to walk. These conditions can include neurological disorders such as strokes, spinal cord injuries, and traumatic brain injuries. In traditional gait rehabilitation, patients receive manual therapy from a team of physical therapists. While manual therapy can be effective, it can also be time-consuming and resource-intensive, and therapists may not be able to provide consistent and precise support to patients. Gait rehabilitation robots, on the other hand, provide a consistent and precise form of therapy that may help patients make faster and more significant progress. Gait rehabilitation robots can also help reduce the physical demands on therapists and improve the efficiency of therapy sessions. This can allow more patients to receive therapy, which can improve access to care and reduce the burden on health care systems. However, most of existing robotic orthoses have not applied appropriate self-aligning mechanism, gravity-balancing mechanism, or compliant actuators. These limitations should be considered in this proposed research.

This thesis proposes a novel intrinsically compliant gait rehabilitation robot with multiple actuated degrees-of-freedom (DOFs). The robot design is flexible and can be personalised with the use of telescopic pelvis, thigh, and shank sections. This newly designed rehabilitation robotic orthosis has multiple actuated and passive DOFs. Because of the importance of alignment between the designed rehabilitation robot joints and human anatomical joints, the robot design has a self-aligning mechanism. A novel gear-couple mechanism, toothed cam-couple mechanism and four-bar linkage mechanism are designed and applied to the hip, knee, and ankle joints to align the robot joints with anatomical joints during gait rehabilitation.

Simulation-based and motion capture system-based tests are applied to those three mechanisms to evaluate and choose the most effective self-aligning mechanism. The gear-couple mechanism is finally chosen to be applied to the prototype design.

A partial gravity-balancing mechanism is also applied to the designed rehabilitation robot. Gravity-balancing can help overcome the inertia of the rehabilitation robot and can further help reduce joint misalignment. The compliance in the robot is intrinsic due to the use of pneumatic muscle actuators (PMAs). The PMAs have been carefully selected to provide the required torques at the hip, knee and ankle joints during gait rehabilitation. Mechanical amplification of the actuation from the PMAs has been achieved by using gear-couples to replace the usual revolute robot joints. However, with the increase in flexibility of the designed prototype and application of PMAs, which are nonlinear actuators, it is challenging to design the robot control system. This challenge was overcome by developing a system dynamic identification model based on the Koopman operator for the design of a nonlinear model predictive controller (NMPC).

The new robot design, together with its self-aligning and gravity-balancing mechanisms, is discussed in detail in this thesis. Compliant actuation and its amplification are explained and various algorithms that are designed and implemented on the robot system as robot firmware are explained. A NMPC is designed and developed to control the rehabilitation robot. The experimental setup and evaluation of the robot design, together with the nonlinear model predictive controller, was carried out with healthy users and yielded the intended results. The robotic orthosis along with the NMPC could successfully guide the healthy human subject along the pre-defined trajectory.

Acknowledgement

I would like to express my special thanks to my supervisor Associate Professor Shahid Hussain for his guidance, support, and encouragement throughout this research work. His contagious enthusiasm for this project was the greatest motivation. The Rehabilitation Engineering Research Laboratory he established at the University of Canberra provided me with valuable research experience. I would also like to thank my co-supervisor Professor Roland Goecke for his encouragement and advice during the research. As an interdisciplinary project, I would also like to thank Associate Professor Prashant Jamwal at the Robotics Faculty, Nazarbayev University; Dr Mergen H. Ghayesh at the School of Mechanical Engineering, the University of Adelaide; and Associate Professor Wayne Spratford at the Faculty of Health, University of Canberra, for their valuable interactions, and their experience and ideas that have helped to shape this project.

I also offer thanks to those in the Rehabilitation Engineering Research Laboratory with whom I have worked, especially Tanishka Goyal, Akim Kapsalyamov, Fahad Hussain, and Faizan Shah for making it such an exciting environment. I would also like to thank the editor, Dr. Rhonda Daniels, for editing this thesis.

Technicians Jamie Plowman, and Jason Weber at the University of Canberra also helped throughout this research in fabricating and improving the mechanical and electronic hardware. Other staff in the Faculty of Science and Technology at the University of Canberra deserve special thanks.

I am forever indebted to my parents for their guidance and support throughout my student life. My younger cousin, Haoyang Zhou, also deserves special recognition. All my friends provided valuable support and encouragement.

Table of Contents

Abstract iii
Certificate of Authorship v
Acknowledgement vii
Table of Contents ix
List of Figures xiii
List of Tables xvii
List of Acronyms and Abbreviations xix
Chapter 1 – Introduction 1
1.1 Human Gait 1
1.2 Causes of Gait Disorders 2
1.3 Traditional Gait Rehabilitation 3
1.4 Limitations of Traditional Rehabilitation Approach 4
1.5 Research Motivation and Impact 5
1.6 Research Aims and Objectives 7
1.6.1 Development of a Prototype of a Gait Rehabilitation Robotic Orthosis 7
1.6.2 Development and Application of a Self-aligning Mechanism 8
1.6.3 Development and Application of a Gravity-balancing Mechanism 9
1.6.4 Application of Appropriate Actuators for the Robotic Orthosis 9
1.6.5 Design and Application of an Appropriate Controller for the Robotic Orthosis 10
1.7 Thesis Overview and Scope 11
1.8 Chapter Summary 11
Chapter 2 – Literature Review 13
2.1 Existing Robotic Orthosis Designs 13
2.1.1 LOKOMAT 13
2.1.2 AutoAmbulator 14
2.1.3 ALEX, ALEX II and ALEX III 15
2.1.4 Robotic Exoskeleton from Vanderbilt University 16
2.1.5 Robotic Exoskeleton from South China University 17
2.1.6 WPAL from Fujita Health University 17
2.1.7 HAL from University of Tsukuba 18
2.1.8 MLLRE 19
2.1.9 LOPES and LOPES II 20
2.1.10 GT-1 and Haptic Walker 21

2.1.11 Knee–ankle–foot Robot from National University of Singapore 22
2.1.12 ICRO 23
2.1.14 Knee–ankle–foot Robot from University of Michigan 23
2.1.15 Robotic Exoskeleton from University of Salford 24
2.2 Actuators for Robotic Orthoses 26
2.3 Self-Alignment for Robotic Orthoses 27
2.4 Gravity-Balancing of Robotic Orthoses 28
2.5 Control Strategies for Robotic Orthoses 28
2.6 Chapter Summary 30
Chapter 3 – Robotic Orthosis Mechanical Design 33
3.1 Introduction 33
3.2 Biomechanics of Human Gait 34
3.2.1 Planes and Axes 34
3.2.2 Hip, Knee and Ankle Complex 35
3.3 Robot Design Requirements and Specifications 36
3.3.1 Design Requirements 37
3.3.2 Design Specifications 39
3.4 Mechanism Design 41
3.4.1 Robot Hip and Pelvis Joint Design 41
3.4.2 Robot Knee Joint 43
3.4.3 Robot Ankle Joint 45
3.5 Self-Aligning Robot Joints 46
3.6 Gravity-Balancing Mechanism 49
3.7 Compliant Actuation 51
3.8 Robotic Orthosis Prototyping and Instrumentation 53
3.8.1 Prototype Components for the Self-Alignment Mechanism 55
3.8.2 Prototype Component for the Gravity-Balancing Mechanism 56
3.8.3 Prototype Instruments 57
3.9 Safety 58
3.10 Design Capability Analysis 59
3.11 Chapter Summary 60
Chapter 4 – Development and Comparison of various Self-Alignment Mechanisms for Robotic Orthosis 61
4.1 Introduction 61
4.2 Estimation of Knee Rotation and Displacement 63

4.3 Gear Couple Mechanism 65
4.4 Toothed Cam Couple Mechanism 67
4.5 Four-Bar Linkage Mechanism 71
4.6 Performance Evaluation and Comparison of the Three Mechanisms 73
4.6.1 Simulation-based Evaluation and Comparison 73
4.6.2 Motion Capture System-based Evaluation and Comparison 75
4.7 Chapter Summary 77
Chapter 5 – Design Analysis 79
5.1 Introduction 79
5.2 Robot Kinematic Analysis 80
5.2.1 Forward Kinematics 83
5.2.2 Inverse Kinematics 84
5.2.3 AI-Based Inverse Kinematic Modelling 86
5.3 Robot Dynamic Modelling 90
5.4 Results and Discussion 91
5.5 Chapter Summary 95
Chapter 6 – Control and Experimental Evaluation 97
6.1 Introduction 97
6.2 System Identification using Koopman Operator 99
6.3 Nonlinear Model Predictive Controller Design 103
6.4 Experiment Setup 105
6.5 Data Collection and Robot System Identification 107
6.6 Results 108
6.7 Chapter Summary 114
Chapter 7 – Conclusion 115
7.1 Major Outcomes and Contributions 115
7.1.1 Robotic Orthosis Design and Analysis 115
7.1.2 Application of a Self-aligning Mechanism 116
7.1.3 Application of a Gravity-balancing Mechanism 117
7.1.4 Application of Compliant Actuators 117
7.1.5 Nonlinear Model Predictive Control 118
7.2 Limitations 118
7.3 Future Work 119
Appendix A – Solution of Forward Kinematics 121
Appendix B – Dynamic Modelling 125

Appendix C – Ethics Approval 129
Appendix D – Consent Forms 133
Appendix E – Publications and Submissions 137
References 139

List of Figures

Figure 1–1. Gait Cycle [50]..... 2
Figure 1–2. Traditional Body Weight Supported Treadmill Training [15]..... 4
Figure 2–1. LOKOMAT [62]..... 14
Figure 2–2. AutoAmbulator [177].. 14
Figure 2–3. Active Leg Exoskeleton (ALEX) [178]..... 15
Figure 2–4. Vanderbilt University Robotic Exoskeleton [78]. 16
Figure 2–5. Robotic Exoskeleton from South China University [79]..... 17
Figure 2–6 WPAL [81]. 18
Figure 2–7. Hybrid Assistive Limb [82]. 18
Figure 2–8. MLLRE [84]. 19
Figure 2–9. (a) LOPES [88], (b) LOPES II [88]..... 20
Figure 2–10. Gait Trainer GT-1 [89]. 21
Figure 2–11. Haptic Walker [179]. 22
Figure 2–12. Knee–ankle–foot Robot Prototype from National University of Singapore [180]. 22
Figure 2–13 ICRO [94]. 23
Figure 2–14. Knee–Ankle–Foot Robot from University of Michigan [95]. 24
Figure 2–15. Robotic Exoskeleton from University of Salford [96]..... 24
Figure 3–1. Planes and Axes which Bisect the Human Body [50]. 35
Figure 3–2. Motions Provided by Human Joints [10].. 36
Figure 3–3. Schematic Drawing of the Robotic Orthosis showing all the DOFs. R1(a,b). Revolute Joint for Hip Abduction/Adduction; R2. Revolute Joint for Hip External/Internal Rotation; R3. Revolute Joint for Hip Flexion/Extension; R4. Revolute Joint for Knee External/Internal Rotation; R5. Revolute Joint for Knee Flexion/Extension; R6. Revolute Joint for Ankle Abduction/Adduction; R7. Revolute Joint for Ankle Flexion/Extension; R8. Revolute Joint for Ankle Inversion/Eversion; T1. Pelvis Vertical Translation; T2. Pelvis Lateral Translation; T3. Hip Joint Vertical Translation; T4. Knee Joint Vertical Translation; T5. Ankle Joint Vertical Translation..... 40
Figure 3–4. Telescopic Pelvis Support on the Gait Robot. 42
Figure 3–5. The Hip Joint Linked with the Pelvis Support on the Gait Robot. 43
Figure 3–6. The Knee Joint with the Meshing Gears and Damper. 44
Figure 3–7. Robot Shank and Ankle Joint. 45

Figure 3–8. Amplification of PMA Using Gears. 46
Figure 3–9. Schematic Drawing of Self-Aligning Mechanism. 48
Figure 3–10. Implementation of Gravity-Balancing Mechanism Applied on the Prototype. .. 49
Figure 3–11. New Gait Robot Prototype (PMAs not shown here). 55
Figure 3–12. Prototype Components for Self-Aligning Mechanism. 56
Figure 3–13. Prototype Component for Gravity-Balancing Mechanism. 57
Figure 3–14. Schematic of the Prototype Instruments. 58
Figure 4–1. Movement of the Femur on Tibia Plateau Inside the Knee Joint. 65
Figure 4–2. (a) CAD design of robot Knee Joint with Gear Couple Mechanism. (b) Prototype of knee joint with Gear Couple Mechanism. 66
Figure 4–3. CAD design of the robot knee joint with toothed Cam Couple Mechanism. 68
Figure 4– 4. (a) Prototype of knee joint with Cam Couple Mechanism (b) Cam Couple Joint. 69
Figure 4–5. Line Sketch to show the Linear Displacement in the Robot Knee Joint (dimensions in mm). 70
Figure 4– 6. (a) Human Knee Rotation Trajectory. (b) Designed Cam Mechanism Trajectory. 71
Figure 4–7. CAD design of robot Knee Joint with Four Bar Linkage Mechanism. 71
Figure 4–8. Line Sketch of Robot Knee Joint with Four-Bar Linkage Mechanism. 72
Figure 4–9. Prototype of Knee Joint with Four-Bar Linkage Mechanism. 72
Figure 4–10. Instantaneous Contacting Point Trajectory of Gear Couple Mechanism. 74
Figure 4–11. Instantaneous Contacting Point Trajectory of Cam Couple Mechanism. 74
Figure 4–12. Range of motion of Four Bar Linkage Mechanism.. 75
Figure 4–13. (a) Motion capture system. (b) Change of position of the robotic knee joint for three mechanisms obtained by using motion capture system. 77
Figure 5–1. Schematic Drawing of Designed Prototype for Analysis. 80
Figure 5–2. MANFIS-Based Inverse Kinematic Optimisation. 86
Figure 5–3. ANFIS Architecture for IK Solver. 86
Figure 5–4. Antagonistic PMA and Joint Rotation. 88
Figure 5–5. Overview of the Gait Robot Hardware. 89
Figure 5–6. Controller Schematics. 90
Figure 5–7. Fuzzy Controller Design Showing Fuzzy Variable and Fuzzy Rule-Based for Inferencing Output Pressure. 90
Figure 5–8. Schematic Drawings of Dynamic Model. 90

Figure 5–9. Estimated Joint Errors Using Inverse Kinematics Solver in ANFIS. 92
Figure 5–10. Displacement (a) along x-axis, (b) along y-axis, (c) along z-axis, (d) resultant displacement. Velocity (e) along x-axis, (f) along y-axis, (g) along z-axis, (h) resultant velocity. Acceleration (i) along x-axis, (j) along y-axis, (k) along z-axis, (l) resultant acceleration of the endpoint (ankle joint) with hip rotation only. 93
Figure 5–11. Displacement (a) along x-axis, (b) along y-axis, (c) along z-axis, (d) resultant displacement. Velocity (e) along x-axis, (f) along y-axis, (g) along z-axis, (h) resultant displacement. Acceleration (i) along x-axis, (j) along y-axis, (k) along z-axis, (l) resultant acceleration of the endpoint (forefoot) with hip, knee and ankle rotation. 94
Figure 6–1. Schematic Diagram of the Gait Rehabilitation Robot with Nonlinear Model Predictive Controller based on Koopman Operator. 105
Figure 6–2. Experimental Setup for the Gait Rehabilitation Robot with a Healthy Human User. 106
Figure 6–3. Required Orientation and the Actual Orientation attained by the a) Hip, b) Knee and c) Ankle Joints. 109
Figure 6–4. Errors between Required Orientation and Actual Orientation for the Ankle, Knee, and Hip Joints. 109
Figure 6–5. Actuator Lengths for attaining the Required Orientation of a) Hip, b) Knee and c) Ankle Joints. 110
Figure 6–6. Acceleration of a) Hip, b) Knee and c) Ankle Joints. 111

List of Tables

Table 2–1. Overview of Existing Robotic Gait Rehabilitation Orthoses. 25
Table 3–1. Actuated, Passive and Blocked Degrees of Freedom (DOFs) of the robotic Orthosis Compared with Real Human Gait. 38
Table 3–2. Design Parameters. 39
Table 5–1. Parameters for Position Analysis. 81
Table 5–2. Element of the Generalised Homogeneous Transformation Matrix. 82
Table 6–1. Algorithm for System Identification. 100
Table 6–2. Range of Motion and Mean Trajectory Tracking Error for Hip, Knee, and Ankle Joints 113
Table A–1. Elements of the Homogeneous Transformation Matrix 123

List of Acronyms and Abbreviations

Active Leg Exoskeleton	ALEX
Body Weight Support	BWS
Centre of Mass	COM
Degrees-of-Freedom	DOFs
Forward Kinematics	FK
Gait Trainer	GT
Gait Cycle	GC
Hybrid Assistive Limb	HAL
Intrinsically Compliant Robotic Orthosis	ICRO
Inverse Kinematics	IK
Lower-extremity Powered Exoskeleton	LOPES
Mobile Lower Limb Robotic Gait Rehabilitation Exoskeleton	MLLRE
Nonlinear Model Predictive Controller	NMPC
Pneumatic Muscle Actuator	PMA
Spinal Cord Injuries	SCI
Wearable Power-Assist Locomotor	WPAL

Chapter 1 – Introduction

Robots are widely used in factories, laboratories, warehouses, the military, and transportation. Robots can help solve those repetitive, boring, inhospitable, dangerous, and impractical activities or tasks, which are difficult for humans to achieve. Although the application of robots in the field of industrial automation has a long history, the current trend of using robotic devices to provide medical care is increasing because of the increasing number of people affected by neurological disorders and the ageing of the global population [1-4]. An important application of robots in health care is to rehabilitate gait for those patients who have had a stroke or spinal cord injuries (SCI) instead of using physical therapists to do so [5-7]. Many researchers focus on the development of robotic devices to help patients with gait rehabilitation. Those designed robotic devices may help provide repetitive, low-cost, long-term, and customised gait training for patients with stroke or SCI related disabilities [6, 7]. Mechanism design, actuation and control systems of those devices play a significant role in rehabilitation due to the fact that non-ergonomic designs may lead to increased cardiorespiratory load and discomfort which could lead to additional gait disorders. This research aims to design and develop an intrinsically compliant gait robot with multiple degrees-of-freedoms (DOFs) to alleviate the prevalent issues.

This chapter provides background knowledge related to this research. Some basic definitions of human gait and causes of gait disorders are explained and the process of conventional gait rehabilitation with and without a body weight support (BWS) system is introduced.

1.1 Human Gait

In the biomechanics literature, gait is usually used as a synonym for walking. Human gait refers to locomotion achieved through the movement of human limbs. The human body's forward propulsion can be classified as bipedal and biphasic. [8, 9]. During the gait, periodic movement is achieved. Thus, the concept of a gait cycle (GC) has been developed to describe

the sequence of motion events from the heel strike of one foot to the next heel strike of the same foot [10]. Figure 1–1 shows the human gait cycle, consisting of the stance phase and the swing phase. The stance phase represents approximately 62% of the cycle, while the swing phase occupies around 38%. The stance phase describes the entire time the foot is in contact with the ground and the limb is bearing weight, while the swing phase is the part of the cycle during which the reference foot is not in contact with the ground and swings above the ground [11].

1.2 Causes of Gait Disorders

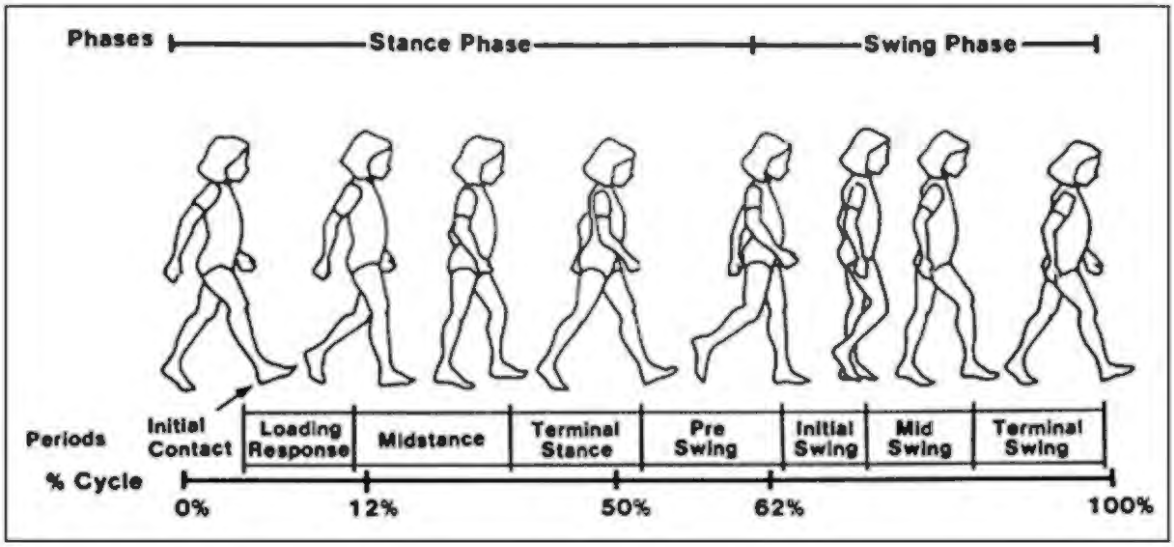

Figure 1–1. Gait Cycle [50].

Neurological disorders, such as stroke or SCI, result in gait disorders, which require physical therapy. Stroke is a kind of sudden and rapidly progressive cerebral ischemic (cerebral infarction) or cerebral haemorrhage (parenchymal haemorrhage, ventricular haemorrhage, subarachnoid haemorrhage) disease [12]. Stroke causes damage to the brain and is Australia's leading killer after coronary heart disease and a leading cause of disability [13]. Approximately 54,000 Australians suffer a stroke each year [13]. Stroke is an important factor that leads to human dyskinesia. Stroke patients face difficulties and restrictions in their daily activities. Total

financial costs of stroke in Australia were estimated to be five billion Australian dollars yearly [13]. Spinal cord injury is a serious complication of spinal fracture or dislocation. It leads to motor dysfunctions, sensory dysfunctions, sphincter dysfunctions, abnormal muscle tone, and corresponding changes in pathological reflexes appear in the corresponding segments that are damaged. Spinal cord injury also limits the gait of affected patients, and they cannot perform their activities of daily living. Patients with mild stroke and incomplete spinal cord injury can regain their ability to walk by undergoing the rehabilitation process.

1.3 Traditional Gait Rehabilitation

Traditional gait physical therapy includes manually assisted treadmill or overground walking to increase the range of motion of lower limb joints in order to retrain the neuromuscular system. A body weight support (BWS) is also provided during the treadmill training of neurologically impaired patients. Figure 1–2 shows the BWS treadmill training process. A harness is connected to the metal frame or ceiling and supports a patient using BWS. While the patient is walking on the treadmill, the harness and BWS assist and reduce the weight on the patient's feet. A team of two or three physical therapists guide the lower limbs of the patient on predefined paths and stabilise the patient’s pelvis during BWS treadmill training (Figure 1–2). Applying BWS for gait rehabilitation can help patients to improve their endurance, range of motion, balance and coordination, and muscular strength [14-16].

Figure 1–2. Traditional Body Weight Supported Treadmill Training [15].

1.4 Limitations of Traditional Rehabilitation Approach

The traditional approach for rehabilitation such as manually assisted BWS treadmill training needs cooperation and effort from both therapists and patients. However, the conventional approach generally takes extensive time to treat a patient as a patient can only undertake a limited number of short duration therapy sessions due to the limited availability of physical therapists. For a speedy recovery, patients need to undergo repetitive, intensive, and customised gait therapy. In order to allow neuroplastic changes needed for motor learning to occur in specific neural networks which mediate motor function, it has been shown from literature that repetition must be high at 100 repetitions per session. [17]. This will aid in the fast recovery of neurologically impaired patients.

Manual physical therapy sessions also have limited capability to record and objectively assess a patient's progress and recovery, and evaluation is solely dependent on physical therapists' judgment and assessment. This subjectivity in the rehabilitation of neurologically impaired patients presents a limitation [18, 19]. Manual gait therapy is also not ergonomically feasible for physical therapists. The labour-intensive process of manual gait therapy can cause musculoskeletal injuries resulting in back pain for physical therapists as evident from various studies reported in literature [20, 21]. Robot-assisted gait rehabilitation overcomes these limitations and improves treatment outcomes, and also optimises physiotherapists' interventions and time [22].

Therefore, it is important to develop innovative robotic technological solutions for the gait limb rehabilitation of neurologically impaired patients. These technological advances also greatly expand the rehabilitation tasks a therapist can prescribe and can help reduce hospitalisation, while accelerating the recovery of lower limb movement. Accelerated recovery from neurological injuries improves quality of life and assists in patients' return to independent living.

1.5 Research Motivation and Impact

It is important to design and develop novel robotic systems for gait rehabilitation of neurologically impaired patients. These robots can provide accessible, intensive, customised and low-cost physical therapy to patients which may aid in their speedy recovery [23]. The active participation of patients in their rehabilitation could also be enhanced by using rehabilitation robots. The rehabilitation robots are generally programmable to provide personalised training of different intensity and modes according to the nature and disability level of each patient [24]. In addition, rehabilitation robots are usually integrated with a variety of sensors which can provide accurate information to therapists. Based on this objective sensor-

based data physical therapists can adjust the rehabilitation plan based on the progress and recovery of the patient [24-27].

Rehabilitation robots can also ease the burden on physical therapists and a single physical therapist could simultaneously supervise multiple patients undergoing robot-assisted gait rehabilitation. Robots could also reduce the financial budget on the health care system and the social security system, by enabling patients to perform daily living activities [23]. Moreover, these robots are more suitable for repetitive exercise tasks during the rehabilitation process, which can ensure the intensity, efficacy, consistency, and accuracy of the rehabilitation process [19, 28-33].

Several robots have been developed and reported in the literature for the gait rehabilitation of neurologically impaired patients and are discussed in more detail in Chapter 2. However, there are limitations in the mechanism design, actuation, and control systems of these gait rehabilitation robots. These robots use highly stiff and non-backdrivable actuators, such as DC motors, which may cause discomfort to patients. These non-backdrivable actuators also create inaccuracies in estimation of the human–robot interaction force which is vital for the control of these rehabilitation robots. The alignment of robot joints with anatomical joints of patients is not accurate during the rehabilitation process[22]. Some of these robot prototypes do not have full or partial gravity-balancing of a human leg during the motion.

Developing a robotic orthosis (*i.e.* robotic exoskeleton) with intrinsically compliant actuators for gait rehabilitation is vital for the safety of patients and is the first motivation for conducting this research. An intrinsically compliant actuator provides a safe avenue for rehabilitation. The robotic orthosis should also be capable of providing the major ranges of joint motion during the rehabilitation process. Ensuring joint alignment between the robotic orthosis joints and anatomical joints is also critical for safeguarding patients as well as for providing accurate

robotic moments at the anatomical joints and this forms the second motivation for this research. The self-aligning mechanism and gravity-balancing mechanism should be developed for the gait rehabilitation robotic orthosis in order to provide better rehabilitation training and ensure the safety of patients. The control of the intrinsically compliant robotic orthosis with a self-aligning and gravity-balancing mechanism is a challenging task due to the nonlinear and time-varying behaviour of actuators and forms the third motivation for this research [34].

This research may have socio-economic impact in Australia and worldwide. Stroke remains one of the leading causes of disability and causes a huge impact on the socio-economic system [35]. This research may provide a better rehabilitation robot, which can provide accessible, intensive, customised, and low-cost physical therapy to stroke survivors [23]. The proposed rehabilitation robot, by allowing the survivors to engage in their daily living activities, may help reduce financial pressures on health care and social security systems [23].

1.6 Research Aims and Objectives

The aim of this research is to develop an intrinsically compliant robotic orthosis for gait rehabilitation, which can perform the major ranges of joint motion while providing joint alignment to patients during the training process. The research aim is further explained with the following five research objectives.

1.6.1 Development of a Prototype of a Gait Rehabilitation Robotic Orthosis

A treadmill-based gait rehabilitation robotic orthosis will be designed and developed. The developed robotic orthosis should meet the required dynamic capabilities in terms of velocities, acceleration and force/torque. The robotic orthosis should provide sufficient degrees-of-freedom (DOFs) to provide naturalistic motion patterns. In addition, the developed robotic orthosis should have good stability and rigidity.

1.6.2 Development and Application of a Self-aligning Mechanism

The need to avoid misalignment of the robotic orthosis joint with the alignment of the human joint is a major practical problem for the comfort and usability of rehabilitation robots. A robotic orthosis normally has simple revolute joints, while human joints have translating axes of rotation. As such the two, robot and human joints, cannot remain aligned during motions. Consequently, this axis misalignment induces compensatory movements that may not only impede recovery but can also cause discomfort to patients due to undesired residual forces. Thus, it is important to incorporate self-aligning mechanisms in the design of the robotic orthosis.

Therefore, researchers have proposed novel self-aligning mechanisms that can be used in rehabilitation robots. Analytically, it has been shown that the use of a self-aligning mechanism may reduce the residual forces and torques substantially [36-38]. Recently, robots using a self-aligning mechanism have been designed and proposed for lower limb rehabilitation [39-42] as well as for robot-assisted rehabilitation of upper limbs [43-45]. Nevertheless, most of the self-aligning mechanisms for lower and upper limb robots are either too complex to be practically used or they still produce residual or uncompensated forces and torques.

Assumptions that these aligning mechanisms are massless, frictionless, and infinitely stiff do not practically hold during the design of physical prototypes. The finite mass of these aligning mechanisms induces unpredictable forces and torques, which adversely affect their intended objective. The presence of friction in the mechanism may prevent the mechanism from dynamically aligning in real time. Compliance in the linkages of the aligning mechanisms may also induce passive movements that may give rise to uncertain kinematic behaviour. Therefore, it is challenging to design and develop an aligning mechanism that has low mass and frictions and is sufficiently robust to transfer motions without altering them.

Apart from the above attributes, a good aligning mechanism should also have a good decoupling approach, which allows large residual forces to be transferred to the exoskeletal system [36, 46-48]. Decoupling of joint rotations and translations also plays an important role in achieving the self-alignment of robotic orthoses. An aligning mechanism with a provision for decoupling can reduce the interaction stiffness between the robot and the human lower limbs. A novel passive self-aligning mechanism is developed during this research to address the noted challenges of the existing mechanisms.

1.6.3 Development and Application of a Gravity-balancing Mechanism

A partial gravity-balancing mechanism is incorporated in the design of the robotic orthosis in order to compensate for some of the weight of the prototype. With the inclusion of a gravity-balancing mechanism, patients may have more comfort and face fewer difficulties during the rehabilitation process.

1.6.4 Application of Appropriate Actuators for the Robotic Orthosis

Actuation in rehabilitation robots plays an important role and compliant actuators, such as pneumatic muscle actuators (PMAs), are preferred over stiff electromagnetic actuators due to their lightweight, compliant nature, and skeletal muscle-like behaviour. Due to these advantages, PMAs are used in the design of the robotic orthosis in this thesis research.

A few designs of gait rehabilitation robots actuated by PMAs have been proposed in the literature. However, only two DOFs have been implemented in these designs, due to design complexities that arise from the use of the PMAs. Moreover, most of the robots do not have a telescopic feature and instead have fixed link lengths, which prevents their use for a wide range of people who would require length adjustments. One example is [49] where only one leg of the 2-DOFs robot is presented and the design is not adaptable to different user sizes.

Further, it is known that an average torque of 60 Nm is needed to move the hip joint, while 15 to 20 Nm torque is sufficient for the knee joint motions during the human gait [50]. Therefore, for the hip motions, two antagonistically actuated pneumatic muscle actuators (inflated with 6-bar pressure and separated by 6 cm) must individually produce force more than 2000 N. In [49], such torque is claimed to have been achieved with less than 3 bar pressure, which appears to be unrealistic. In [51], the authors presented a 2-DOFs gait robot that is claimed to provide the required hip and knee torques with 20 mm and 10 mm diameter pneumatic muscle actuators. The data sheet from the FESTO® does not verify this claim [52] and, according to this data sheet, the maximum possible force from a 9-metre-long actuator of 20 mm diameter is only 150 kg. Beyl *et al.* in [53] presented a single leg of their pneumatic muscle actuated gait robot with just one DOF at the knee joint. Huang et al. [54] proposed a 2-DOFs robot design and tested its hip joint motions, assuming the weight of a human leg as 5 kg, which is an unrealistically low measure.

Three important inferences can be drawn from the above discussion. First and foremost is that there is no 3-DOFs pneumatic muscle actuated gait robot proposed in the literature so far. Second, all intrinsically compliant gait robots have fixed link lengths and cannot be adapted to different user sizes. Finally, the above-mentioned gait robots cannot provide the required torques at the hip and the knee joints, which are crucial for effective rehabilitation treatment. The proposed design of the robotic orthosis in this thesis overcomes these limitations.

1.6.5 Design and Application of an Appropriate Controller for the Robotic Orthosis

Control of the robotic orthosis powered by pneumatic muscle actuators and incorporating a self-aligning mechanism is a challenging task due to the highly nonlinear and time varying nature of the actuation system. In this research, a Koopman operator-based system identification approach [55-58] is developed to model the combined dynamics of humans and a robotic orthosis. For modelling the nonlinear dynamics of the system, the orientation of the

hip, knee, and ankle joints and the actuator lengths were considered. Based on this model, a nonlinear model predictive control system is developed to ensure that the robot follows the desired trajectory.

1.7 Thesis Overview and Scope

This thesis details the research work carried out to meet the five objectives. Chapter 2 presents a literature review to discuss the current state-of-the-art in the field of robot assisted gait rehabilitation. Chapter 3 presents a robotic orthosis design that meets design requirements and specifications. Chapter 4 presents three different self-aligning mechanisms. They are simulated and tested to determine a better self-aligning mechanism for the designed prototype. The kinematics and dynamics of this prototype are analysed in Chapter 5. Chapter 6 discusses the control of the designed prototype and experimental evaluation and results. Chapter 7 presents the contribution of this research, limitations of the designed rehabilitation robotic orthosis, and future research directions.

1.8 Chapter Summary

This chapter presented background knowledge on human gait and causes of human gait impairments, such as stroke and spinal cord injuries. Popular conventional approaches of gait rehabilitation were briefly introduced. Manually assisted treadmill training based on body weight support was discussed. The need to develop robotic gait rehabilitation solutions was emphasised as a research motivation. The research aims and objectives were discussed, and the thesis overview and scope presented.

Chapter 2 – Literature Review

Several robotic gait rehabilitation robotic orthoses have been developed during the last three decades by the rehabilitation engineering research community. This chapter presents the state-of-the-art in the mechanism designs, actuation methods and control mechanisms in these existing robotic orthoses.

2.1 Existing Robotic Orthosis Designs

Robotic orthoses are wearable robots that work in close proximity to human anatomical joints [24]. These robotic orthoses have also been referred to in the literature as robotic orthoses and several of these have been reported in the literature with various applications such as load carrying augmentation in the military [35], rehabilitation of neurologically impaired patients [22] and in the construction industry [59]. The mechanical design is an important aspect in the development of these robotic orthoses as it forms the basic structure to work with human limbs. Gait rehabilitation robotic orthoses are designed to assist neurologically impaired patients to restore their walking ability during the process of physical therapy. Therefore, it is important for rehabilitation engineers to consider and determine the kinematics and dynamics in the design of these robotic orthoses [60]. Recent emphasis has been placed on selecting the correct number of degrees of freedom for these robotic orthoses [48, 61]. Various robotic orthoses for gait rehabilitation of neurologically impaired patients are introduced in this section.

2.1.1 LOKOMAT

LOKOMAT (Figure 2–1) is the first commercially available rehabilitation orthosis designed to help patients move their hip and knee joints in the sagittal plane while walking on a treadmill by using DC motors as actuators [62-64]. LOKOMAT applies a passive parallelogram mechanism, which can help patients to feel less constrained during the rehabilitation process.

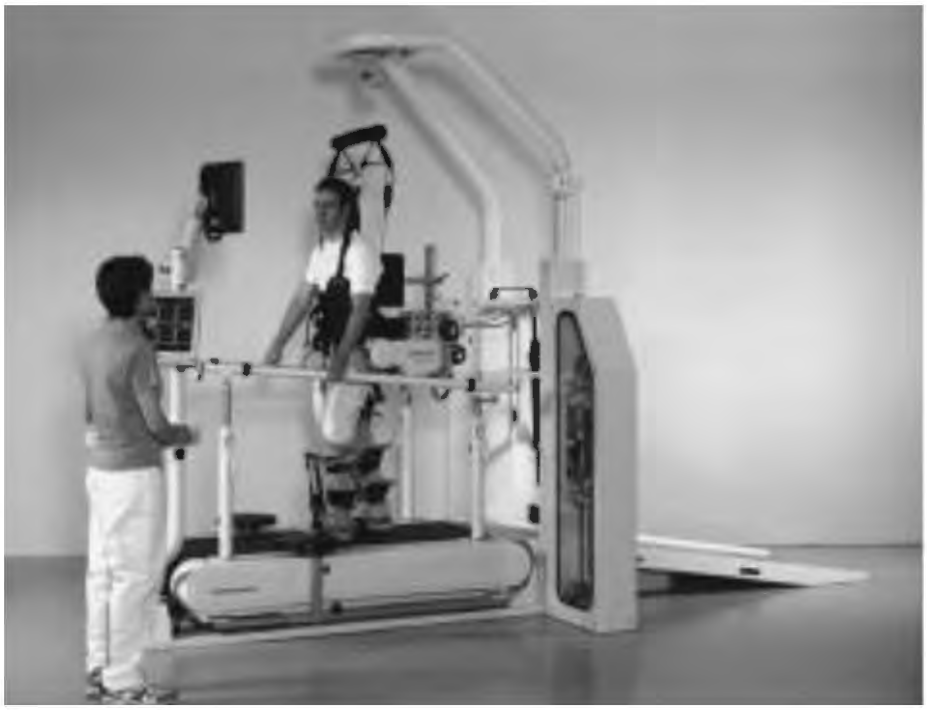

Figure 2–1. LOKOMAT [62].

2.1.2 AutoAmbulator

Another treadmill based robotic orthosis is AutoAmbulator (Figure 2–2). AutoAmbulator is a four DOFs prototype, which uses two robotic arms to support the patient's body to help them step onto a treadmill [65-67]. AutoAmbulator can be strapped to a patient's thigh and ankle. The DC motors can actuate the robot and make the patient walk in a natural gait pattern. This device can only provide gait training process for patients on a treadmill but allows patients to adjust the treadmill speed based on their performance and recovery [62-68].

Figure 2–2. AutoAmbulator [177].

2.1.3 ALEX, ALEX II and ALEX III

The Active Leg Exoskeleton (ALEX) is an example of an active unilateral robotic orthosis, which overcomes the limitations of a passive robot, allowing the patient's impaired leg to move freely while constraining harmful motions [69-71]. ALEX (Figure 2–3) can provide both hip and knee rotations actively in the sagittal plane and hip abduction/adduction motion passively [72, 73]. In addition, ALEX uses the concept of gravity-balancing by using springs and linkage mechanisms [74]. The second prototype of the ALEX project is ALEX II. It has one more DOF than ALEX, which allows passive ankle plantar/dorsiflexion, so it can provide a more naturalistic motion pattern for stroke patients during the gait training process [75, 76]. Both ALEX and ALEX II are actuated by DC motors.

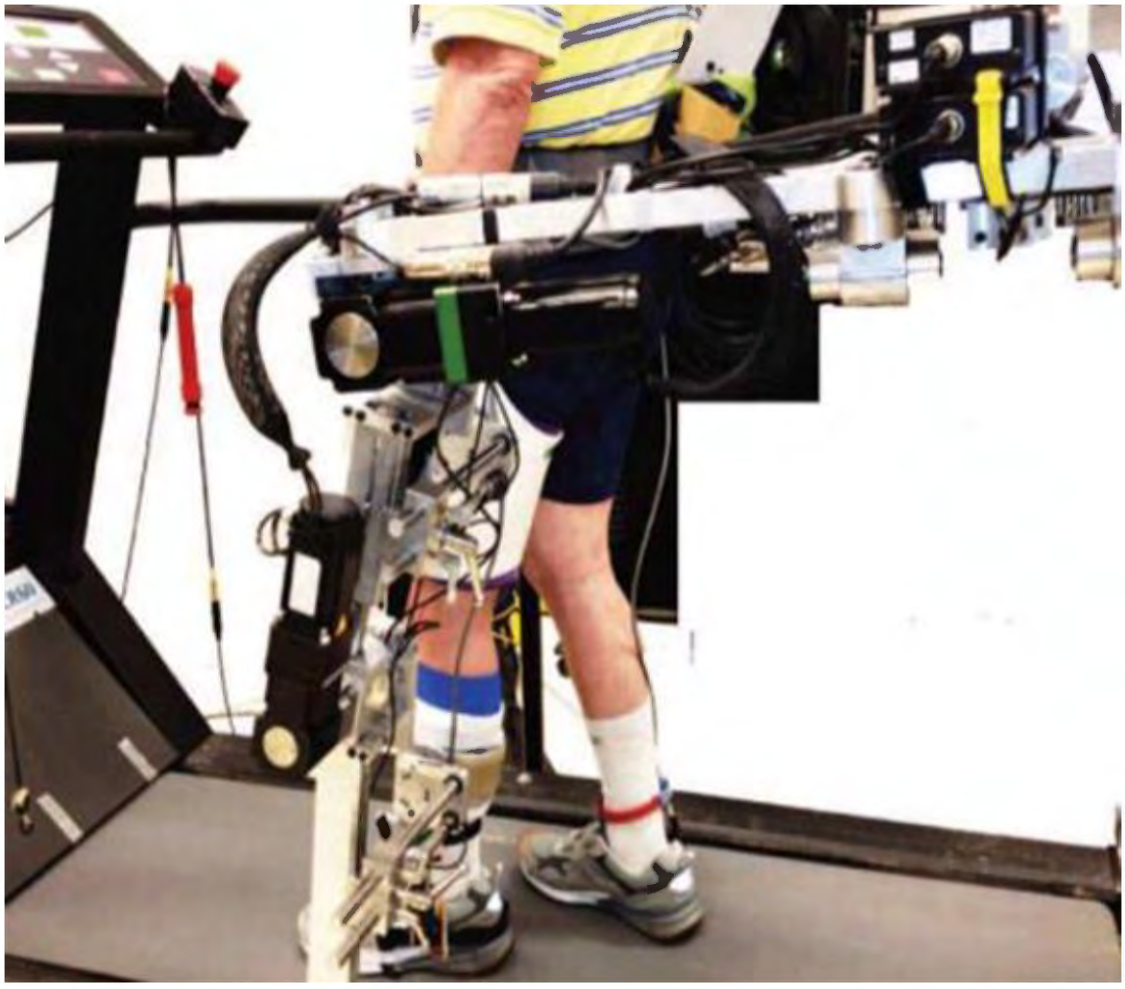

Figure 2–3. Active Leg Exoskeleton (ALEX) [178].

ALEX III is a more developed prototype actuated by DC motors. The parallelogram mechanism and belts help ALEX III to be actuated in 12 DOFs during the rehabilitation process

[61]. ALEX III is a bilateral robotic device compared to the unilateral ALEX II. It has two four-DOFs legs and can provide active vertical motions, anterior/posterior, superior/inferior, and lateral motions on the pelvis. Thus, ALEX III has a total of twelve DOFs, with eight active DOFs and four passive DOFs.

2.1.4 Robotic Exoskeleton from Vanderbilt University

The Vanderbilt University Exoskeleton (Figure 2–4) allows patients to retrain their gait by over ground walking. This prototype is actuated by a brushless DC motor and provides rotations on the sagittal plane of hip and knee joints [77, 78]. This exoskeleton uses a novel idea of embedding an extra battery to power the DC motors for prolonged working duration. There is no mechanism to support passive hip abduction/adduction, but it can be provided by adding compliance to hip brace material and structure. This exoskeleton also uses a passive ankle–foot mechanism to provide stability and transfer the weight of the exoskeleton to the ground.

Figure 2–4. Vanderbilt University Robotic Exoskeleton [78].

2.1.5 Robotic Exoskeleton from South China University

A gait rehabilitation robotic exoskeleton, actuated by a brushless DC motor (Figure 2–5), has been developed by South China University [79]. The South China University's prototype has four DOFs. One rotational DOF works for ankle plantarflexion/dorsiflexion motion while another DOF works for knee flexion/extension motion. The other two rotational DOFs can help patients do hip abduction/adduction and flexion/extension motions. This prototype can support patients to walk over ground [79].

Figure 2–5. Robotic Exoskeleton from South China University [79].

2.1.6 WPAL from Fujita Health University

A Wearable Power-Assist Locomotor (WPAL) (Figure 2–6), which aids paraplegic patients, has been developed by Fujita Health University [80]. DC motors are used to actuate this prototype and it provides motions to the sagittal plane of hip, knee and ankle joints. Paraplegic patients can walk over ground using the Wearable Power-Assist Locomotor [80, 81].

Figure 2–6 WPAL [81].

2.1.7 HAL from University of Tsukuba

The Hybrid Assistive Leg (HAL) was developed by the University of Tsukuba to assist paraplegic patients (Figure 2–7). The prototype provides active motions in the sagittal plane of hip and knee joints by using DC motors, and the ankle motions are provided by passive spring mechanisms [82, 83].

Figure 2–7. Hybrid Assistive Limb [82].

2.1.8 MLLRE

With a similar structure to HAL, a mobile lower limb robotic gait rehabilitation exoskeleton (MLLRE) (Figure 2–8) was developed for body weight support training [84]. This robotic orthosis is actuated by DC motors. It has two active joints for hip extension/flexion and knee extension/flexion. Ankle plantar/dorsiflexion is passively achieved by applying a spring lifter [84].

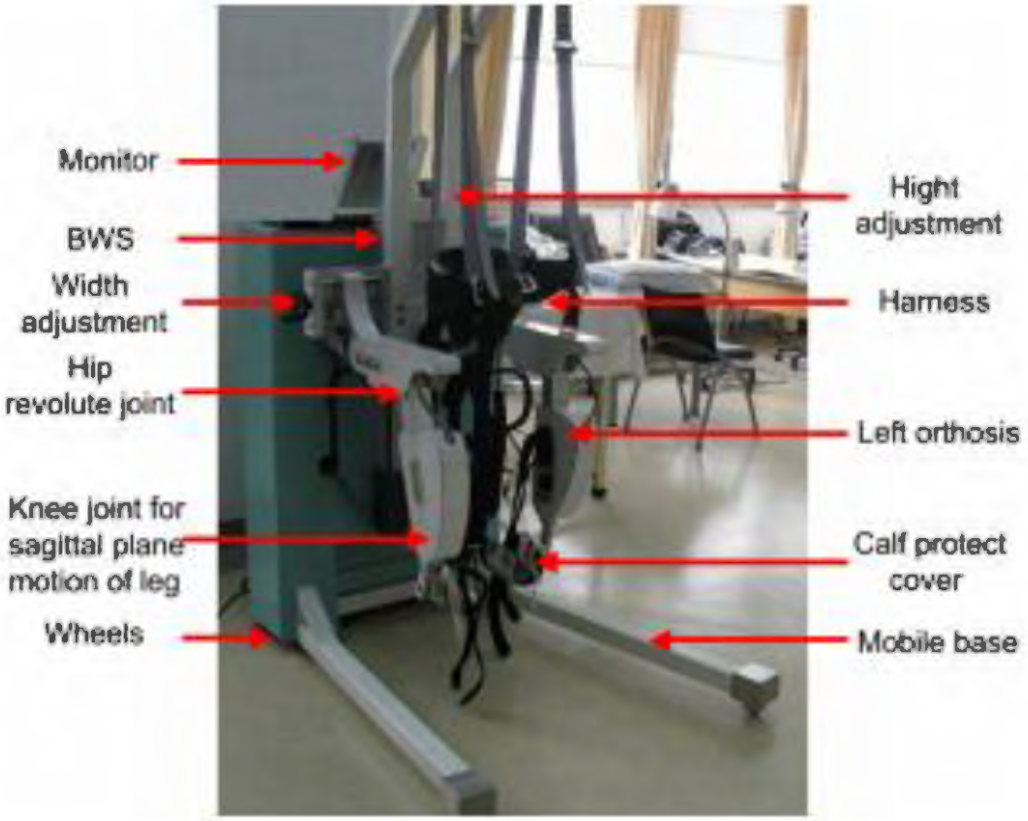

Figure 2–8. MLLRE [84].

2.1.9 LOPES and LOPES II

Another treadmill training-based rehabilitation robot is LOPES (Lower-extremity Powered Exoskeleton), which is designed to help patients regain lost motor control [85, 86]. LOPES (Figure 2–9a) has six DOFs and uses serial elastic actuation to provide compliant assistance to stroke patients. It allows hip and knee extension/flexion in the sagittal plane and hip abduction/adduction. LOPES can also achieve forward and sideway linear motions [87]. LOPES II (Figure 2–9b), a prototype modified from LOPES, has been developed with eight active DOFs to achieve knee flexion/extension, hip flexion/extension and hip abduction/adduction motions for both legs. Forward/after and mediolateral motions on the pelvis part can also be achieved in this modified prototype [88].

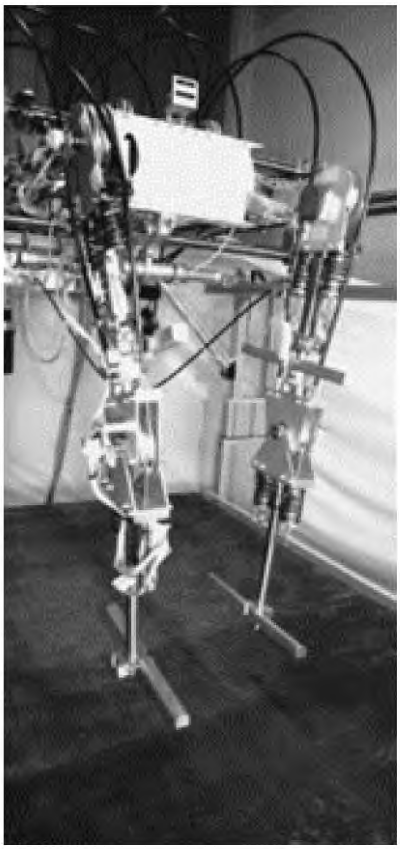

(a)

(b)

Figure 2–9. (a) LOPES [88], (b) LOPES II [88].

2.1.10 GT-1 and Haptic Walker

The Gait Trainer GT-1 was invented by Hesse et al. [89]. The GT-1 (Figure 2–10) applies the principle of a movable foot pedal, which is controlled by a planetary wheel system and simulates foot movement during the standing and swinging phases of the gait cycle [68]. The patient's feet are strapped to foot pedals during the gait training. In this case, the patient's feet trajectory mimics over ground walking which provides more range of hip and knee motions. GT-1 has no active actuation, but requires less effort from therapists for the rehabilitation process [89].

As a result, the team that designed Gait Trainer GT-1 developed the Haptic Walker (Figure 2–11), the first gait rehabilitation device that does not have to be strapped to the limbs of patients during over ground training [90, 91]. The Haptic Walker can achieve a higher

Figure 2–10. Gait Trainer GT-1 [89].

percentage of the stance phase in the gait cycle compared to GT-1 during the rehabilitation process. This prototype can simulate a better gait cycle for patients [90].

Figure 2–11. Haptic Walker [179].

2.1.11 Knee–ankle–foot Robot from National University of Singapore

A knee–ankle–foot robot has been developed by the National University of Singapore (Figure 2–12). This knee–ankle–foot robot is designed for gait rehabilitation based on a series elastic actuation mechanism [92]. This prototype consists of two separate modules, an ankle–foot module and a knee module. In other words, this prototype could be used to rehabilitate the

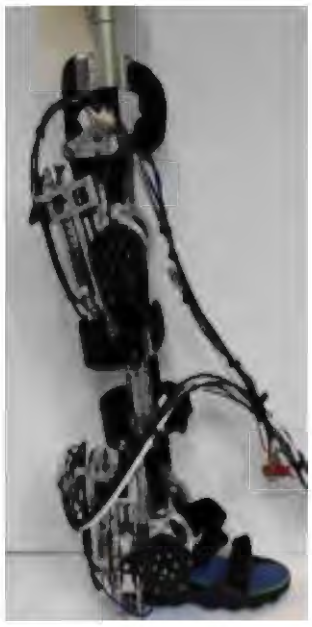

Figure 2–12. Knee–ankle–foot Robot Prototype from National University of Singapore [180].

ankle joint or the knee joint independently by the series elastic actuation. The actuation is transferred to robot joints by using a four-bar linkage mechanism [92, 93].

2.1.12 ICRO

An Intrinsically Compliant Robotic Orthosis (ICRO) (Figure 2–13) has been developed for BWS treadmill training [94]. This prototype has six DOFs with two actuated ones providing power to the hip and knee sagittal plane motions. Other types of motion are passive [94]. The ICRO is powered by PMAs.

Figure 2–13 ICRO [94].

2.1.14 Knee–ankle–foot Robot from University of Michigan

Another pneumatically operated knee-ankle-foot orthosis (Figure 2–14) has been developed by the University of Michigan [95]. It is actuated by PMAs, which can provide motions in the sagittal plane for knee and ankle joints [95].

Figure 2–14. Knee–Ankle–Foot Robot from University of Michigan [95].

2.1.15 Robotic Exoskeleton from University of Salford

A robotic orthosis powered by PMAs has also been developed by the University of Salford (Figure 2–15). It provides knee extension/flexion motions, ankle plantarflexion/dorsiflexion motions, hip flexion/extension, and abduction/adduction motions [96, 97]. Table 2–1 summarises existing robotic gait rehabilitation orthoses.

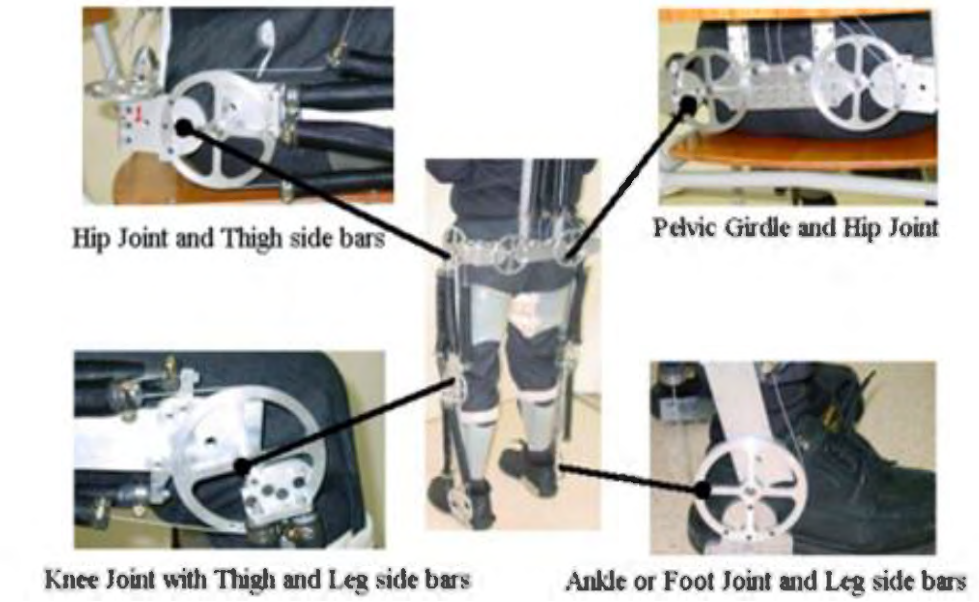

Figure 2–15. Robotic Exoskeleton from University of Salford [96].

Table 2–1. Overview of Existing Robotic Gait Rehabilitation Orthoses.

Robotic Orthosis	**Actuation Type**	**Degrees-of-Freedom**			**Gravity-Balancing**
		Active DOFs	**Passive DOFs**	**Total DOFs**	
LOKOMAT [62]	DC motors	2	0	2	-
AutoAmbulator [177]	DC motors	-	-	4	-
ALEX [178]	DC motors	2	1	3	Applied
ALEX II [178]	DC motors	2	2	4	Applied
ALEX III [178]	DC motors	8	4	12	Applied
Vanderbilt University Robotic Exoskeleton [78]	DC motors	2	0	2	-
Robotic Exoskeleton from South China University [79]	DC motors	2	2	4	-
WPAL [81]	DC motors	3	0	3	-
HAL [82]	DC motors	2	1	3	-
MLLRE [84]	DC motors	2	1	3	-
LOPES [88]	Serial elastic actuation	-	-	6	-
LOPES II [88]	Serial elastic actuation	8	0	8	-
GT-1 [89]	-	-	-	-	-
Haptic Walker [179]	-	-	-	-	-
Knee–Ankle–Foot Robot from National University of Singapore [180]	Serial elastic actuation	-	-	-	-
ICRO [94]	PMAs	2	4	6	-
Knee–Ankle–Foot Robot from University of Michigan [95]	PMAs	-	-	2	-
Robotic Exoskeleton from	PMAs	-	-	4	-

University of Salford [96]					

Note: '-' sign means the literature does not clearly indicate the mentioned parameters.

2.2 Actuators for Robotic Orthoses

Pneumatic cylinders, DC motors, series elastic actuators, and fluidic muscles are commonly used as actuation for robotic orthoses [24, 98, 99]. A pneumatic cylinder is capable of converting the compressed air pressure into mechanical energy and driving it to make linear reciprocating or rotating motion. The diameter of the inner cylinder represents the output force of the pneumatic cylinder. The design of the inner surface needs to reduce friction resistance to prevent wear and corrosion. The advantage of the cylinder is that it moves very fast. However, it is difficult to control the speed and the power/weight ratio is only 16:1 [60]. Due to its good speed regulation performance, DC motors have had a wide use. DC motors with large starting torque can convert direct current energy into mechanical energy. DC motors can regulate stepless speed uniformly and smoothly under heavy load, and the speed regulation range is wide. The limitation of DC motors is a low power/weight ratio, which is close to pneumatic cylinders [61, 78]. Some existing robotic orthoses apply series elastic actuators (SEA). SEA usually have an elastic element, which is connected with a source of mechanical energy output [100]. Compared to those rigid actuators, this type of actuation has lower mechanical output impedance. It also has good tolerance to impulse loads and good peak power output. Series elastic actuators can also passively store mechanical energy and provide benefits in control of robots [85, 100].

The pneumatic muscle, which is also known as air muscle or fluidic muscle, is a flexible/compliant actuator that mimics the movement of human skeletal muscles. The pneumatic muscle consists of a contraction system and a connector. This contraction system consists of a segment of sealed rubber tube wrapped in a high-strength fibre. The fibre forms a three-dimensional rhomboid network structure. The initial force of air muscles is much larger

than traditional pneumatic cylinders with the same diameter. Even in the case of overload, the dynamic characteristics of pneumatic muscles are still stable and good. Pneumatic muscles can reach a power/weight ratio as high as 400:1 and a power/volume ratio of 1 W/cm^3 with small, light, and simple construction. They are compliant and highly backdrivable having a minimum end point actuator impedance [101, 102].

2.3 Self-Alignment for Robotic Orthoses

The need to avoid misalignment of the orthosis joints with the corresponding anatomical joints is a major practical challenge for the comfort of patients and the usability of robotic orthosis. Due to the large variability between users, alignment mismatches are not easy to eliminate and can result in a high degree of stress on the attachment system and Musculoskeletal System [36, 46-48]. Previously, self-aligning mechanisms have been suggested in literature that could compensate muscle contractions but leave many residual forces which would pass directly to the skeletal system. A more efficient self-alignment mechanism should have a good decoupling approach, which allows large forces to be carried by the orthosis while reducing residual moments from the musculoskeletal system [36, 46-48]. One of the methods to achieve self-alignment is to use a four-bar linkage mechanism. Four bar linkage is relatively simple to be designed by using movable closed-chain linkage with four joints. This mechanism can help to reduce the misalignment during robotic orthosis assisted rehabilitation [36]. Decoupling of joint rotations and translations plays an important role in self-alignment of robotic orthoses. Interaction stiffness between the robotic orthosis and anatomical lower limbs can be reduced by this mechanism [46]. Whenever misalignment generates a reaction force and the resulting combined human–robotic orthosis system is not in the equilibrium balance state, the orthosis linkages should have the ability to move themselves until a new residual zero-force position is reached [46, 47].

2.4 Gravity-Balancing of Robotic Orthoses

Gravity-balancing is a mechanism often applied in industrial devices. This mechanism has also been used to reduce the forces needed to compensate the weight of the robotic orthosis during the rehabilitation process [103]. Counterweights, springs, and auxiliary parallelograms have been used to determine the centre of gravity for the design of ALEX [103]. The theory of using both auxiliary parallelograms and springs has proven to be effective in achieving full or partial gravity-balancing for human legs within the desired range of motion [69, 103]. Martin et al. have also proved that using flexure springs can achieve gravity-balancing with an increase in 94% of the power/weight ratio by reducing 81% of the spring strength at the same time [104]. However, those gravity-balancing theories have not yet been physically implemented in the design of robotic orthoses [69, 103, 104].

There are still some limitations associated with these published gait rehabilitation robots. Table 2–1 clearly shows that some existing designs use highly stiff and non-back drivable actuators, such as DC motors, and that the alignment of robotic orthosis joints with anatomical joints of patients is not accurate during the rehabilitation process. Besides, most prototypes do not have full or partial gravity-balancing of a human leg during the motion, which may also cause misalignment during the gait training and cause discomfort to patients during the training process.

2.5 Control Strategies for Robotic Orthoses

The aim of the control strategy of a robotic orthosis for rehabilitation purposes is to simulate physical engagement with the subject by providing continuous guidance along the predefined path. Additionally, the described path must be anatomically and ergonomically feasible. Therefore, designing effective control schemes has been an important field of research. These

control strategies can be broadly classified into two categories: Trajectory tracking and Assist-as-Needed control (AAN).

Trajectory tracking is the conventional form wherein the robotic orthosis guides the subject's limbs along the predefined trajectories [105]. It is generally used for preliminary evaluation of the robotic orthosis. Orthoses like LOKOMAT implemented a proportional-derivative based trajectory tracking controller [106]. The controller guides the user's hip and knee joints in the sagittal plane. Another orthosis, SCUT [107], applied a backstepping control algorithm to improve the accuracy of the trajectory tracking controller. However, these robotic orthoses used a DC motor, which increases the rigidity of the robotic orthoses. With the context of trajectory tracking control, a pneumatically actuated ICRO used a nonlinear sliding mode controller [108]. Pneumatic muscle actuators are inherently nonlinear and time varying, which necessitated the use of a sliding mode controller. Although trajectory tracking controllers aid in establishing the efficiency of robotic orthoses, they do not take the subject's voluntary participation into consideration. Therefore, Assist-as-Needed controllers were designed to understand the patient's disability level, increase the patient's involvement, and provide a more proficient mode of rehabilitation.

Several gait rehabilitation robots have been developed with various AAN based strategies. The control scheme of the LOKOMAT [109] was modified to include an inverse dynamics model. The user's contribution in the form of joint moment from the inverse dynamics model was then used to implement impedance control [110]. Other gait rehabilitation robots used an AAN control scheme based on various laws. For example, LOPES implemented AAN by proposing a virtual mode control law [111]. Similarly, an adaptive controller was also developed for ICRO by augmenting the sliding mode control with an inverse dynamics model [112].

However, in a system with multiple active and passive degrees of freedom, implementation of an inverse dynamics model is computationally expensive and can cause lag. Moreover, the nonlinear and time variant nature of the PMAs add another layer of complexity to controller design. Hence, several attempts have been made to include neural network models to identify the dynamics of a multilayered nonlinear system. However, such models have constraints as they lack interpretability and explainability [113]. Another method is the implementation of a data driven model, such as the Koopman operator, to identify the nonlinear system [114]. Koopman-based methods yield linear models of nonlinear systems that can be used to design a model-based controller like the linear quadratic regulator (LQR) [115, 116] or model predictive controller (MPC) [117, 118]. The Koopman operator has been used to construct a dynamic model for a soft robotic arm in [56]. Based on the identified model, a linear and a nonlinear model predictive controller were designed to compare their efficiency in controlling the soft robotic arm. Koopman operators have also found an application in modelling a linear, control-oriented model for soft robotic swimmers [119].

Although the literature has mentioned various instances of application and efficacy of the Koopman operator in identifying the nonlinear system dynamics, this has not been applied for a gait rehabilitation robot with multiple passive and active degrees of freedom.

2.6 Chapter Summary

This chapter provided an overview of the existing robotic gait rehabilitation systems with an emphasis on robotic orthoses. It discussed mechanism design and the mechanical capabilities of these robotic orthoses in terms of actuated and passive DOFs. Various types of actuation systems developed for these robotic orthoses have also been presented. Mechanisms for gravity-balancing and for providing self-alignment for these robotic orthoses have also been detailed. This chapter also concluded with a discussion of the control strategies developed for these robotic orthoses. Most of existing robotic orthoses don’t have enough DOFs to provide complex

gait training. Some expensive and non-back drivable actuators are applied to those robotic orthoses. Majority of these rehabilitation robots don't have gravity-balancing system which can help to achieve a good alignment between underlying human and robotic orthosis. A novel robotic orthosis should be developed to improve the drawbacks of those existing robotic orthoses.

Chapter 3 – Robotic Orthosis Mechanical Design

This chapter presents a novel intrinsically compliant robotic orthosis powered by PMAs for treadmill-based rehabilitation of neurologically impaired patients. The mechanism of the designed prototype is bio-inspired to achieve self-alignment with the corresponding anatomical joints. Gravity-balancing mechanisms have also been incorporated in the design of the robotic orthosis. Based on the biomechanics of human gait, the design requirements and specifications of the robotic orthosis are devised and, later, the robotic orthosis prototype mechanism design is provided in detail.

3.1 Introduction

Robot-assisted gait training can be effective in reducing the workload of physical therapists and the financial burden on health care systems [64, 73]. Robotic orthoses can provide repetitive and periodic rehabilitation training sessions for an extended duration, and the quality of rehabilitation training can be maintained at a higher level. Moreover, the use of robot-assisted gait training can reduce the subjectivity of manual training, thereby providing patients with efficient rehabilitation more objectively. Among the various robotic orthoses mentioned in Chapter 2, some have been commercialised. These robotic orthoses attempt to mimic the natural gait of humans to help neurologically damaged patients recover faster and more efficiently.

To further improve the efficiency of rehabilitation training and, at the same time, reduce the discomfort that patients with neurological impairment may experience during rehabilitation training, a self-aligning mechanism is applied to the new robot design. Although several studies [46, 120] have provided concepts or designs for self-aligning mechanisms, there is currently no evidence of which mechanism is better. The ALEX series prototypes [71, 73] provide an example of applying a gravity-balancing mechanism by using springs and parallelogram mechanisms. An effective gravity-balancing mechanism can help reduce discomfort for patients

and allow robotic orthoses to provide better self-alignment. Thus, it would be useful to have an efficient self-aligning mechanism and a gravity-balancing mechanism in the newly developed gait rehabilitation robotic orthosis. To power the robotic orthosis, PMAs are a good choice because they offer higher power/weight and power/volume ratios at relatively reduced cost [121, 122]. PMAs are elastic and can provide compliance in the actuation.

In this thesis, a compliantly actuated robot-assisted gait rehabilitation orthosis with a self-aligning mechanism and a gravity-balanced mechanism is developed. The developed robotic orthosis can be used during treadmill rehabilitation sessions. This chapter briefly introduces the biomechanics of human gait, various design requirements and specifications, and the development process of the robotic orthosis mechanisms and actuation.

3.2 Biomechanics of Human Gait

3.2.1 Planes and Axes

The human body can be divided by three planes: the sagittal plane, the frontal or coronal plane, and the transverse or horizontal plane[50]. Figure 3–1 shows these three planes. The sagittal plane can bisect the human body into a left half part and a right half part. The frontal or coronal plane can bisect the human body into a front half part and a back half part. The transverse or horizontal plane can bisect the human body into an upper half part and a lower half part[50].

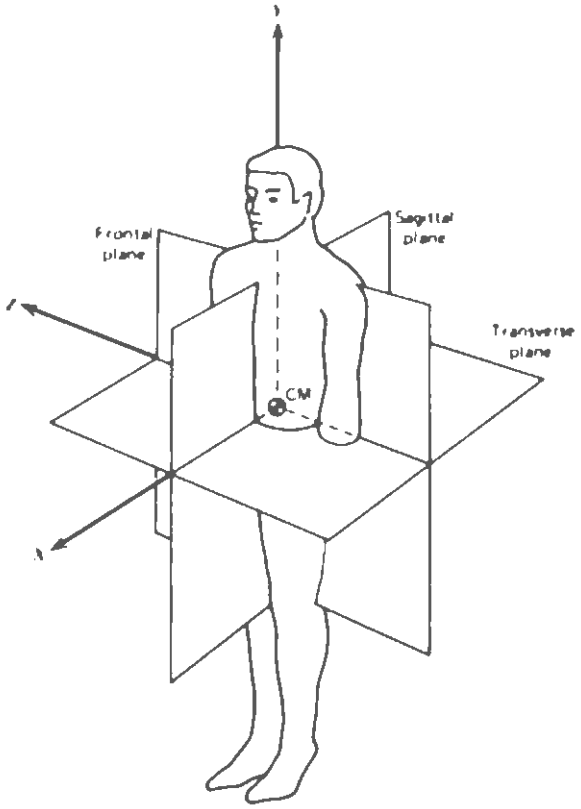

Figure 3–1. Planes and Axes which Bisect the Human Body [50].

3.2.2 Hip, Knee and Ankle Complex

Figure 3–2 clearly shows the motion type and their directions. Motions can occur on the plane along the axis. There are three main types of motions: flexion and extension, abduction and adduction, and internal/external rotation [50]. Flexion and extension motions occur on the sagittal plane. They are about the mediolateral axis, which runs side to side through the centre of mass of the body [10, 50]. Abduction and adduction motions occur on the frontal or coronal plane. They are about the anteroposterior axis, which runs anterior and posterior from the plane [10, 50]. Internal/external rotation motions occur on the transverse or horizontal plane. They are about the longitudinal axis [10, 50].

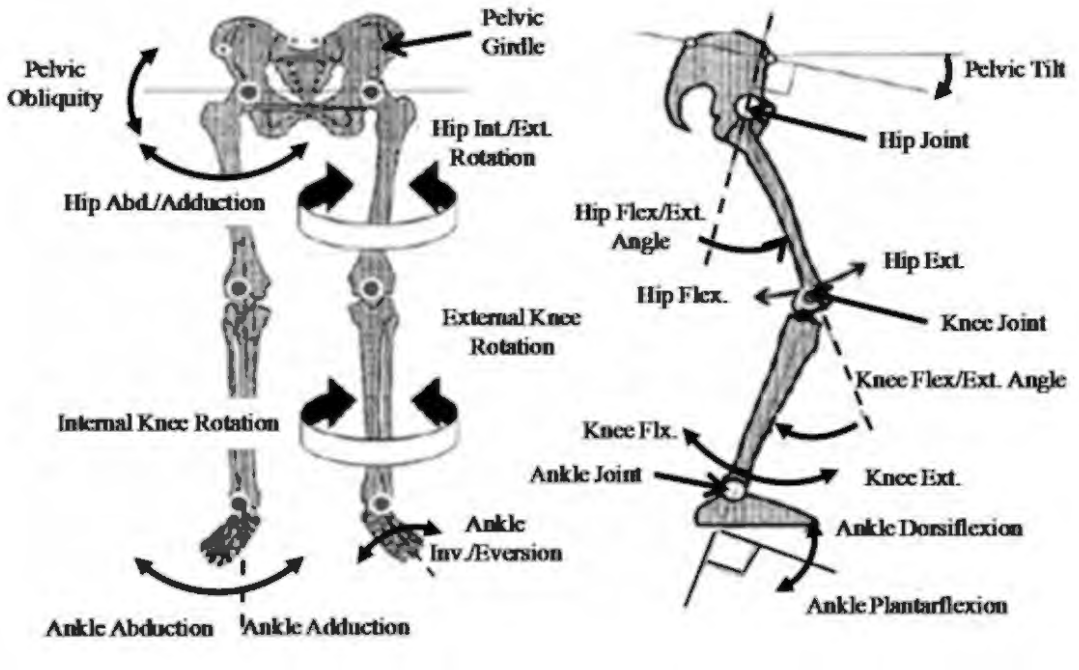

Figure 3–2. Motions Provided by Human Joints [10].

The human lower limb has three joints: the hip, knee and ankle [50]. The hip joint can provide flexion/extension on the sagittal plane, abduction/adduction on the frontal or coronal plane and internal/external rotation on the transverse or horizontal plane. Thus, the hip joint should be considered as three degrees of freedom (DOFs). The number of DOFs is equal to the total number of independent displacements or aspects of motion. The knee joint can provide flexion/extension on the sagittal plane and rotation on the transverse plane. However, in the design of the robotic orthosis in this research, it is still considered as a single DOF in sagittal plane. For the ankle joint, plantarflexion and dorsiflexion occur on the sagittal plane, abduction and adduction occur on the frontal plane, while inversion and eversion occur on the transverse plane (3 DOFs) [50].

3.3 Robot Design Requirements and Specifications

To solve the above-mentioned issues with the existing robotic gait rehabilitation orthoses (mentioned in Chapter 2), the research presented in this thesis has developed an intrinsically

compliant robotic orthosis for gait rehabilitation. This research aims to improve the functional and structural limitations of existing robotic gait orthoses for treadmill training. The novel robotic gait orthosis should be capable of performing the major ranges of joint motion, while providing joint alignment with anatomical joints during the rehabilitation. A gravity-balancing mechanism was also developed and incorporated in the design of the robotic gait orthosis.

3.3.1 Design Requirements

First, a robotic orthosis should provide a realistic walking experience. A realistic gait experience can help neurologically impaired patients experience only minimal kinematic constraints during treadmill training. It may also help to improve the speed of recovery for neurologically disordered patients. Robotic joints should provide a sufficient range of motion for patients to experience a relatively realistic gait. Robotic orthosis should also limit knee extension to prevent unnecessary injury. Therefore, the designed robotic orthosis should have active (*i.e.* actuated) hip, knee and ankle joints, and some passive motion mechanisms. The hip joint should provide active flexion/extension motion on the sagittal plane, passive abduction/adduction on the frontal or coronal plane, and passive rotation on the transverse or horizontal plane. The hip joint on the gait robot design should therefore provide three DOFs. The robot knee joint should be able to provide actuated flexion/extension on the sagittal plane and small passive rotation on the transverse plane. However, owing to the small transverse rotation available, the knee joint is considered to have a single DOF. The robot ankle joint may provide actuated plantarflexion/dorsiflexion on the sagittal plane, passive abduction/adduction on the frontal plane, and passive inversion/eversion on the transverse plane [50].

Robotic gait training orthosis joints should maintain good alignment with human anatomical joints. Patients may experience discomfort if the robotic orthosis and anatomical joints are not properly aligned during the rehabilitation process [37]. Therefore, it is necessary to ensure the robotic orthosis joints are well aligned with the anatomical joints. Thus, the development and

application of the self-aligning mechanisms is a crucial task in the design of robotic orthoses. For the gait pattern provided by the robotic orthosis to approximate the real human gait, the translations of some orthosis joints should also be considered. During the gait cycle, there are only translations occurring on the pelvis in the vertical and lateral directions. Thus, the forward/backward translation and all rotations of the pelvis should be blocked in the mechanism design. For the hip, knee and ankle joints, vertical translations should be achieved by the orthosis mechanism to maintain a good alignment between anatomical joints and robotic orthosis joints. Table 3–1 clearly shows all the DOFs that should be achieved, and all motions that should be blocked or limited in the robotic orthosis design.

Table 3–1. Actuated, Passive and Blocked Degrees of Freedom (DOFs) of the robotic Orthosis Compared with Real Human Gait.

DOFs	**Natural Gait**	**Robot Design**		
		Actuated	**Passive**	**Blocked**
Pelvis to fixed ground	3 Rotations & 3 Translations	-	Lateral Translations Vertical Translations	Forward/Backward Translations All Rotations
Hip	3 Rotations	Flexion/Extension	Abduction/Adduction Ex/Internal Rotation Vertical Translation	-
Knee	2 Rotations	Flexion/Extension	Ex/Internal Rotation Vertical Translation	-
Ankle	3 Rotations	Plantar/Dorsiflexion	Abduction/Adduction Inversion/Eversion Vertical Translation	-

The actuation system of the designed robotic gait training orthosis should be powerful enough to generate the required joint torque and provide sufficient joint ranges of motion. The robotic orthosis and its actuation system should be as lightweight as possible, so that advanced control strategies such as impedance control can be implemented [85, 87]. A lighter weight of the robotic orthosis will also help achieve better joint alignment between the robotic joints and the anatomical joints. Therefore, a full or partial gravity-balancing mechanism should also be incorporated in the design to keep the mechanism in equilibrium at various configurations. In

addition, the variety in patients' anthropometric parameters is another factor to consider during the design. Since the designed robotic orthosis is intended to be provided to different users with different anthropometric characteristics and age range, it would be very effective to add a telescopic structure to the main parts of the robot orthosis. Safety is also a major factor, and it should be considered at every stage of robotic orthosis development. In the design of robotic orthotics, the control system cannot be completely relied on to ensure the range of motion of the joints. During the design of the robotic orthosis, it is best to consider adding several mechanisms to limit the range of motion of the joints to ensure the safety of patients. Table 3–2 below shows all the DOFs the designed robotic orthosis should achieve, and their design parameters including ranges of motion and joint torque are listed. These data are collected from Winter's textbook [50].

Table 3–2. Design Parameters.

DOF	Range of Motion	Joint Torque
Hip Flexion/Extension	$+60^{\circ}/-60^{\circ}$	60 Nm
Knee Flexion/Extension	$+0^{\circ}/-60^{\circ}$	60 Nm
Ankle Plantar/Dorsiflexion	$+15^{\circ}/-15^{\circ}$	40 Nm
Pelvis Lateral Translations	+0.01m/-0.01m	Passive Motion
Pelvis Vertical Translations	+0.01m/-0.01m	Passive Motion
Hip Abduction/Adduction	$+8^{\circ}/-8^{\circ}$	Passive Motion
Hip Ex/Internal Rotation	$+12^{\circ}/-12^{\circ}$	Passive Motion
Hip Vertical Translation	+0.05m/-0.05m	Passive Motion
Knee Ex/Internal Rotation	$+6^{\circ}/-6^{\circ}$	Passive Motion
Knee Vertical Translation	+0.05m/-0.05m	Passive Motion
Ankle Abduction/Adduction	$+6^{\circ}/-6^{\circ}$	Passive Motion
Ankle Inversion/Eversion	$+3^{\circ}/-3^{\circ}$	Passive Motion
Ankle Vertical Translation	+0.03m/-0.03m	Passive Motion

3.3.2 Design Specifications

Figure 3–3 shows the conceptual design of robotic orthosis with all the required DOFs as listed in Table 3–2.

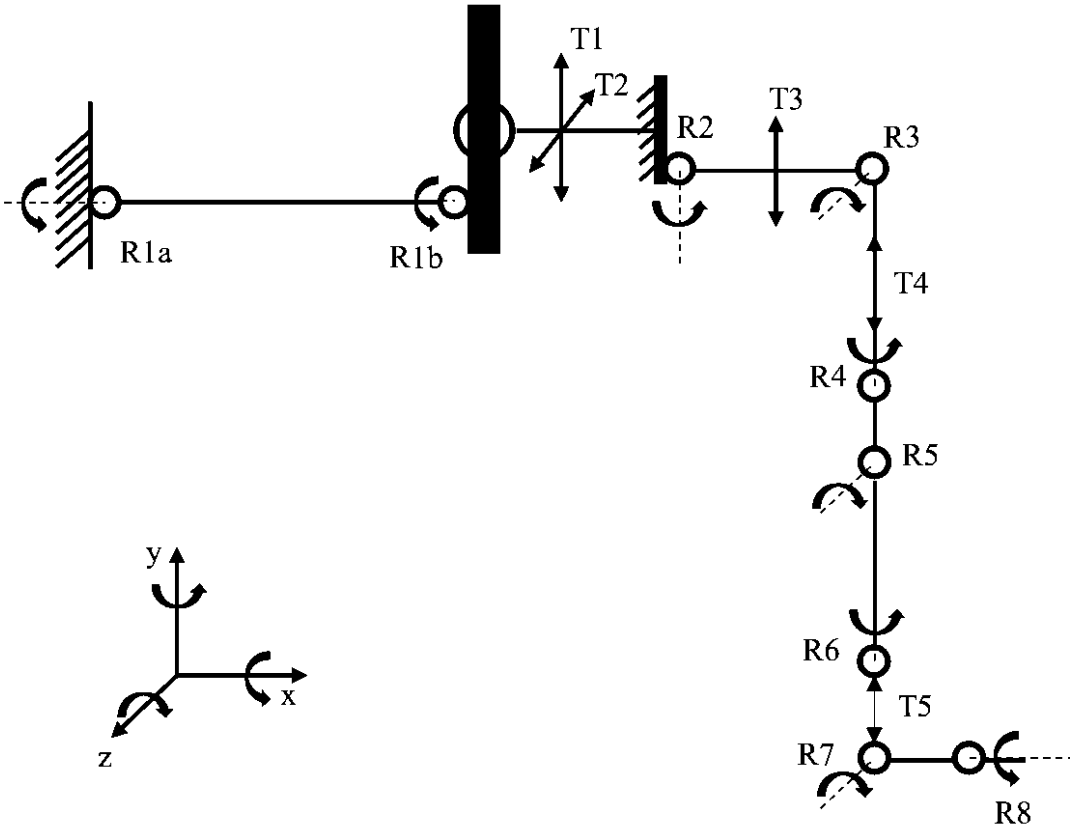

Figure 3–3. Schematic Drawing of the Robotic Orthosis showing all the DOFs. R1(a,b). Revolute Joint for Hip Abduction/Adduction; R2. Revolute Joint for Hip External/Internal Rotation; R3. Revolute Joint for Hip Flexion/Extension; R4. Revolute Joint for Knee External/Internal Rotation; R5. Revolute Joint for Knee Flexion/Extension; R6. Revolute Joint for Ankle Abduction/Adduction; R7. Revolute Joint for Ankle Flexion/Extension; R8. Revolute Joint for Ankle Inversion/Eversion; T1. Pelvis Vertical Translation; T2. Pelvis Lateral Translation; T3. Hip Joint Vertical Translation; T4. Knee Joint Vertical Translation; T5. Ankle Joint Vertical Translation.

Here, the symbol R refers to Revolute Joints, while T refers to Translations. Break lines represent the axes along which rotations occur. The direction of the three axes, x, y and z, are defined in Figure 3–3. R1(a, b) represents the passive revolute joint for hip abduction and adduction along the x-axis. R2 refers to the passive revolute joint for hip external and internal rotations along the y-axis. R3 is the active revolute hip joint, which represents hip extension

and flexion along the z-axis. It implies that the designed prototype has one actuated joint and two passive joints at the hip joint. R4 represents the passive revolute joint for knee external and internal rotations. R5 is the actuated revolute knee joint for extension and flexion. However, usually this designed knee joint of robotic orthosis is considered as a single DOF because the range of internal and external rotation on the knee joint is not significant during the rehabilitation process. R6 is the passive revolute joint for ankle abduction and adduction. R7 is the actuated revolute ankle joint which provides ankle plantarflexion and dorsiflexion. R8 represents the passive revolute joint for ankle inversion and eversion. Thus, the ankle joint of the designed prototype has three DOFs. T1 and T2 represent the vertical and lateral translation on the pelvis, respectively. T3, T4 and T5 are the vertical translations for hip, knee and ankle joints, respectively. Those actuated and passive DOFs should help ensure the designed prototype has enough range of motion and achieves joint self-alignment.

3.4 Mechanism Design

3.4.1 Robot Hip and Pelvis Joint Design

The robot prototype has provisions for the pelvic motions and allows trunk motion during the gait motion. The pelvic part of the gait robot is designed to be telescopic to accommodate users with different anthropometric parameters. The height of the pelvic joints should be more than the height of hip joints with reference to the ground [123] and, therefore, there are two L-shaped links provided to raise the pelvic joints (Figure 3–4). Such design flexibility has no adverse effect on the robot's gait motion. At the top of the pelvic joints, there is a hook to hold a spring with high elastic coefficient, which is used for gravity-balancing of the robotic orthosis. The telescopic design at the pelvis support helps in adjusting the distance between the two robotic orthosis legs (Figure 3–4). In the proposed robotic orthosis, braces and cotton sheets were used for wearing which decreases discomfort to the wearers.

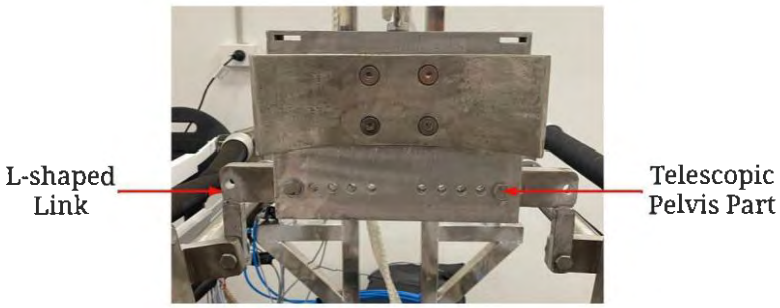

Figure 3–4. Telescopic Pelvis Support on the Gait Robot.

The ends of the pelvis support and the hip joints on the robot (Figure 3–5) are joined together with the help of a connecting shaft, which is made of two segments connected through a flexible coupling at the centre to adapt for any misalignment. The pelvis part is pinned with the connecting shaft to passively allow for the abduction/adduction motion at the pelvis joint. The connecting shaft also has two PMAs mounted on it and their antagonistic actuation moves the robot hip joint in its sagittal plane. The large torque requirement (60 Nm) at the hip joint is achieved by using longer PMAs with large diameters (40 mm). The longer PMAs cannot be accommodated vertically in the robot leg and, therefore, are installed between the robot leg and its supporting frame (Figure 3–5). The actuating ends of the two PMAs are connected with a special ‘T-section’ link, which houses a gear at its tail. The antagonistic motion of the PMAs rotates the ‘T-section’ and this in turn rotates the gear attached at the tail of the ‘T-section’ link. This gear in turn is meshed with another gear, which is mounted on the top of the robot’s thigh part, and the antagonistic actuation of the PMAs moves the robot thigh segment in the sagittal plane. The PMAs have linear encoders attached and can provide information on their individual displacements.

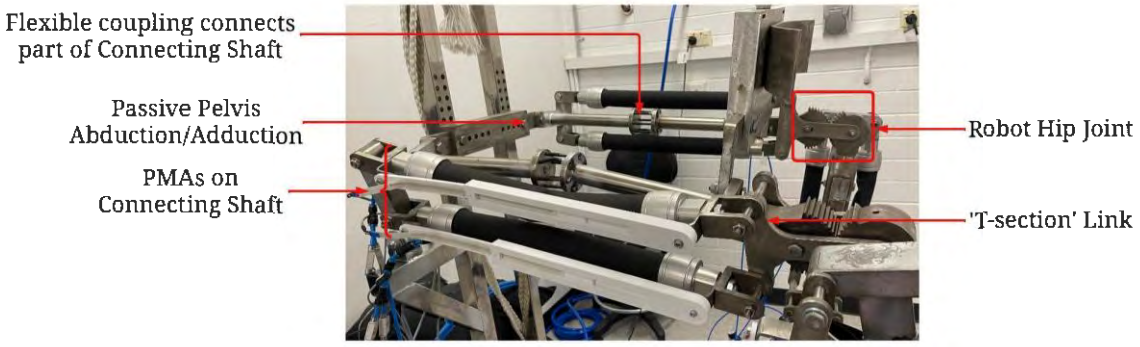

Figure 3–5. The Hip Joint Linked with the Pelvis Support on the Gait Robot.

3.4.2 Robot Knee Joint

There is another pair of PMAs used to actuate the robot knee joint and these are mounted on the thigh part of the robot. The thigh and the shank segments are designed in two parts (the upper and the lower parts), which can slide into each other. This feature makes the thigh and shank sections telescopic to accommodate adjustments required when the gait robot is used by different subjects. The telescopic feature on the thigh segment has six holes, which are 20 mm apart, while the shank telescopic feature has five holes spaced at 20 mm.

Besides adapting the robot design to different users, the telescopic feature also improves portability and saves storage space since the entire robot structures can be downsized by sliding parts of the thigh and shank segments into each other. It is not possible to change the nominal lengths of the PMAs during such adjustments and, therefore, the PMAs are mounted only on the lower thigh part, which is also the sliding thigh part. This is an important design feature of this robot, which allows telescopic thigh and shank sections without altering the lengths of PMAs.

The knee joint is formed with two meshing gears of the same pitch, a non-moving gear G1 at the top and a movable gear G2, which also acts as the robot knee joint (Figure 3–6).

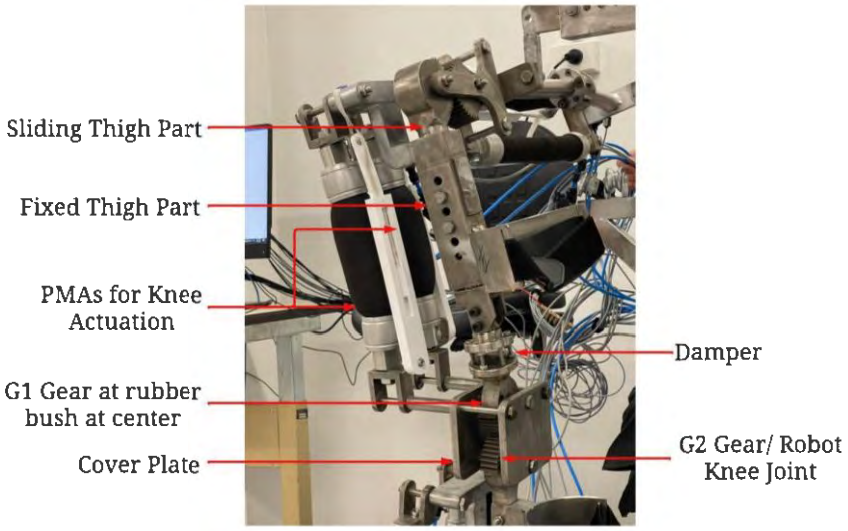

Figure 3–6. The Knee Joint with the Meshing Gears and Damper.

The non-moving gear (G1) is fixed at the end of the thigh segment, whereas the other meshing gear (G2) is connected with the shank of the robot and can rotate. The two actuating ends of the PMAs (which are used to actuate the knee joint) and the axis of G2 are rigidly connected at three points on a cover plate forming another 'T-section' such that during the antagonistic actuation of the PMAs, an anticlockwise moment (up to 60 Nm) from the PMAs rotates the gear G2 over G1 anticlockwise from 0 to 60 degrees. The top meshing gear G1 also has a lock that prevents gear G2 from rotating in the clockwise direction and, therefore, the knee joint can only have flexion motion and cannot extend. The PMAs used cannot contract more than 10% of their nominal lengths and this limits the achievable rotational motions at the robot joints. To achieve the required hip, knee and ankle motions, the actuation from PMAs needs to be amplified. There are two ways to achieve larger actuation from PMAs, either by using PMAs of longer nominal length or by amplifying the actuating signal by mechanical means. The telescopic feature in the thigh and the shank sections poses a constraint on the PMA lengths to be short. Therefore, in the proposed gait robot design, the actuation is mechanically amplified by using two meshed gears G1 and G2. It is evident from Figure 3–8 that a 30 degrees rotation received from antagonistic actuation of PMAs can be converted to 60 degrees rotation of the

shank segment. Two cover plates are provided on both sides of the gears G1 and G2 for safety reasons. The cover plates prevent the user's clothes from being snagged into the gears.

3.4.3 Robot Ankle Joint

As discussed in the previous sections, the robot shank part is also telescopic and so has been designed in two parts that can slide into each other, adjusting its length to accommodate different subjects. The PMAs, which are used to actuate the ankle joint, are mounted on the sliding part of the robot shank and, therefore, their lengths do not require being altered during such length adjustments (Figure 3–7).

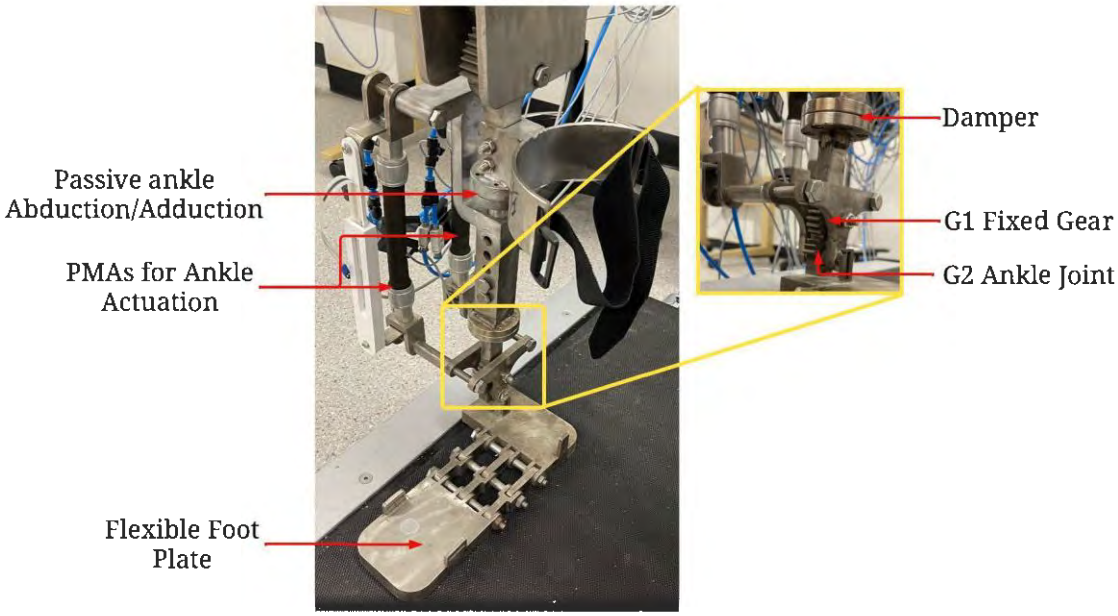

Figure 3–7. Robot Shank and Ankle Joint.

The human ankle joint has three rotational DOFs collectively provided by the ankle and the subtalar joints, which are commonly referred to as the ankle complex. The three DOFs are plantarflexion/dorsiflexion in the sagittal plane, eversion/inversion in the frontal plane, and abduction/adduction in the transverse plane. However, during the gait motion, the ankle predominantly moves in the sagittal plane with small rotations ($< 7.5^0$) in the frontal and transverse planes [124]. The ankle joint in the proposed robot design can provide actuated

plantarflexion–dorsiflexion motions, while the other two rotations are provided passively. A flexible coupling, provided on the top non-sliding part of the shank, facilitates small passive abduction–adduction, which is required during walking. The damper, provided on the sliding part of the robot shank, allows small eversion–inversion besides serving as a safety device for the PMAs as explained in the previous section. Two meshing gears G1 (fixed) and G2 (movable) are used to provide ankle sagittal plane motion (Figure 3–7) in the same manner as they were used in the robot knee joint. The flexible foot plate in the gait robot conforms to the sole of the user's shoes and allows passive metatarsal motion during gait.

3.5 Self-Aligning Robot Joints

As mentioned in section 2.3, a good self-aligning mechanism should be applied on the proposed robotic orthosis to provide better performance during gait rehabilitation process.

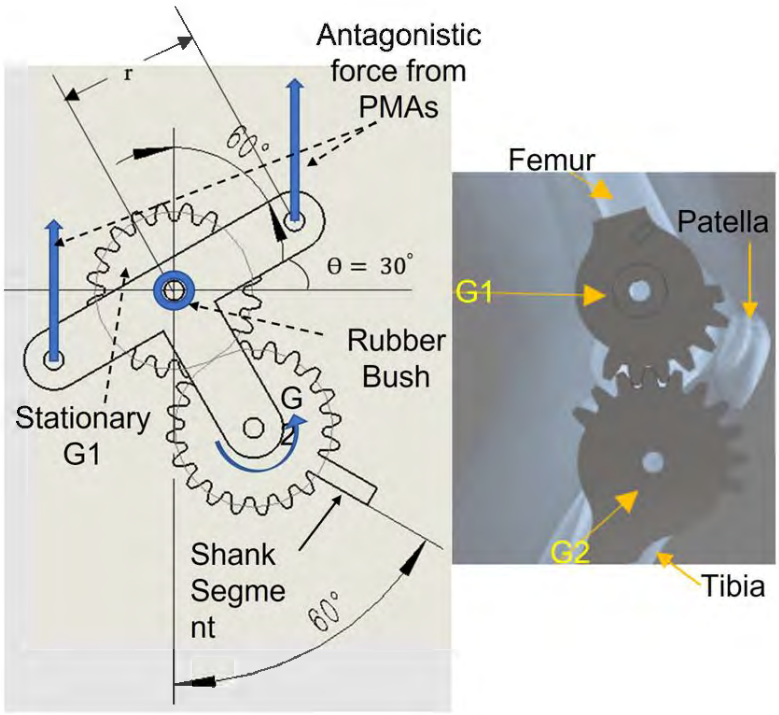

Figure 3–8. Amplification of PMA Using Gears.

The human knee joint complex is formed by the patella bone together with the ends of the femur and tibia bones. It is a complex joint that provides multiple DOFs during walking over ground at natural speeds. While flexion–extension is the most pronounced rotation, a small internal–external rotation and abduction–adduction is also observed during the gait cycle [125].

The proposed novel design of a gait robot offers passive internal–external rotation and abduction–adduction motions besides active flexion–extension motion at the knee joint. Gears G1 and G2, that form the robot knee, have rubber bushes at their centres to eventually provide small passive motion in the transverse and the coronal planes. The cushioning effect of the rubber bushes also emulates the cartilages in the human knee acting as shock absorbers.

A damper consisting of damper springs is provided on the robot thigh part immediately before gear G1 as shown in Figure 3–6. This damper serves two important purposes and the first one is to passively contribute towards the internal–external rotation and abduction–adduction motions of the knee joint. Second, the damper also serves as a safety device for the PMAs. In fact, to achieve the antagonistic actuation of two PMAs, one of them is contracted by inflating with high pressure (up to 8 bar). Since the actuating ends of the two PMAs are coupled through a link that forms a moment arm, contraction in one causes extension in another PMA. However, during this process, the link forming the moment arm also undergoes a small displacement, which cannot be restrained. The damper serves the important task of providing the necessary small displacement at the moment arm and, thereby, prevents the PMAs from potentially bursting from high inflating pressure.

The approach of using gear couples and dampers to achieve self-alignment is known as the decoupling method. As reported in published research [46], during normal human gait, there is not only rotation occurring in the sagittal plane, but also the vertical translation. The decoupling approach works on the idea that it is not necessary to achieve both rotation and translation in one mechanism. In the designed rehabilitation robotic orthosis, there are two mechanisms working for one joint to achieve vertical translation and sagittal plane rotation, respectively (Figure 3–9).

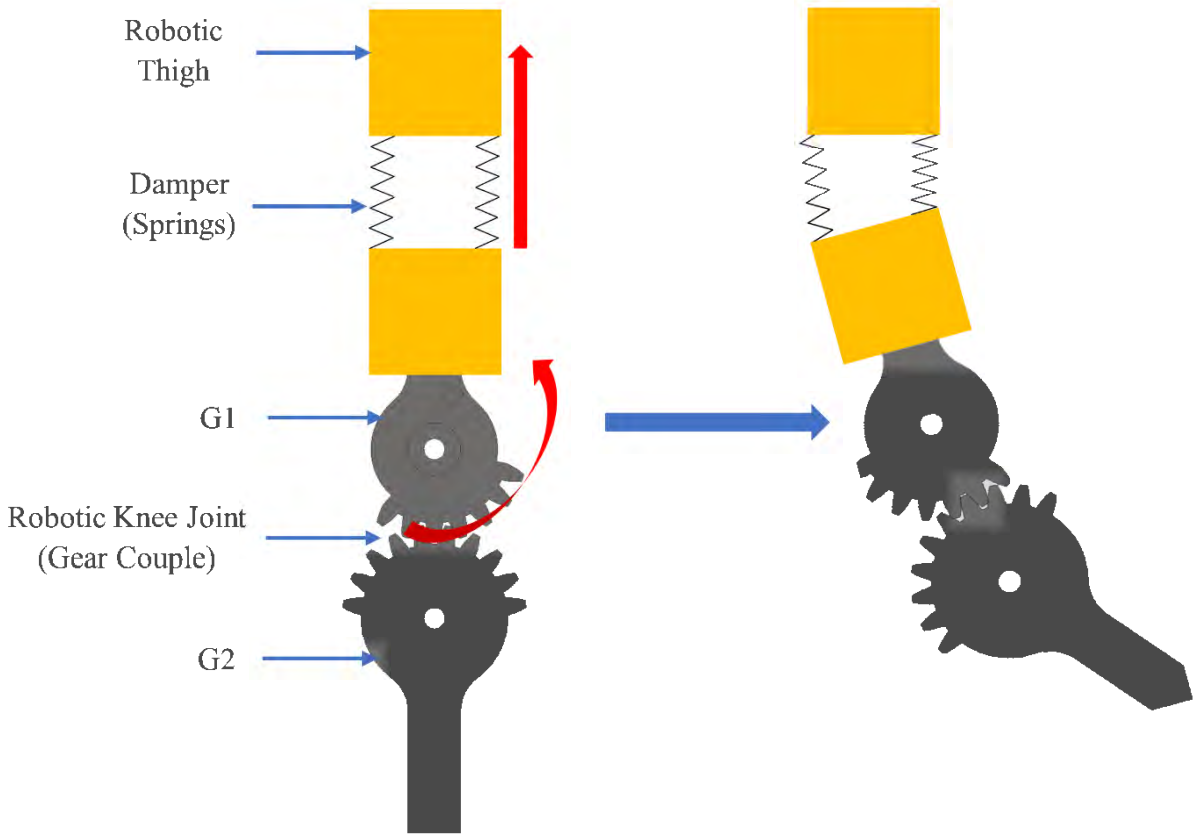

Figure 3–9. Schematic Drawing of Self-Aligning Mechanism.

When the robotic knee joint (designed as a couple of gears instead of the usual bushing and bearing joint) is actuated, G2 starts rotating by following the edge of G1 to achieve the robotic knee joint rotation. At the same time, the damper (consisting of six strong compression springs) also starts working. The side of the damper, where knee flexion acts, will contract more, while another side will contract less. By this process, the overall distance between two yellow blocks (which represent the robotic thigh segment) also decreases in order to achieve knee joint vertical

translation occurring during normal human gait. This type of decoupling mechanism helps to facilitate the self-alignment on the robotic knee joint. The same mechanisms have also been developed for the orthosis hip and ankle joints.

3.6 Gravity-Balancing Mechanism

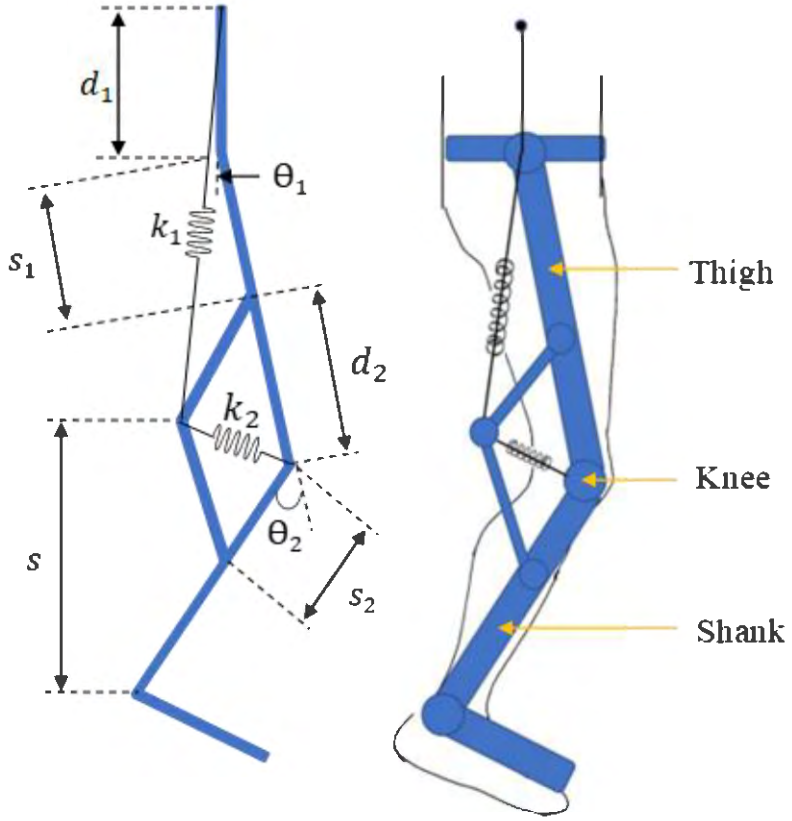

Figure 3–10. Implementation of Gravity-Balancing Mechanism Applied on the Prototype.

As discussed in section 2.4, the proposed robotic orthosis design needs to be gravity-balanced to avoid potential slippage when it is fixed to users' limbs as well as to compensate the effects of orthosis inertia. In other words, the actuator forces should not be required at the joints to maintain system equilibrium at various configurations. A gravity-balancing mechanism can also reduce the forces needed to actuate the robotic orthoses during the course of rehabilitation, by reducing the inertia of robotic orthosis [103]. Counterweights, springs and auxiliary parallelograms, which are used to determine the centre of gravity, are three commonly used gravity-balancing methods [103]. The theory of using both auxiliary parallelograms and springs

has proven to effectively achieve full or partial gravity-balancing for human legs within the range of motion [69, 103]. It is also found that flexure springs can achieve gravity-balancing by increasing the power/weight ratio [104]. To date, these developments are still at the theoretical stage and have not been physically implemented [69, 103, 104].

In the proposed design of a robotic orthosis, gravity-balancing was applied to the two DOFs, namely flexion as well as extension at hip and knee joints of the robot. A hybrid method of gravity-balancing was adapted whereby springs are used and placed appropriately after identifying the centre of mass of the robot elements. Partial gravity-balancing has been obtained for the robotic orthosis to offer a wide-ranging degree of gravity-balancing to users of varying physical characteristics by applying different spring stiffness and an installation position on the designed prototype [126].

First, the link dimensions of the robot are used to find the trajectory of the centre of mass (COM) of its elements in the sagittal plane. Masses of the thigh and shank sections are assumed to be lumped as point masses at their respective COM. Later, the parameters and positions of the springs are selected in such a manner that the total potential energy of the robot system remains constant in various configurations. It should be noted here that the positions of the springs can be changed suiting an individual user's anthropometric measurements. As Figure 3–9 shows, the potential energy of the robot system can be defined as the sum of the potential energies of the springs and the gravitational potential energy as explained below:

$$P = P_S + P_g = {}^1\!/_2\, k_1 x_1^2 + {}^1\!/_2\, k_2 x_2^2 - Mg(S) \tag{3.1}$$

Here, $x_1 = (d_1 + S_1 \sin\theta_1 + S_2 \sin\theta_2)$ and x_2 can be obtained using the cosine law as $x_2^2 = S_2^2 + d_2^2 - 2S_2 d_2 \cos\theta_2$. Spring stiffnesses k_1 and k_2 are derived from the above relation (3.1) using the condition for static balancing or the condition of minimum potential energy. The spring stiffnesses in terms of the robot mass and its configuration are defined below:

$$k_1 = \frac{Mg}{d_1} \tag{3.2}$$

$$k_2 = \frac{MgS_1}{d_1 d_2} \tag{3.3}$$

The prototype developed during the course of this research is not optimised for weight, rather it has been developed to demonstrate the design efficacies and, therefore, it weighs 110 kg. The weight of the robot thigh segment of one of the legs is 25 kg. The total weight of the shank and foot segments in one of the robot legs is 30 kg. The weight of the human test subject's thigh segment is found to be 6.4 kg, whereas their shank and foot segments weighed 3.6 kg. Stiffnesses of the springs using these values can be derived in terms of the adjustable distances d_1 and d_2, as $k_1 = \frac{245}{d_1}$ and $k_2 = \frac{294}{d_2}$.

3.7 Compliant Actuation

As discussed in the previous section, pneumatic muscle actuators (PMAs) are used to actuate the proposed gait robot. This actuator is made of a segment of sealed rubber tube wrapped in high-strength fibre. This fibre forms a three-dimensional rhomboid network structure around the rubber tube to allow deformations [127]. The initial force of air muscles is much larger than the traditional pneumatic cylinders with the same diameter. Even in the case of overload, the dynamic characteristics of pneumatic muscles remain stable [101, 102]. PMAs exhibit a five times higher power/weight ratio and power/volume ratio in comparison to the usual DC motors or hydraulic cylinders [128]. When the PMAs are inflated, the diameter of their internal air bladder increases together with the protective outer sheath and the length contracts. This lengthwise contraction and the axial force generated due to inflation is used for the actuation.

These PMAs have properties similar to human skeletal muscles and, therefore, they have been widely used in robotic manipulators and rehabilitation prototypes [129]. However, their transient and nonlinear behaviour, which mainly comes from the hysteresis effect of the inside

latex tube, is difficult to model and there have been many attempts by researchers in the past to model the dynamics of PMAs. In one of the earliest works [122], a linearised model was proposed relating the extension and force at constant pressure. Improvements to this model were later suggested in [130-132] that improved the positional accuracy up to 5%. Later, a three-element mechanical model of PMAs was proposed by [133, 134] and is commonly used to describe PMA dynamics.

If the pressure-dependent damping, spring and force elements of PMAs are represented by B, K and F, respectively, their system model can be described by the following differential equation:

$$M\ddot{x} + B(P)\dot{x} + K(P)x = F(P) - Mg \tag{3.4}$$

Here, M, P and 'g' are the mass, pressure, and the gravitational acceleration, respectively, and the damping can be defined as: $B(P) = \begin{cases} B_i P + B_{i0} \\ B_d P + B_{d0} \end{cases}$, where indices '$i$' and '$d$' are used for different damping characteristics of PMAs during inflation and deflation. The stiffness and the force elements are given as $K(P) = KP + K_0$, and $F(P) = FP + F_0$, respectively.

If the input variable to the PMAs, which is pressure, is defined as $u = P_t - P_0$ and the output displacement is denoted by $x = x_t - x_0$, the dynamic equation (3.4) can be rewritten as (3.5):

$$\ddot{x} + B^*\dot{x} + K^*x = (p\dot{x} + qx + r)u \tag{3.5}$$

Here, $B^* = (BP + B_0)/M$, $K^* = (KP + K_0)/M$, $p = B_0/M$, $q = K_0/M$, and $r = (FP - Mg)/M$. Unknown parameters, such as B^*, K^*, p, q and r are obtained through experiments performed with PMAs to obtain a transfer function of the PMA system relating pressure and its length.

The PMAs used in the thesis research work are sourced from Festo® [135] and during the experiments conducted they exhibited contraction up to 25% of their nominal lengths when

inflated with 6 bar air pressure. Nominal lengths of the PMAs used for robot knee actuation are 200 mm, whereas their diameters are 40 mm, and they can provide approximately 6000 N axial force.

A different approach is adopted to relate the internal pressure and the force produced in PMAs whereby the work done by the force exerted by the PMA is studied together with the stored strain energy density (ΔW). For a small change in PMA length, the input energy can be accounted for as below [130]:

$$P\Delta V = F\Delta L + V_e\Delta W \tag{3.6}$$

The initial volume and the inflation pressure of the muscle are represented by V_e and P, respectively. A change in the volume of a PMA is indicated by ΔV and the force and axial displacements are given by F and ΔL, respectively. Rewriting (3.6) in the differential form:

$$F = P\frac{dV}{dL} - V_e\frac{dW}{dL} \tag{3.7}$$

The above equation gives us the required transfer function relating input pressure and force from PMAs. To avoid contraction beyond allowable limits, and a potential explosion of the air muscle, the robot thigh and shank segments consist of damper springs. When the air muscle on one side contracts to drive the knee joint, the air muscle on the other side elongates. Here, the damper provides a small contraction to the thigh segment in the middle, so that the air muscle on the other side can be extended by an acceptable amount.

3.8 Robotic Orthosis Prototyping and Instrumentation

The gait robot is mounted on a supporting frame, which also has a body weight support (BWS) system. The unweighing achieved through the BWS system helps patients walk comfortably and can also improve their balance and coordination. It can help keep patients upright and centred, coordinates their steps, and prevents falls. The BWS also helps patients walk for a longer duration, shortening the recovery period. Finally, the BWS system also induces

confidence in patients, who can use the robot system in a safe manner. With the BWS system, patients can rehabilitate their gait safely and easier, and it can improve their confidence to train for further tasks.

The PMAs required for actuating the hip joint are found to be too long and there is not enough space to install the air muscles on the thigh structure. Hence, the air muscles for the hip joints are installed between the robot and the supporting frame. Due to this new arrangement of PMAs, it is possible to achieve passive abduction–adduction motion of the hip joint.

The overall structure of the designed prototype and supporting frame is shown in Figure 3–11. The robotic orthosis is kept 70 mm above the bottom of the supporting frame. This height difference is provided for its intended use with a treadmill. To reduce the overall weight of the robot, aluminium alloy is chosen to be the main material for fabrication. However, due to the large loading and axial forces in the structure, the gears, screws, nuts, and supporting frames are fabricated with steel. The following sections separately show the main components with important functions.

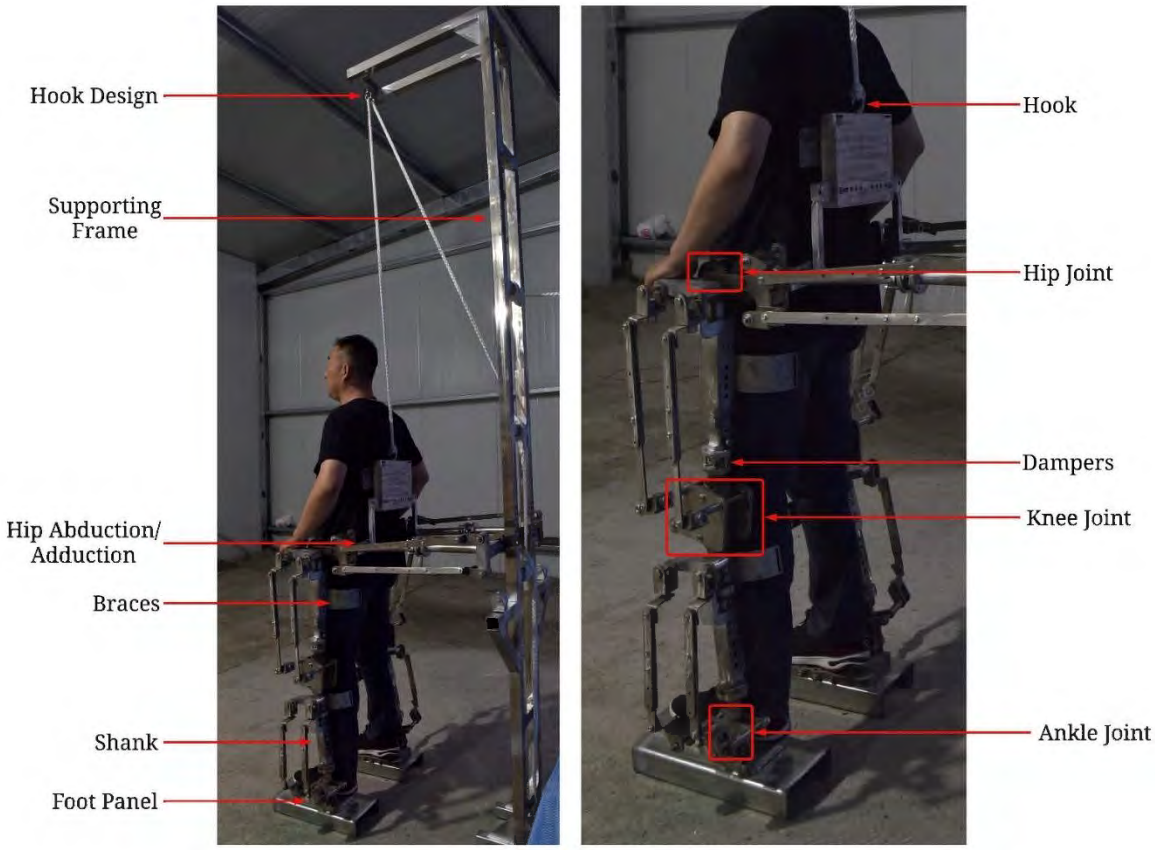

Figure 3–11. New Gait Robot Prototype (PMAs not shown here).

3.8.1 Prototype Components for the Self-Alignment Mechanism

Figure 3–12 shows the robotic knee joint, which has a self-aligning mechanism. As discussed in Section 3.5, G1, G2 and damper can help to obtain self-alignment. Two PMAs are used to actuate robotic knee flexion and extension. Potentiometers can measure the change in length of PMAs during the rehabilitation process. Pressure sensors can measure the pressure applied to the PMAs. The data from these sensors can be used to develop the feedback control system. Solenoid valves are used to control the applied pressure to PMAs.

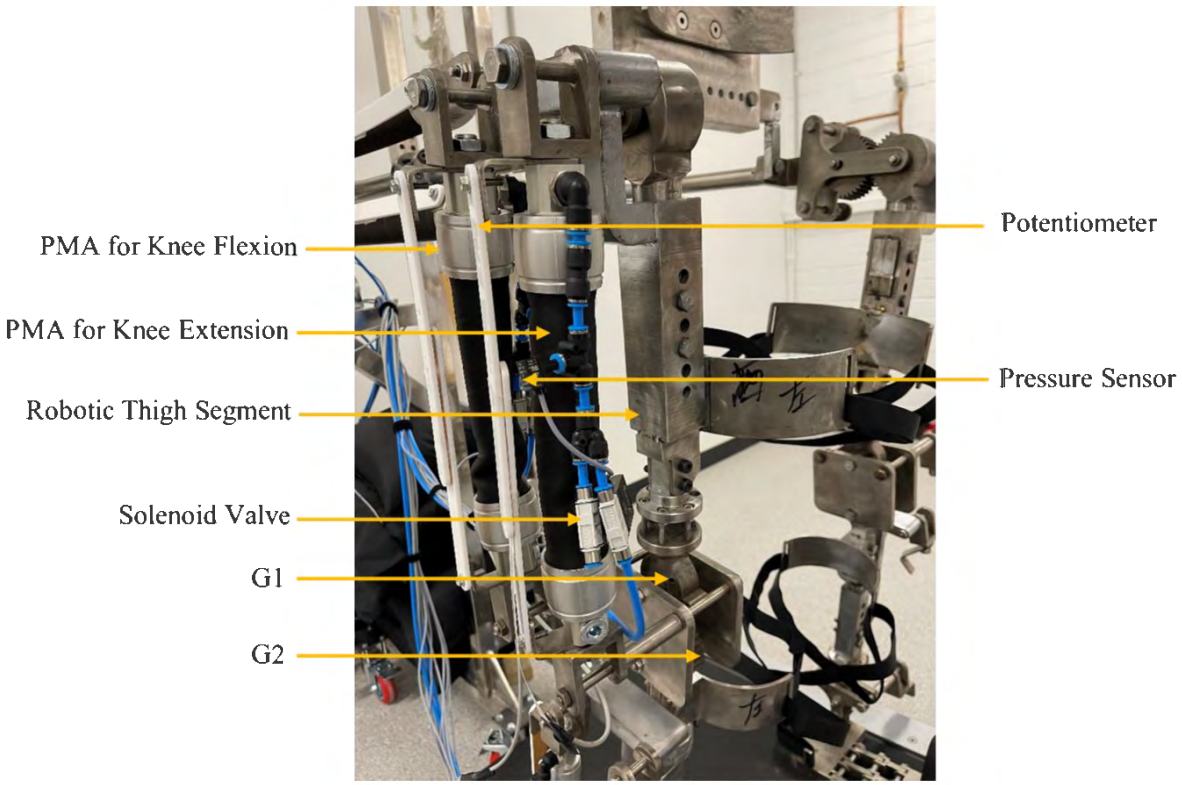

Figure 3–12. Prototype Components for Self-Aligning Mechanism.

3.8.2 Prototype Component for the Gravity-Balancing Mechanism

Figure 3–13 shows the gravity-balancing mechanism as detailed in Section 3.6. This combination of springs (highlighted by red colour) can help to achieve partial gravity-balancing. Two strong extension springs are attached for one leg with fishing lines to form a similar mechanism as shown in Figure 3–10.

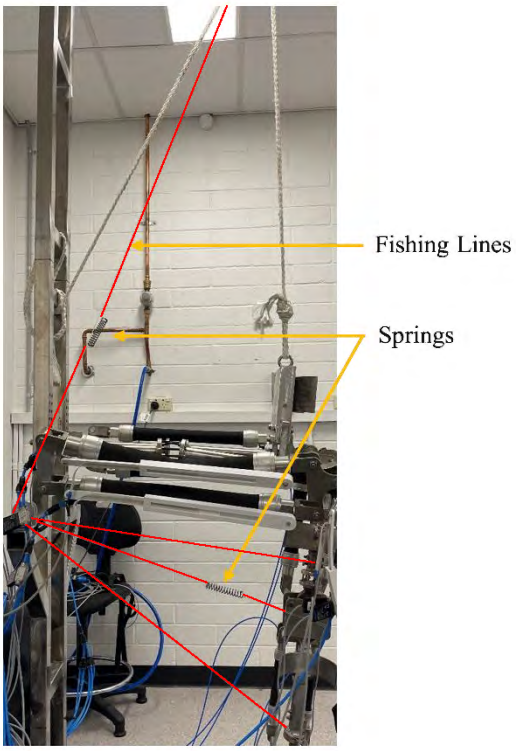

Figure 3–13. Prototype Component for Gravity-Balancing Mechanism.

3.8.3 Prototype Instruments

The gait robot uses sensors to measure pressure and displacement, then calculates force in real time. The pressure sensor is mounted for the compressor, and the pressure measurements are used to determine the force generated by each PMA. The position sensors are installed on the robotic joints. The Block Diagram (Figure 3–14) shows the instruments of the prototype. The controller with a completed circuit can help to control and actuate the prototype.

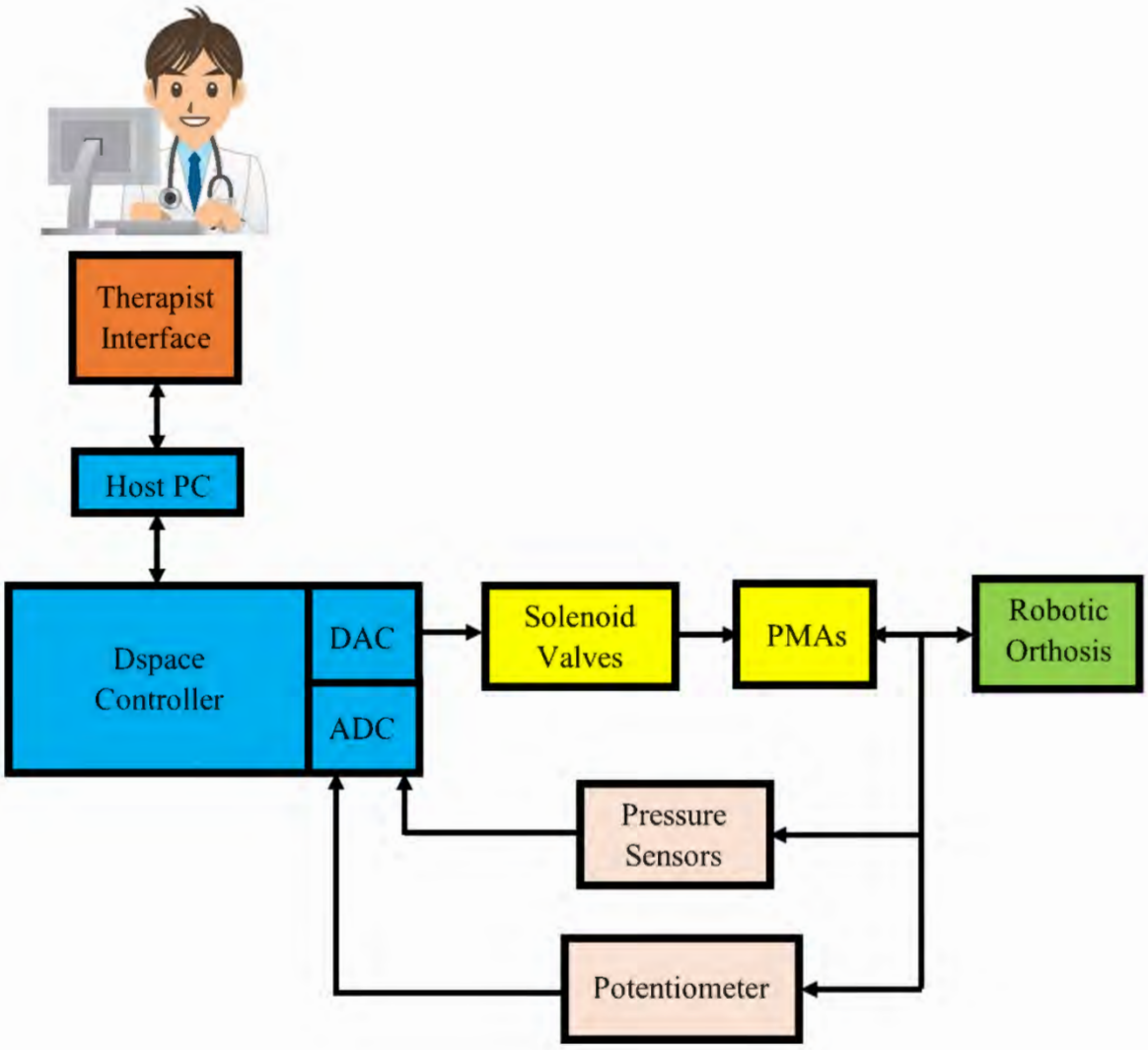

Figure 3–14. Schematic of the Prototype Instruments.

3.9 Safety

Safety is an important factor in designing robotic orthoses for gait rehabilitation. Since the patients who use such robotic orthoses usually have limited mobility due to stroke, it is particularly important to incorporate some protection mechanisms into the robotic orthosis for the safety of users. The robot orthosis developed in this research uses gear-couple as joints, so some concave–convex structures are added onto the sides of the gears to constrain the robot's joint rotation range. The rotation range of the knee joint is set to be -60 to 0 degrees, the hip joint is -60 to 60 degrees, and the ankle joint is -15 to 15 degrees. Such a mechanical structure can prevent the excessive range of motion of the robotic orthosis from causing secondary injury

to the user. In addition, two emergency stop buttons are added to the control system, which both the user and the supervisor can press to stop the movement of the robotic orthosis under any circumstances. After pressing the emergency stop button, all PMAs start exhausting air to allow the robotic orthosis to return to its natural vertical attitude. In addition, since the robotic orthosis developed in this research is for treadmill rehabilitation training, the treadmill used also has two emergency stop switches. One is located next to the treadmill screen, and the user or supervisor can press this button at any time to stop the treadmill. Another safety switch is a bracelet tied to the user's wrist. If the user accidentally falls during rehabilitation training, the line connected to the bracelet is pulled out of the treadmill, and the treadmill stops working immediately.

3.10 Design Capability Analysis

In design capability analysis of robotic orthoses, two key factors need to be specifically assessed. The first factor is the maximum range of motion of the robotic joints. The second factor is the maximum torque that each robotic joint can provide.

By measuring the angles, the maximum ranges of motion of the robotic joints have been recorded during the testing of the orthosis. The range of motion of the hip joint is approximately -15 to 30 degrees, the knee joint is around -60 to 0 degrees, and the ankle joint is about -10 to 20 degrees. This data is also discussed in Section 5.5. The maximum range of motion designed for the knee and ankle joints was successfully achieved, but the range of motion of the hip joint failed to perfectly meet the design requirements proposed in Table 3–2.

After testing the maximum torque each joint can provide, Festo PMAs can provide a peak torque of about 300 Nm at the hip joint and knee joints, and a peak torque of up to 75 Nm at the ankle joint. This is substantially more than the design requirements in Table 3–2.

3.11 Chapter Summary

This chapter presented an intrinsically compliant robotic orthosis for gait rehabilitation capable of performing the major ranges of joint motion, while providing joint alignment with gravity-balancing to patients in the training process.

Self-aligning mechanisms, a partial gravity-balancing mechanism, and lightweight actuators (pneumatic air muscles) are successfully incorporated in the design of the robotic orthosis which makes the proposed robotic orthosis ergonomic to the wearers. Safety mechanisms are added both in the robotic orthosis design and in the control systems to protect patients. The robotic orthosis design capability has been validated. However, the robot design needs to be analysed to establish its feasibility for use in gait rehabilitation. The design analysis, control systems and experimental evaluations with healthy users are discussed in the following chapters.

Chapter 4 – Development and Comparison of various Self-Alignment Mechanisms for Robotic Orthosis

4.1 Introduction

For long, we have been trying to mimic human functions in robots to help us in hazardous, monotonous, and repetitive works. Biological knowledge acquired from the human system is effectively being used and applied to design or develop new machines, equipment, materials, and complicated bionics systems [136, 137]. The essence of bionics lies in the research on biological structure, biological character, principle of biological systems and creatures' behaviour to provide new design concepts, working principles and mechanisms for engineering technologies [137, 138]. Bionics is a young interdisciplinary subject that consists of bioscience, materials, mathematics and mechanics, information science, engineering, and system science [137].

This chapter focuses on the design and development of robot knee joint devising a novel self-aligning mechanism for the gait rehabilitation robotic orthosis by incorporating the concepts from bionics. The designed robotic orthosis prototype should mimic the biological structure of human knee. By the application of mechanical bionics, some advanced prosthetic implants have been developed. In these designs and prototypes, the concept of bionics is also effectively applied [138, 139]. The human knee joint anatomy allows complex movements while carrying the weight of the upper body section. The anatomical structure of the knee joint has the patella bone that meets at the patellar surface of the femur, and the medial and lateral condyles of the femur are opposite to the medial and lateral condyles of the tibia, respectively. The joint capsule of the knee joint is thin and loose. They are attached to the periphery of each joint surface, and ligaments are reinforced around it to increase the stability of the joint. During the flexion and extension of the human knee joint, sliding and rolling (or translation and rotation) occur according to the shape of the bones and ligaments, where the sliding motion is not negligible.

The need to prevent robotic orthosis from aligning with human joint alignment is an important practical problem for the comfort and usability of rehabilitation robots. Robotic orthoses normally have simple revolute joints, while human joints have translating axes of rotation. As such the two, robot and human joints, cannot remain aligned during motions. The knee joint, however, is assumed to be a fixed single rotation joint mechanism by many existing robotic orthoses. As a result of this simplification of the joint mechanism, it is inevitable that the joints of the robotic orthosis and the joints of the person wearing it will be distorted. Misalignment of the robotic orthosis joints and the wearer's joints can reduce the power transmission efficiency of the robot actuators, while also causing discomfort to the wearer as the rehabilitation robot hinders their movement [48]. This axis misalignment also induces compensatory movements that will not only impede recovery but will also cause discomfort to the subjects due to undesired residual forces. Such misalignment may also be caused by the compression of soft tissues interacting physically with the robot or due to the use of flexible braces while fixing robots on the subjects' limbs. Thus, achieving self-aligning for rehabilitation robots becomes a challenging and active area of research in the field of rehabilitation robotics.

Subsequently, researchers have proposed novel self-aligning mechanisms that can be used in robots. Analytically, it has been shown that the use of a self-aligning or allying mechanism may reduce the residual forces and torques substantially [36-38]. Lately, robots employing a self-aligning mechanism have been designed and proposed for lower limb rehabilitation [39-42] as well as for robot-assisted rehabilitation of the human upper limbs [43-45]. Nevertheless, most of the self-aligning mechanisms for lower and upper limb robots are either too complex to be practically used or they still produce residual or uncompensated forces/torques.

Assumptions that these allying mechanisms are massless, frictionless, and infinitely stiff do not practically hold during implementations. The finite mass of these allying mechanisms

induces unpredictable forces and torques, which adversely affect their intended objectives. The presence of friction in the mechanisms may prevent them from aligning dynamically in real-time. Compliance in the linkages of the allying mechanisms may also induce passive movements that may give rise to uncertain kinematic behaviour. Therefore, it is challenging to design and develop an allying mechanism that has low mass and frictions and is sufficiently robust to transfer motions without altering them.

Apart from the above attributes, a good allying mechanism will also have a good decoupling approach, which allows large residual forces to be transferred to the exoskeletal system [36, 46-48]. Decoupling of joint rotations and translations also plays an important role in achieving the self-alignment of robotic orthoses. An allying mechanism with a provision for decoupling can reduce the interaction stiffness between the robot and the human lower limbs.

Subsequent to further analysis of mechanisms, it was found that a robot knee joint can be designed mimicking human knee joint in three different ways, such as, using gear couple, through a cam couple or by designing appropriate four bar linkage. Therefore, following the above-mentioned three ways, three different mechanisms have been designed and analysed in this proposed research. In this Chapter, conceptualization and development of these three mechanisms are discussed in order to provide the self-alignment between robotic orthosis knee joint and human knee joint. The design, performance evaluation and comparison of these three mechanisms is also discussed in detailed.

4.2 Estimation of Knee Rotation and Displacement

Knee movement is a result of combined displacements due to the angular and linear motions between the tibia and femur bones. The rotation of the femur in the sagittal plane can be explained by sliding and rolling. While sliding is the rotation without displacement of the centre of rotation of the femoral curvature, rolling is the rotation with simultaneous displacement of

the centre of rotation which is further dependent on the radius of curvature of the femoral surface. The sliding and rolling components of the distance, between femoral point (PF) and tibial point (PT), are presented by D_{FTS} and D_{FTR} here and can be mathematically expressed as follows:

Displacement due to pure sliding (D_{FTS}) is given by:

$$d_{fts} = R \times \tan \alpha \tag{4.1}$$

Similarly, displacement due to pure rolling motion of tibia on femur (D_FTS) is given by:

$$d_{ftr} = R \times \tan \beta - R \times \beta \tag{4.2}$$

Here, R is the radius of curvature (roc) of the femoral condyles, α and β are the angular displacements during sliding and rolling of tibia on femoral condyles. The total angular displacement at knee ($\theta; 0 \leq \theta \leq 55^0$) can be taken as sum of α and β, i.e., $\theta = \alpha + \beta$. The relations mentioned above (4.1 & 4.2) can help in estimating the overall linear shift between tibia and femur during a gait cycle.

Total displacement can be expressed as:

$$d_{ft} = k_1 d_{fts} + k_2 d_{ftr} \tag{4.3}$$

Here, $k_1 \& k_2$ ($0 \leq k_1, k_2 \leq 1$) are the contributions of the two displacements ($d_{fts} \& d_{ftr}$) and vary between 0 and 1. It is important to note here that the sliding and rolling between tibia and femur bones occur simultaneously during gait motion and, therefore, their individual values (4.1 & 4.2) cannot be separated. In fact, during the gait motion, contributions from the two displacements keep changing and therefore the overall displacement at certain point of time in gait can be expressed with (4.3). Further, carrying out a numerical analysis with the anatomical data of human knee, it was found that the total displacement between the tibia and the femur bones during gait motion can be 0 to 6 mm.

Hand Calculations:

Considering the ROC for the medial femoral condyle as 17 mm and α and β approximated as 20^0 each, the two displacement values can be calculated as shown below:

$d_{fts} = 17 \times \tan 20^0 = 6.18\, mm$; and

$d_{ftr} = 17 \times \tan 20^0 - 17 \times \left(20^0 * \frac{\pi}{180^0}\right) = 0.25\, mm$;

Further assuming equal contributions of the sliding and the rolling motions (i.e., $k_1 = k_2 = 0.5$), the total displacement shall be $3.22\, mm$ $(d_{ft} = 0.5d_{fts} + 0.5d_{ftr} = 3.22\, mm)$. On the other hand, the maximum displacement (when $k_1 = 1;\ k_2 = 0$), from the above data, can be $d_{ft} = d_{fts} + 0 \times d_{ftr} = 6.18\, mm$.

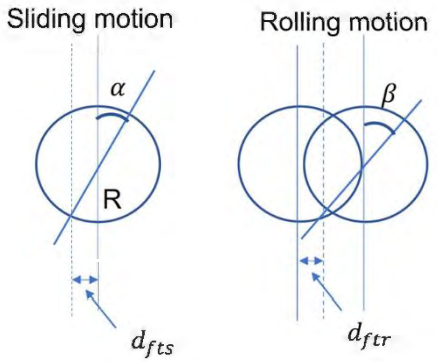

Figure 4–1. Movement of the Femur on Tibia Plateau Inside the Knee Joint.

4.3 Gear Couple Mechanism

The first design developed for providing the self-alignment between human knee joint and the robotic orthosis knee joint uses the concept of spur gear meshing. In this design (Figure 4–2), the knee joint is formed with two meshing gears of the same pitch, a non-moving gear (thigh gear attached to the femur part of the robotic orthosis) at the top and a movable gear (shank gear attached to the tibia part of the robotic orthosis). The two meshing gears together act as the robot knee joint. The non-moving gear (thigh gear) is fixed at the end of the thigh segment, whereas the other meshing gear (shank gear) is connected with the shank of the robot and can rotate. The gear ratio of G1 and G2 is 2, which means the number of teeth on G1 is twice the

number of teeth on G2. Thus, the G2 will rotate 60 degrees, when there is only 30 degrees actuating rotation applied on this mechanism.

The two actuating ends of the PMAs (which are used to actuate the knee joint) and the axis of shank gear are rigidly connected by long fasteners at three points on a cover plate. This cover plate forms a 'T-section' such that during the antagonistic actuation of the PMAs, an anticlockwise moment from the PMAs rotates the shank gear over thigh gear anticlockwise from 0 to 60 degrees (Figure 3–8). Amplification in the angular displacement at knee joint is achieved with the use of the gear couple as shown in Figure 3–8. The top meshing gear (thigh gear) also has a lock that prevents shank gear to rotate in the clockwise direction and, therefore, the knee joint can only have flexion motion and cannot extend. The idea of using gear couples instead of traditional bushing and bearing mechanism is generated from the concept of bionics.

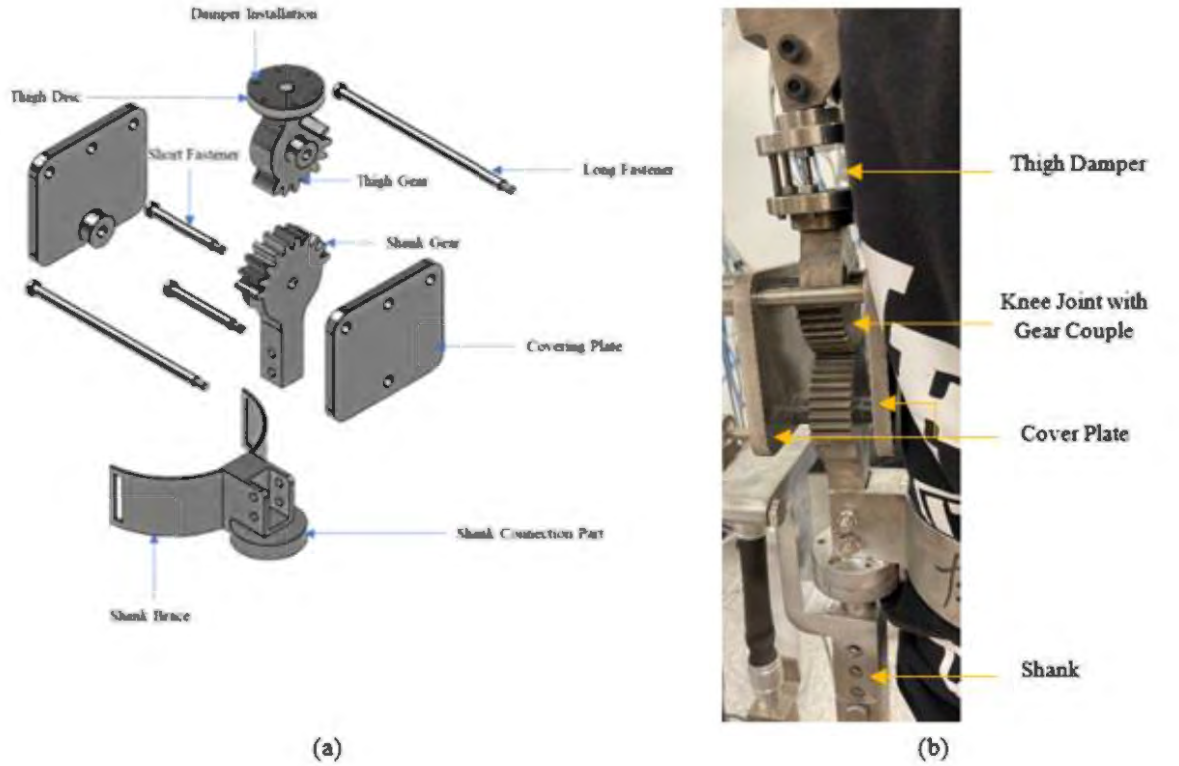

Figure 4–2. (a) CAD design of robot Knee Joint with Gear Couple Mechanism. (b) Prototype of knee joint with Gear Couple Mechanism.

The two angular displacements, one from the 'T' shaped link and the other from the gear mounted on this link gets added up such that, $\theta_{resultant} = \theta_{T-link} + \theta_{gear}$.

The coupled spur gears resembled the combination of femoral condyle and tibial plateau. The module coefficient was selected to be 3.5 with 36 teeth on one gear, which is sufficient to withstand the forces that will act on each individual tooth during motion. Also, a pressure angle of 20 degrees and face width of 56.75 mm significantly decrease the amount of stress applied per unit area.

The gear combination could provide the required knee rotation and further using different ROCs for the two mating surfaces of the two spur gears, it is possible to obtain the required displacement of the centre of rotation of the knee joint. Such an analysis is discussed in the next Section.

4.4 Toothed Cam Couple Mechanism

To have a bio-inspired design for the gait rehabilitation robot, toothed cam couple mechanism may better simulate real human knee joint structure than gear couple mechanism. Cam is a mechanical linkage used for precisely transmitting motion from protruding part of a wheel to a roller which is moving close to its edge [140, 141]. According to the research from prosthetics, for instance, human knee joint consists of femur, patella, and tibia. Shapes of femur and tibia are irregular, and tibia rotates by following the edge of femur when knee joint is in flexion/extension motion [142, 143]. Thus, it is a novel idea to use a double-cam mechanism in the design of a robotic orthosis knee joint, which is almost the same as the human anatomy to reduce misalignment between robotic orthosis and anatomical knee joint.

Using toothed double-cam mechanism for the design of robotic orthosis knee joint, may help in achieving better self-alignment. As shown in Figures 34 and 35, when the shank cam rotates around the thigh cam by the application of forces generated by PMAs, the joint rotation of robtic

orthosis can almost simulate the extension/flexion of human knee anatomy. Two T-shape components are used for installing actuators and covering the gear teeth to avoid unnecessary damage to underlying human body. On T-shape components, movable design features and spacing is used for installing springs, which help to automatically match the changing distance between two centres of cams during rotation. Furthermore, springs used on the T-shape movable part can be modelled as cartilage on the anatomical joint. Cartilage is a flexible connective tissue. In human anatomy, there is layer of cartilage at the end of each bone to prevent friction and impact between bones [144-146]. Articular cartilage can distribute the force evenly and enlarge load-bearing surface. In this way, the joint can bear larger mechanical load by taking less damage. Articular cartilage is very smooth, so the joint motion can be less damaged and flexible by reducing internal friction between human bones [144-146]. Six small holes on bottom disc of thigh cam are used for installing dampers on the designed prototype. Gear teeth on cams are designed to help in the joint rotation, and the rotation process is almost the same as gear couple mechanism. As the cam curve is designed by using the example of

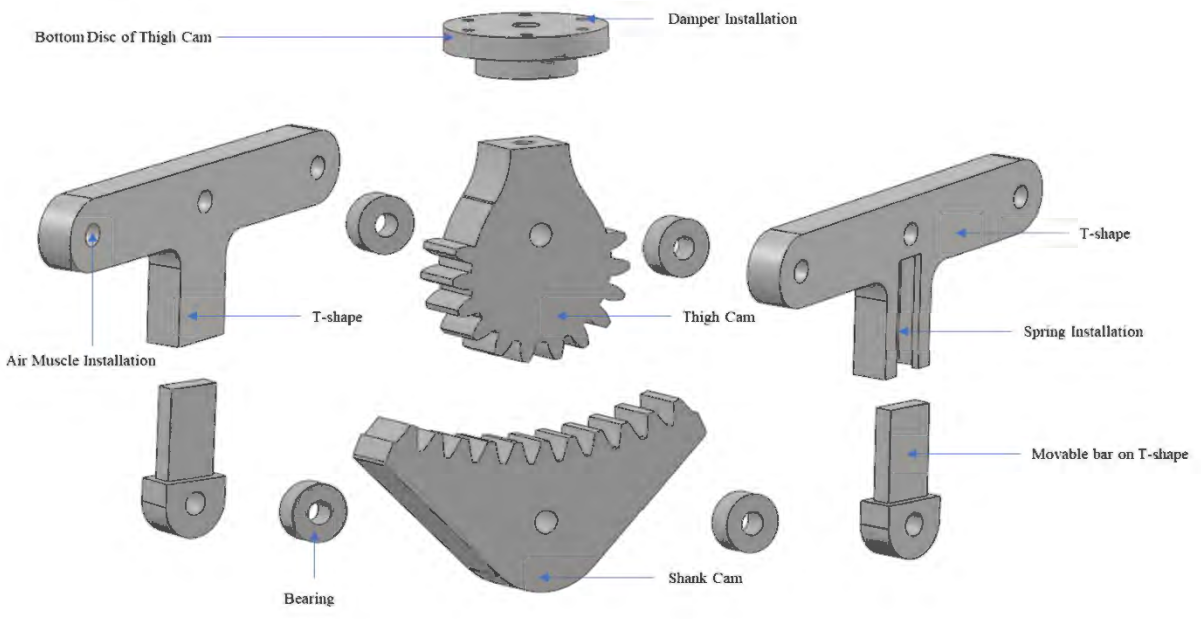

Figure 4–3. CAD design of the robot knee joint with toothed Cam Couple Mechanism.

human anatomy (shown in Figure 4–4), the alignment of robotic orthosis knee joint can be automatically achieved by free rotation of couple of cams (with gear teeth).

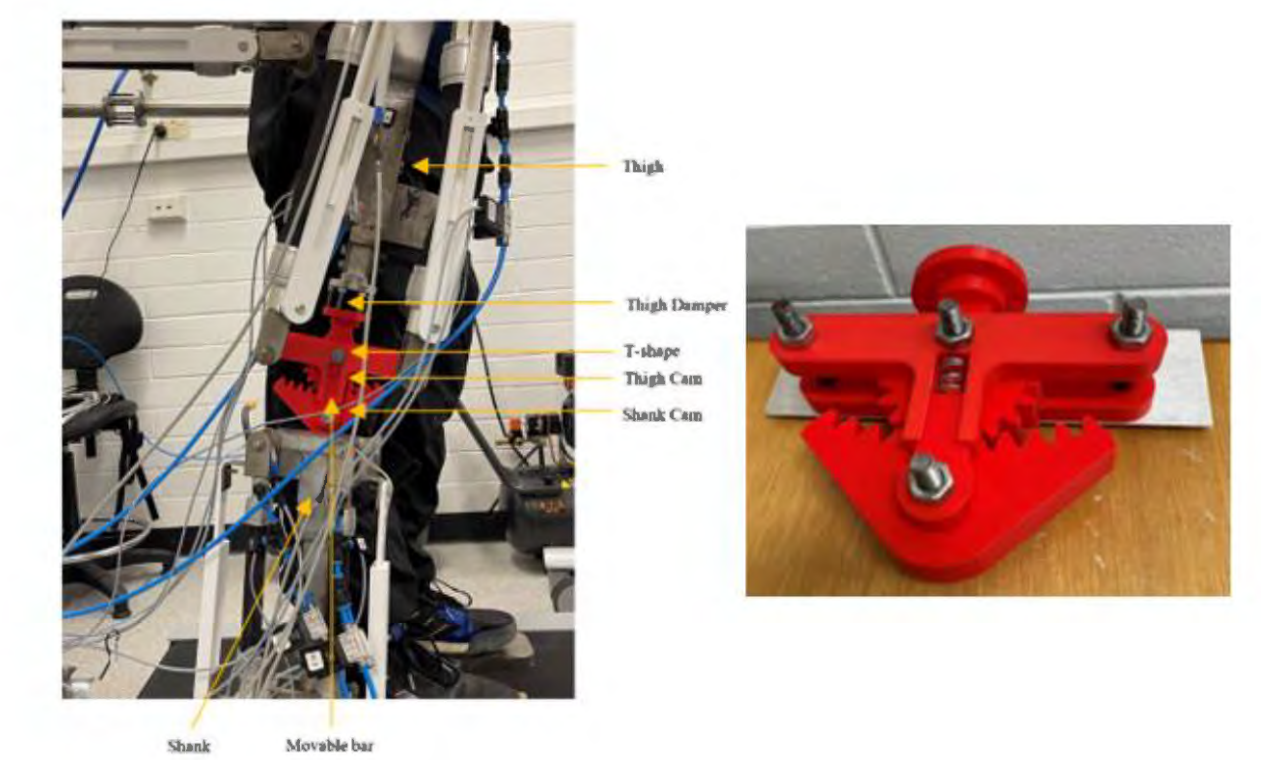

Figure 4–4. (a) Prototype of knee joint with Cam Couple Mechanism (b) Cam Couple Joint.

The curvature profile of the contacting surfaces of the two cam couple constituents causes a translation motion along with the rotational motion. Further, the rotations of the femur and tibial parts are different and are related to the number of teeth on their surfaces or by the factor of the gear ratio, which is $\frac{N_2}{N_1}$. In the proposed design, N_1 (number of teeth on the tibial part) was kept as 11 and N_2 (number of teeth on the femoral part) was chosen to be 14. Therefore, the gear ratio obtained with such configuration was 1.28. Considering the limits for the rotation of a knee joint, there will be certain constraints for the angles of rotation (θ_1 at femoral part and θ_2 at tibial part) as shown in (4–4 & 4–5):

$$0 \leq \theta_1 \leq 47.2^0 \tag{4.4}$$

$$0 \leq \theta_1 \leq 60^0 \tag{4.5}$$

Due to the difference between the curvatures of the mating surfaces, besides rotation, a small amount of translation (dependent on θ_1) will also occur in the sagittal plane between the femoral and the tibial parts. This displacement can be accounted as shown in Figure 4–5. In the line sketch for the robot knee joint, the central distance between the two curvatures is 70 mm and the travel to one of the extremes is 40 mm.

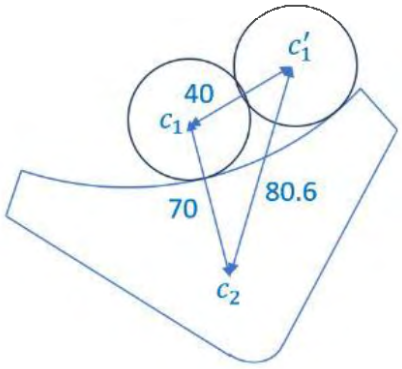

Figure 4–5. Line Sketch to show the Linear Displacement in the Robot Knee Joint (dimensions in mm).

Approximating the triangle $c_1c_2c_1'$ as right-angle triangle, we know that:

$$c_2c_1' = ((c_1c_2)^2 + (c_1c_1')^2)^{0.5} \tag{4.6}$$

This further means that the distance between the centres of the two curvatures changes from $c_1c_2 = 70\ mm$ to $c_2c_1' = 80.6\ mm$. Subsequently, the linear displacement that can be achieved with this special robot knee joint is approximately 10 mm. The requirements as discussed in Section 2 for the linear displacement is 0-6 mm and therefore this robot knee satisfies the requirement completely. The knee join is further shown with its parts and consequent trajectory in Figure 4–6.

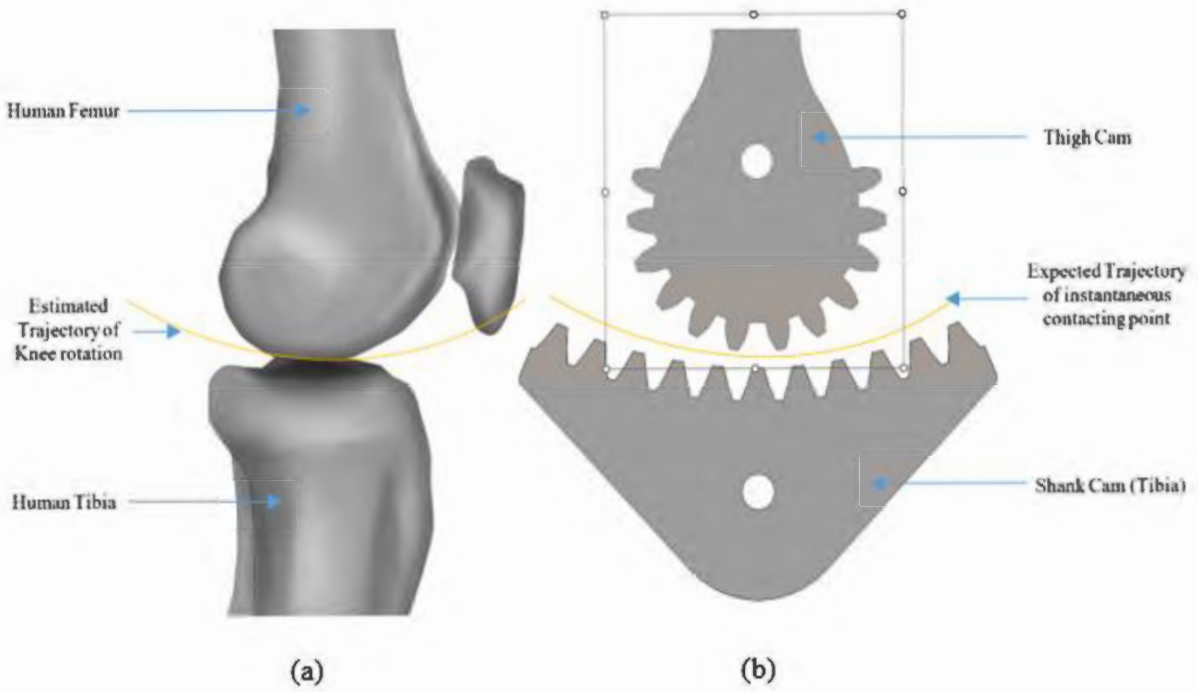

Figure 4– 6. (a) Human Knee Rotation Trajectory. (b) Designed Cam Mechanism Trajectory.

4.5 Four-Bar Linkage Mechanism

Another method to design a self-aligning knee joint mechanism is by using four-bar linkage. The plane link mechanism is a common transmission mechanism, and its most basic and widely used type is a planar four-bar mechanism. Four-bar linkage mechanisms are easy to manufacture and use in the design of robotic systems [147].

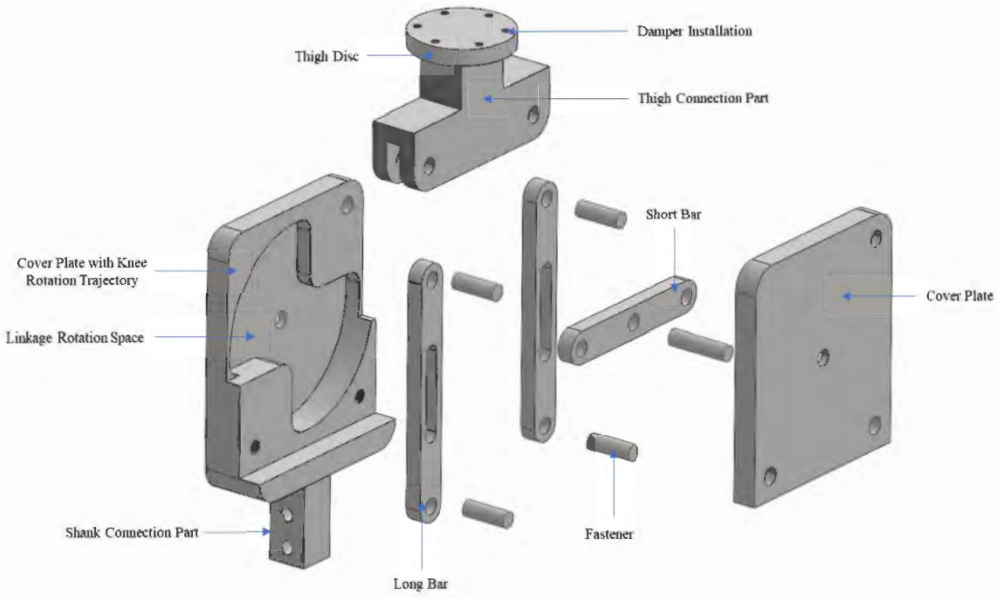

Figure 4–7. CAD design of robot Knee Joint with Four Bar Linkage Mechanism.

The line sketch for the assembly of the robot joint based on four linkages is shown in Figure 4–8. While the linear displacement or the travel obtain at the knee joint using four bar linkages was sufficient, the joint is not strong and durable due to the use of small parts as linkages.

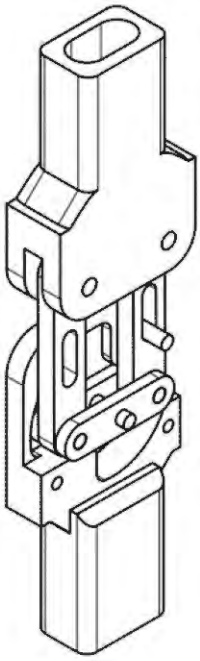

Figure 4–8. Line Sketch of Robot Knee Joint with Four-Bar Linkage Mechanism.

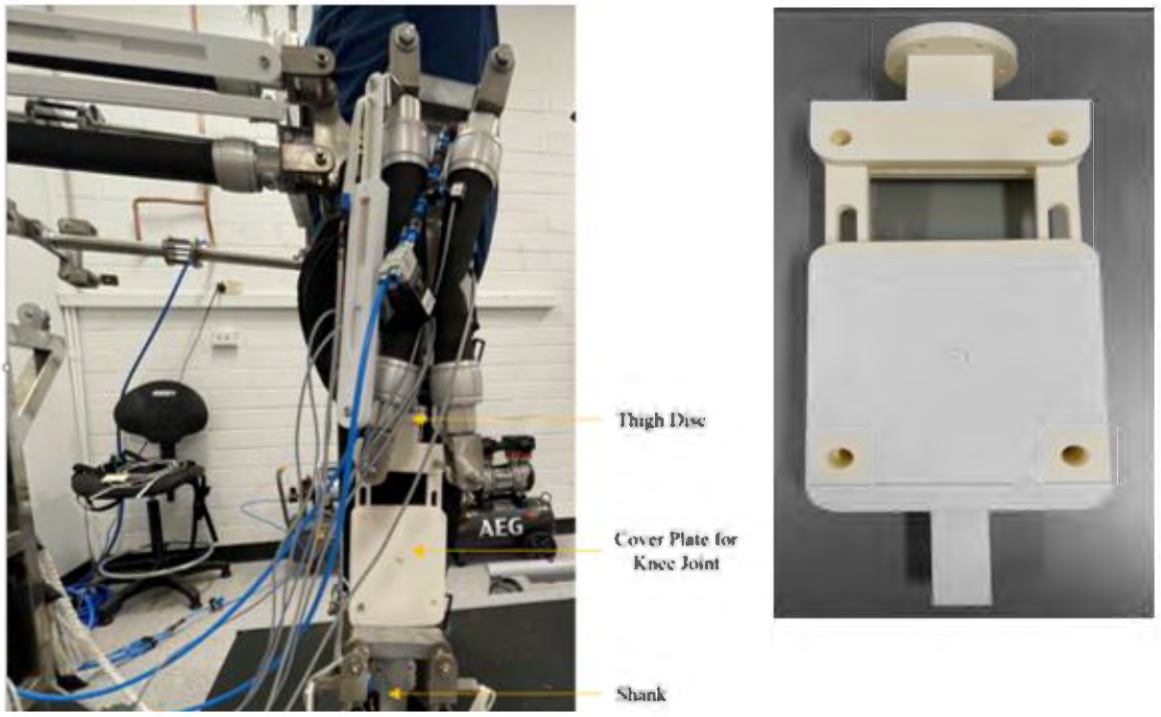

Figure 4–9. Prototype of Knee Joint with Four-Bar Linkage Mechanism.

4.6 Performance Evaluation and Comparison of the Three Mechanisms

4.6.1 Simulation-based Evaluation and Comparison

Figures 4–10, 4–11 and 4–12 show the robotic orthosis knee joint with double-gear mechanism, double-cam mechanism, and four-bar linkage mechanism, respectively. The instantaneous contacting points for double-gear mechanism and double-cam mechanism are located at the contact point when the robotic orthosis is completely in the vertical position. In the four-bar linkage mechanism design, there is no instantaneous contacting point to represent robotic knee joint. Instead, there is a working space (Figure 4–12) in this four-bar linkage mechanism to ensure that robotic knee joint will rotate by following designed trajectory, which helps in achieving self-alignment. The blue crosses in Figures 4–10, 4–11 and 4–12 represent the human anatomical joint position when rotated to 0^o, 30^o, 60^o, and 90^o. Red crosses represent the robotic orthosis knee joint position when it rotates. For most of the previously designed robotic orthosis without any self-aligning mechanism, the red crosses almost lie on the line of the tibia edge, which means the misalignment is too large to be acceptable.

In Figure 4–10, the first design of knee joint with double-gear system is analysed. The results show that the red crosses are close to blue crosses at beginning of the knee rotation, but the misalignment becomes larger when rotation degrees become larger. So, the effective range of motion in which the self-alignment can be achieved is limited.

Double-cam mechanism can easily solve the problem of limited self-alignment range of gear-couple mechanism. Figure 4–11 clearly shows that red crosses are much closer to blue crosses. It still has some misalignment when it rotates to 90^o, however, the knee joint usually does not rotate to 90^o during the normal gait. So, those misalignment beyond 60^o rotation can be ignored.

Figure 4–12 shows the effectiveness of self-alignment between anatomical knee joint and robotic orthosis knee joint by using four-bar linkage mechanism. The red crosses are close to blue crosses during the first 30 degrees of rotation. Then, the four-bar linkage provides a significant vertical translation, which compensates larger misalignment than both gear-couple mechanism and cam-couple mechanism.

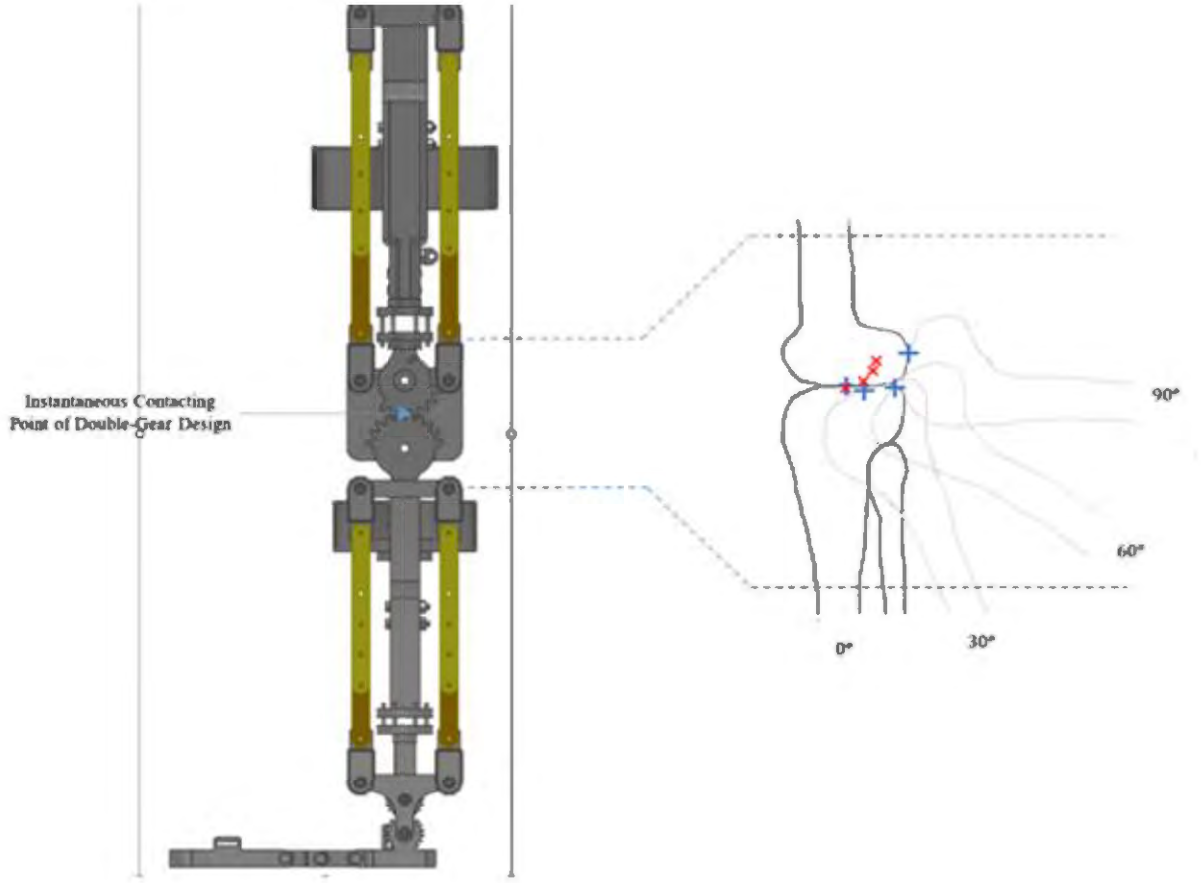

Figure 4–10. Instantaneous Contacting Point Trajectory of Gear Couple Mechanism.

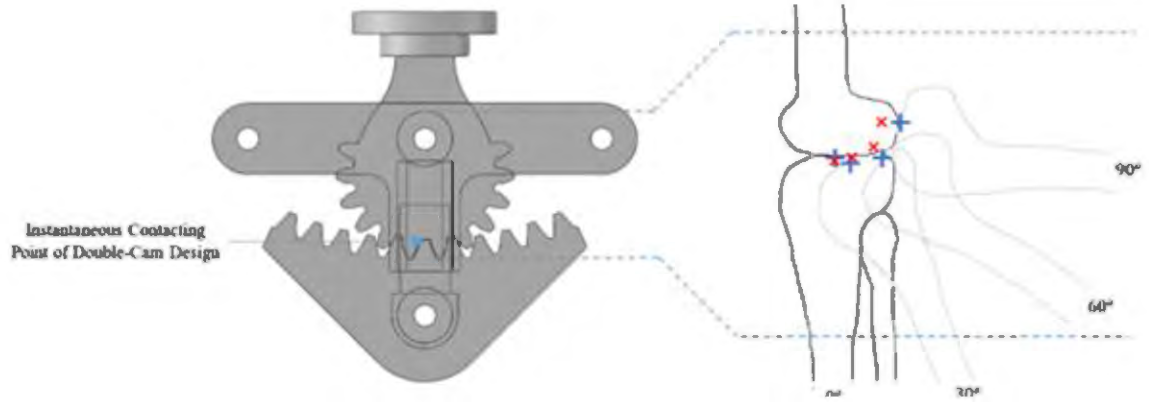

Figure 4–11. Instantaneous Contacting Point Trajectory of Cam Couple Mechanism.

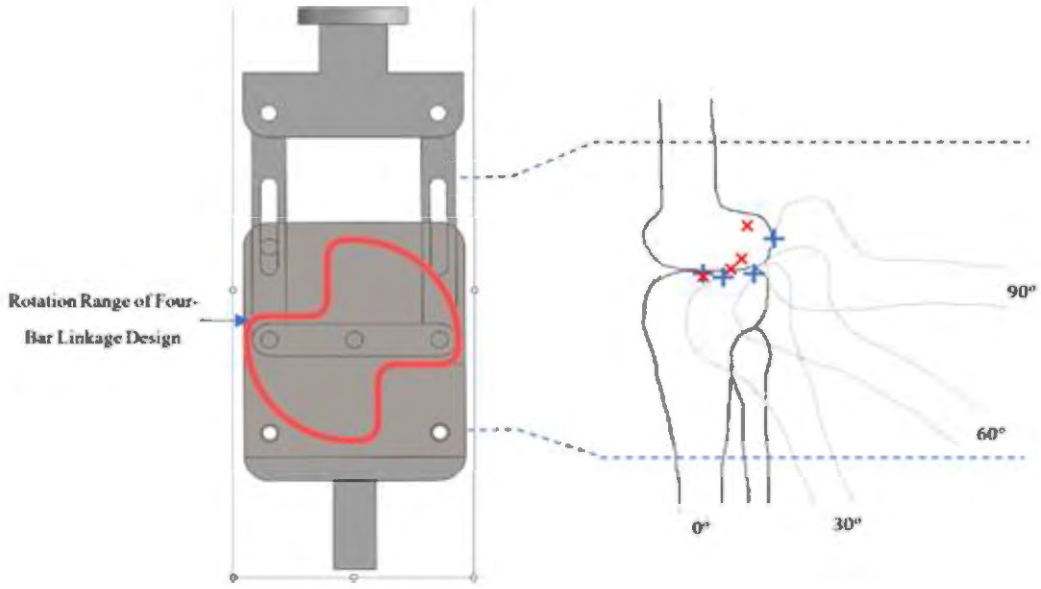

Figure 4–12. Range of motion of Four Bar Linkage Mechanism.

4.6.2 Motion Capture System-based Evaluation and Comparison

Motion capture is an advanced technology that can accurately measure and record all kinds of trajectories and the posture of moving human and objects in real time three-dimensional space. The associated computational technology can reconstruct the state of motion of the human and objects at every time instance in virtual three-dimensional space [148-151]. Motion capture technology can be divided into several categories include optical, inertial, mechanical, acoustic, and electromagnetic [148-151]. In this research, optical motion capture technology was used to acquire the position information of marked points on three different knee joint mechanisms to analyse the effectiveness and accuracy of self-aligning. A high-speed motion capture camera system was used during this work. Figure 4–13 (a) shows the example of using marker-based motion capture to record the position of instantaneous contacting point for the gear couple and cam couple mechanism and the range of motion in the four bar mechanisms. In Figure 4–13 (a), the prototype is using a gear couple as knee joint mechanism. The instantaneous contacting point of two gears was chosen as the marked point to be analysed. When the prototype is actuated, a video is recorded, and the marked point position information

was collected to produce a trajectory of the knee joint. The yellow crosses in the Figure 4–13 (a) are giving an example of the change in position information of instantaneous contacting point of gear couple mechanism. For a cam couple mechanism, the marked point is also chosen to be the instantaneous contacting point of two cams. Moreover, the marked point is chosen as intersection point of two diagonals on the cover plate of a four-bar linkage mechanism.

Figure 4–13 (b) shows the results obtained from the motion capture system for three knee joint mechanisms. The red crosses in the Figure 4–13 (b) represent the human anatomy joint position when it was rotated from 0^o to 90^o. Yellow crosses represent the gear couple knee joint position when it rotates. Blue crosses represent the cam couple knee joint position when it rotates. Green crosses represent the four- bar linkage knee joint position when it rotates. All three mechanisms were also rotated from 0^o to 90^o. For most of the robotic orthosis knee joints designed without any self-aligning mechanism, the marked points almost lie on the line of tibia edge, which means the misalignment of them is too large to be acceptable.

Yellow crosses show that the knee joint trajectory of double-gear mechanism is far away from the usual human anatomy joint position. It shows that the yellow crosses close to red crosses at beginning, but the misalignment becomes larger when the angle increases. A double-cam mechanism can better solve this problem. Figure 4–13 (b) clearly shows that blue crosses are much closer to red crosses. It still has some misalignment when it rotates to 90^o, however, the knee joint will not rotate so much in the normal gait. So, those misalignment after 60^o can be ignored. This data agrees with the modelling results discussed above. However, to achieve self-aligning, the vertical translations should be also considered. A cam couple mechanism can achieve the vertical translations as required for the robot to be aligned with the human anatomical knee joint. Green crosses represent the knee joint mechanism of the four-bar linkage (Figure 4–13 (b)). The motion capture results show that the four-bar linkage mechanism has

better vertical translations as compared to the cam couple mechanism, but its motion trajectory is further from the anatomical knee joint trajectory than cam couple mechanism trajectory.

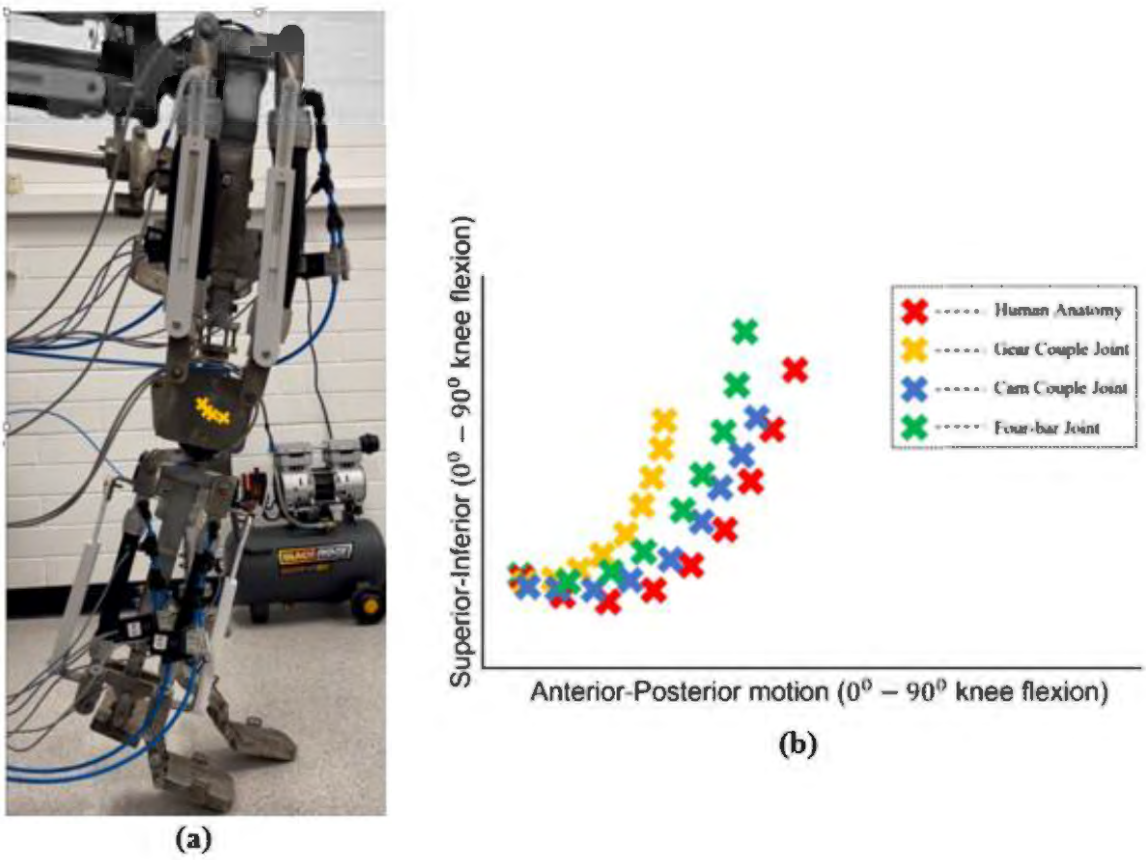

Figure 4–13. (a) Motion capture system. (b) Change of position of the robotic knee joint for three mechanisms obtained by using motion capture system.

4.7 Chapter Summary

In this chapter, self-aligning mechanisms for the alignment of a robotic orthosis knee joint with the anatomical knee joint has been conceptualised and developed. Three different types of self-aligning mechanisms have been developed along with their mathematical models. These mechanisms have been conceptualized based on the biomechanical function of the knee joint. The performance of these three mechanisms has been compared based on the instantaneous contacting point for the gear couple mechanism and cam couple mechanism as well as on the basis of range of motion of the four-bar linkage mechanism. Experimental evaluation and performance comparison of these three mechanisms has also been conducted by using a motion capture system. It was observed that the linear displacement or the travel obtain at the knee joint

using four-bar linkages was sufficient, however, the joint is not strong and durable due to the use of small parts as linkages. Therefore, it was decided to design the knee joint using the two coupled spur gears for greater strength. However, in order to obtain the required linear displacement, it was decided to make the gears of different curvatures as per equations 4.4 to 4.6.

Chapter 5 – Design Analysis

This chapter presents the forward kinematics, inverse kinematics and dynamics for the robotic gait rehabilitation orthosis introduced in Chapter 3.

5.1 Introduction

Kinematics is a branch of mechanics, which describes, and studies changes in an object's position over time. Kinematics is based on the study of the motion of two simplified models of particles and a rigid body, and further studies the motion of deformable bodies. It mainly studies the characteristics of a point such as the equation of motion, trajectory, displacement, velocity and acceleration. Geometry is usually used in kinematics. Kinematics usually does not consider the influence of factors such as force and mass. Descriptions of any movement in kinematics are relative only. Kinematics involves forward kinematics (FK) and inverse kinematics (IK). In robotic analysis, forward kinematics is used to find the position and attitude of the end point effector in the reference coordinate system when the angle of each joint and the parameter of each link are all known. Inverse kinematics is the process to find the corresponding values of joints and links when the position and attitude of the end point effector are known.

Dynamics is fundamental to physics and astronomy, as well as to many engineering disciplines. Advances in mathematics are often associated with solving problems in dynamics. Dynamics mainly studies the relationship between the force acting on an object and the motion of the same object. This research object is a macroscopic object whose motion speed is much smaller than the speed of light. Dynamics can help calculate the force acting on the object if the motion of the object is known, as well as acquire the motion of an object when all forces acting on the object are known.

5.2 Robot Kinematic Analysis

The gait robot discussed here is an open chain mechanism or a serial robot consisting of three closed chains in sequence for hip, knee, and ankle joints. The schematic of the robot is shown with line sketch in Figure 5–1, where various joints are positioned with reference to a global coordinate system (GCS) attached with the robot pelvis joint at 'O'. Here L_1 is referred to as the vertical distance of the left hip joint from GCS in the design, while L_2 represents the horizontal offset between the hip and the pelvis. Length of the thigh segment is L_3 (distance between hip and knee joints) and L_4 is the shank length (distance between knee and ankle joints). S_1 and S_2, respectively, denote the active and the passive rotational DOF at the hip joint while there is a small passive translation (d_3) allowed along S_3 due to the use of damper springs.

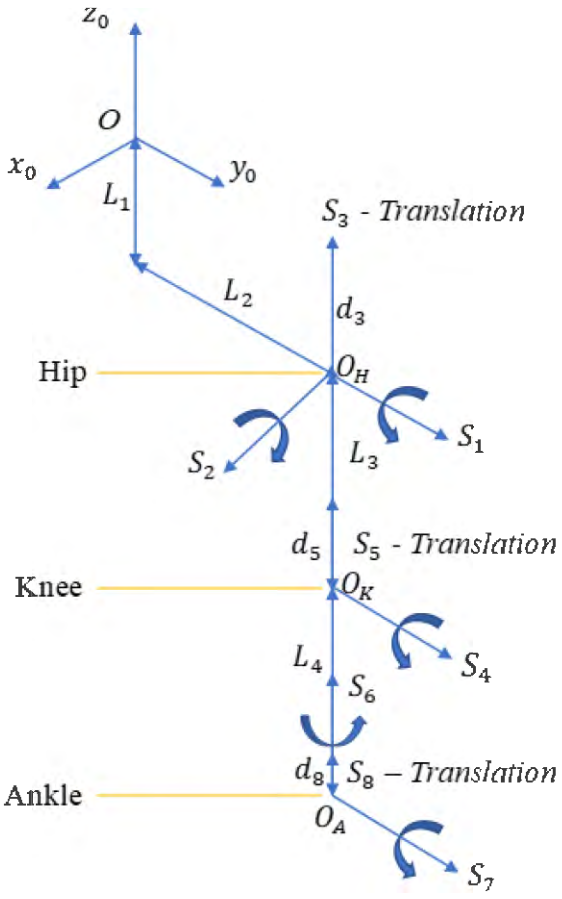

Figure 5–1. Schematic Drawing of Designed Prototype for Analysis.

.

At the knee joint, the gait robot has an active rotational dof shown by S_4 and a small passive translation (d_5) dof along S_5, which comes from the dampers. Further, at the robot ankle joint, the robot has an active rotational dof(S_7) and a small passive rotation (S_6). There is also a small passive translation (d_8) allowed along S_3 due to the damper springs (Figures 3–6 and 5–1). Therefore, the proposed gait robot design has eight dof out of which three are active and the rest five are passive ones.

Screw theory is used in this research to derive and analyze kinematics of the entire mechanism in place of DH parameters and Euler angles. It simplifies the forward kinematics and doesn't require link lengths, twists, link offsets etc. Table 5–1 shows the directions and the positions of the eight dof on the gait robot and these parameters are further used in the current positional analysis and to obtain transformation matrices. For eight dof, there are equal number of transformations, which are normally presented by homogenous transformation matrices.

Table 5–1. Parameters for Position Analysis.

DOF i	S_i $S_x\ S_y\ S_z$	S_{oi} $S_{ox}\ S_{oy}\ S_{oz}$
1	0, 1, 0	$0, L_2, -L_1$
2	1, 0, 0	$0, L_2, -L_1$
3	0, 0, 1	$0, L_2, -L_1$
4	0, 1, 0	$0, L_2, -L_1 - L_3$
5	0, 0, 1	$0, L_2, -L_1 - L_3$
6	0, 0, 1	$0, L_2, -L_1 - L_3 - L_4$
7	0, 1, 0	$0, L_2, -L_1 - L_3 - L_4$
8	0, 0, 1	$0, L_2, -L_1 - L_3 - L_4$

Table 5–2. Element of the Generalised Homogeneous Transformation Matrix.

a_{11}	$(s_x^2 - 1)(1 - C\theta) + 1$
a_{12}	$s_x s_y(1 - C\theta) - s_z\, S\theta$
a_{13}	$s_x s_z(1 - C\theta) + s_y\, S\theta$
a_{14}	$ts_x - s_{ox}(a_{11} - 1) - s_{oy}a_{12} - s_{oz}a_{13}$
a_{21}	$s_y s_x(1 - C\theta) + s_z\, S\theta$
a_{22}	$\left(s_y^2 - 1\right)(1 - C\theta) + 1$
a_{23}	$s_y s_z(1 - C\theta) - s_x\, S\theta$
a_{24}	$ts_y - s_{ox}a_{21} - s_{oy}(a_{22} - 1) - s_{oz}a_{23}$
a_{31}	$s_z s_x(1 - C\theta) - s_y\, S\theta$
a_{32}	$s_z s_y(1 - C\theta) + s_x\, S\theta$
a_{33}	$(s_z^2 - 1)(1 - C\theta) + 1$
a_{34}	$ts_z - s_{ox}a_{31} - s_{oy}a_{32} - s_{oz}(a_{33} - 1)$

Elements of the individual transformation matrices for eight DOFs (Appendix A) can be obtained using Tables 5–1 and 5–2 using the generalised homogeneous transformation matrix (5.1):

$$A = \begin{bmatrix} a_{11} & a_{12} & a_{13} & a_{14} \\ a_{21} & a_{22} & a_{23} & a_{24} \\ a_{31} & a_{32} & a_{33} & a_{34} \\ 0 & 0 & 0 & 1 \end{bmatrix} \tag{5.1}$$

Transformation matrices are important to carry out the kinematic analysis, which is of two types: forward kinematics (FK) and inverse kinematics (IK). To achieve the desired position/velocity of a joint, it is required to know its current positional/velocity from the known position/velocity of the preceding joints. Obtaining the position/velocity of a successive joint $(q_s, \dot{q}_s)$ of an open chain in space using known position/velocity of all preceding joints $\left[(q_p, \dot{q}_p)_{i-1} \cdots (q_p, \dot{q}_p)_1\right]$ is termed forward kinematics (5.2). Later, to move successive joints to different position/velocity in space, it is required to figure out the required position/velocity of all the preceding joints from the known position/velocity of the successive joints and this is done using the inverse kinematic analysis (5.3). If $(q_s, \dot{q}_s)_i$ are the position and velocity of i^{th} successive joint and $\left[(q_p, \dot{q}_p)_{i-1} \cdots (q_p, \dot{q}_p)_1\right]$ are the positions and velocities of all the preceding joints, the forward kinematics and the inverse kinematics can be expressed mathematically as (4.2 & 4.3):

$$(q_s, \dot{q}_s)_i = FK\left[\left(q_p, \dot{q}_p\right)_{i-1} \cdots \left(q_p, \dot{q}_p\right)_1\right] \tag{5.2}$$

$$\left[\left(q_p, \dot{q}_p\right)_{i-1} \cdots \left(q_p, \dot{q}_p\right)_1\right] = IK(q_s, \dot{q}_s)_i \tag{5.3}$$

5.2.1 Forward Kinematics

For an open chain mechanism, forward kinematics always provides closed-form solutions since this is an injective function. In the present case, the overall mechanism has eight DOFs and, therefore, the homogeneous transformation matrix used to perform forward kinematic analysis is given by (5.4).

$$T_8^1 = \prod_{i=1}^{8} [A_i] \tag{5.4}$$

Homogeneous transformation matrices for individual dof is provided in the Appendix A for reference whereas the elements of the homogeneous transformation matrices (5.2) are listed in Table 5–1 in terms of their corresponding angular displacements. The fourth-row elements of (5.2) are taken as $a_{41-44} = (0,0,0,1)$ since the motions are transformed without scaling.

5.2.2 Inverse Kinematics

Inverse kinematics (IK) is performed to find the positions of the preceding joints for the given positions of the succeeding joints and the related link lengths. The required link lengths and the orientations of the preceding joints is required to design an effective controller. Unfortunately, the inverse kinematics analysis of an open chain mechanism does not provide a closed form solution using the conventional approach [152]. In fact, the inverse kinematics analysis provides more than one solution and to obtain an accurate singular solution, analytical and iterative methods are normally employed [153].

However, since the forward and inverse kinematics modules are normally part of the robot closed loop feedback controller, these are executed at higher frequencies. Therefore, apart from accuracy, it is imperative for the forward and inverse kinematics calculations to be computationally efficient. A machine learning based model can be developed to obtain solutions of the inverse kinematics of the gait robot quickly and precisely. To develop such a model, a database is normally required for training and testing the model and obtaining optimal model parameters. Solutions from the forward kinematic analysis (5.2) can be used for this purpose.

During the thesis research, a database was first created by solving the forward kinematics (5.2), which is an injective function. Forward kinematics provides the positions of the end effector or a successive joint as outputs for the input preceding joint positions. Since mapping

between inputs and outputs for a forward kinematics analysis is one-to-one, a database can be prepared which has a value for the end effector position for every set of joint positions. It is possible to develop a machine learning model by training on this database to give joint positions for a given end effector position. A machine learning based model is developed next to test how accurately instructions from therapists about gait trajectories can be quickly and precisely translated in terms of ankle, knee, and hip joint angles. This information is later given to the controller for further execution. In order to obtain joint angles from the information about end effector position, a multiple adaptive neuro-fuzzy inference system (MANFIS) has been developed during this research that contains three individual fuzzy inferencing systems (FIS) (FIS_Ankle, *etc*. shown in Figure 5–2) to provide joint angles at ankle, knee, and hip [154]. This model takes position coordinates of the forefoot containing phalanges as inputs and produces three joint angles through three different ANFIS (adaptive neuro-fuzzy inference system) models and these outputs can be either obtained as three different outputs or as a single vector of three values. Three ANFIS models combined in such a way are called MANFIS (Figure 5–2). Details about construction and training of ANFIS are briefly discussed here, and readers are further advised to refer to [155] for more details.

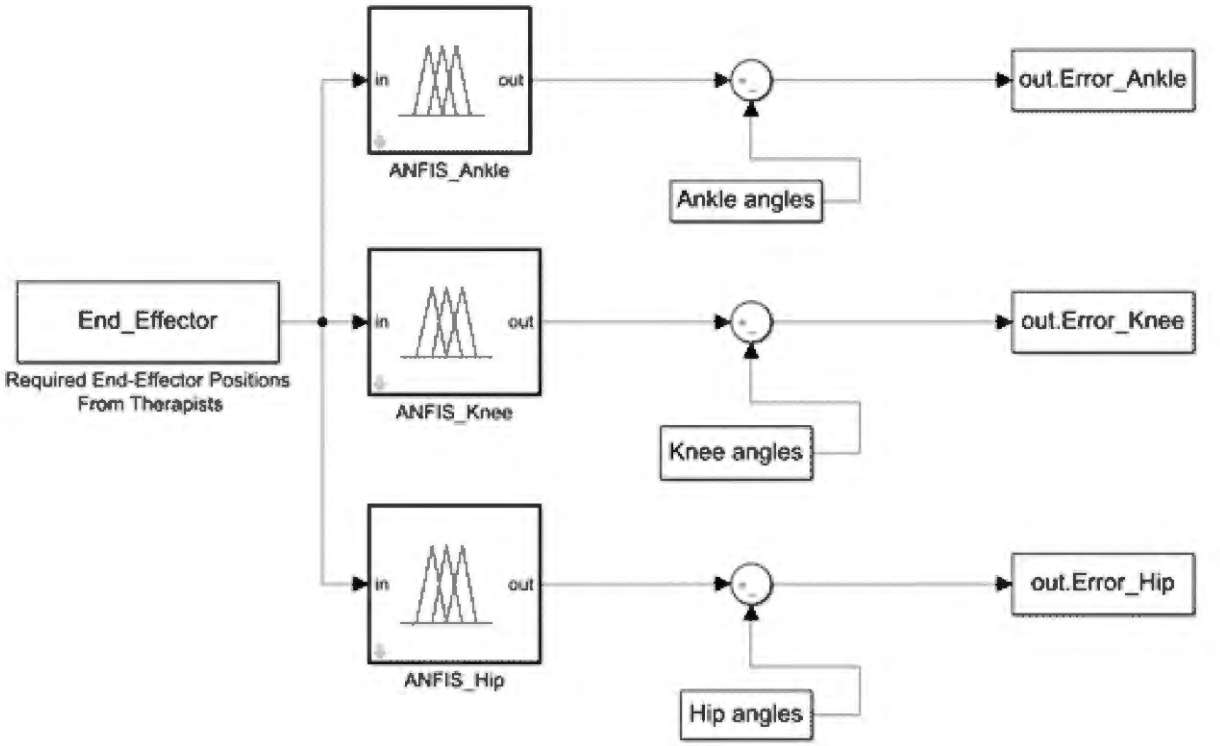

Figure 5–2. MANFIS-Based Inverse Kinematic Optimisation.

5.2.3 AI-Based Inverse Kinematic Modelling

The adaptive network-based fuzzy inference system (ANFIS) uses a 'hybrid learning' rule to optimise the fuzzy system parameters of a first order Sugeno system. A first order Sugeno system can be graphically represented by Figure 5–3.

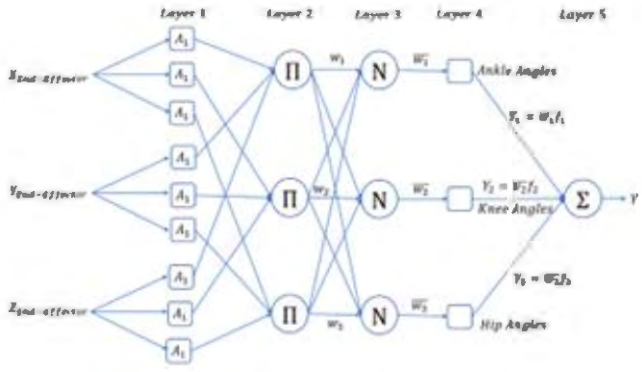

Figure 5–3. ANFIS Architecture for IK Solver.

The ANFIS architecture for a three-input (X, Y, and Z position coordinates of the end effector), first order Sugeno model is shown in Figure 5–3 [156]. Here, a first order polynomial is used to evaluate rule outputs for a given set of inputs using randomly initiated consequence parameters (p, q, r and s), which are later obtained using a least squares algorithm. The polynomial used for n^{th} rule is given as (5.5):

$$f_n = p_n X + q_n Y + r_n Z + s_n \tag{5.5}$$

As such there are two sets of ANFIS parameters that are required to create the models and therefore are identified through training and testing over the database. The first set of parameters are the antecedent fuzzy parameters (also called fuzzy membership functions), namely the mean and the standard deviation since in the thesis work, Gaussian functions are used to define the fuzzy functions. Later, the set of consequence parameters (p, q, r and s) is identified as discussed above. During the thesis research, Marquardt's gradient descent algorithm is used to optimise the antecedent parameters (fuzzy parameters) and a least squares algorithm is used to solve for the consequent parameters. Such training is termed hybrid because two very different algorithms are used to reduce the error. Initially the consequent parameters are updated and then the antecedent parameters are identified by backpropagating the errors.

Outputs from the five layered ANFIS architecture (Figure 5–3) are described below:

Layer 1. Inputs are converted to fuzzy values.

Layer 2. Fuzzy outputs from the rules stored in a variable (w_i).

Layer 3. Weighted average of the outputs ($\overline{w_i}$) from all the rules is calculated.

$$\overline{w_i} = \frac{w_i}{w_1 + w_2 + w_3} \tag{5.6}$$

Layer 4. Rule outputs are found using the consequent parameters.

$$Y_i = \overline{w_i} f_i = \overline{w_i}(p_i X + q_i Y + r_i Z + s_i) \tag{5.7}$$

Layer 5. Solve using regression to find the consequent parameters as shown below.

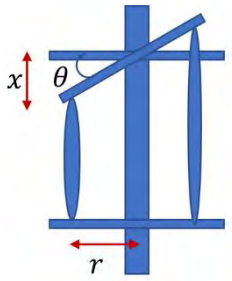

Figure 5–4. Antagonistic PMA and Joint Rotation.

Equation (5.7) is of the form $Y = XW$ where Y is the set of outputs and X is the set of corresponding inputs from the training database. In order to find W, which is the set of consequent parameters, a regression method can be used, such as LU decomposition or QR decompositions or singular value decomposition (SVD). In the thesis work, SVD is used to identify consequent parameters.

The gait robot is intended to move on prescribed trajectories which are normally provided by the therapists in terms of hip, knee, and ankle angles. Since PMAs are used in the proposed gait robot, the prescribed angles at various joints can be achieved by controlling lengths of the PMAs. The angular displacements at joints are further achieved by the coupled motion of the PMAs, therefore, a relation is required to be established between input PMA contraction/extension and the output joint angles. Referring to Figure 5–4, it is apparent that in order to obtain an angular displacement of θ at a joint the required contraction (x) in PMA can be given by $x = r \sin\theta$.

Eventually, to control robot motions the PMA lengths are required to be controlled by inflating and deflating with appropriate pressures. Owing to the transient and nonlinear behaviour of PMAs, in the thesis work, a fuzzy logic controller has been designed to operate the gait robot. The commanded gait robot trajectories are first converted to joint angles, which are further converted to the required PMA lengths at different time instances. The fuzzy logic

controller, therefore, is designed to control PMA lengths to provide the desired joint angles and thereby the gait theories.

An overview of the gait robot hardware is shown in Figure 5–5, whereas working of the controller is explained using a simplified block diagram in Figure 5–7. Commanded trajectory is converted to the desired joint orientations and passed through the inverse kinematics module to convert these to the desired PMA lengths. The fuzzy controller provides the pressure values for a pair of muscles to work antagonistically and implement the required change in joint angle. Three instances of similar fuzzy controllers are used for hip, knee, and ankle joints. The dSPACE® card is used to implement the controller and acts as a hardware interface to facilitate reading sensors (pressure, force and PMA lengths) and writing on the solenoid valves.

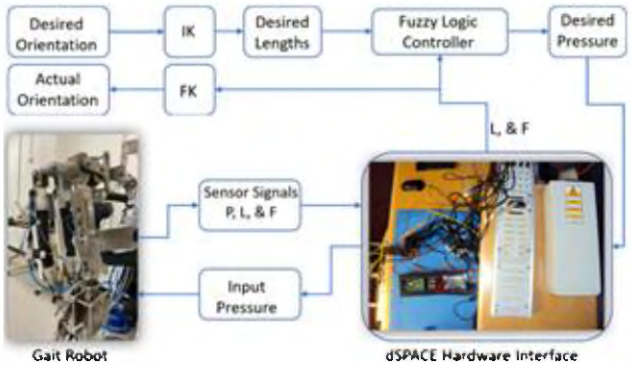

Figure 5–5. Overview of the Gait Robot Hardware.

The error in the commanded joint angles is converted into desired change in PMA lengths and given to three fuzzy controllers designed for hip, knee, and ankle joints. The fuzzy controller designed to be used in the overall controller scheme is shown in Figure 5–6 with further details. The input errors in lengths (± 50 mm) are converted to fuzzy variables using Gaussian fuzzy functions. The rule base is designed to map error in length to appropriate pressure values ($-4\ to\ 6$ bar) and give pressure values as output.

Figure 5–6. Controller Schematics.

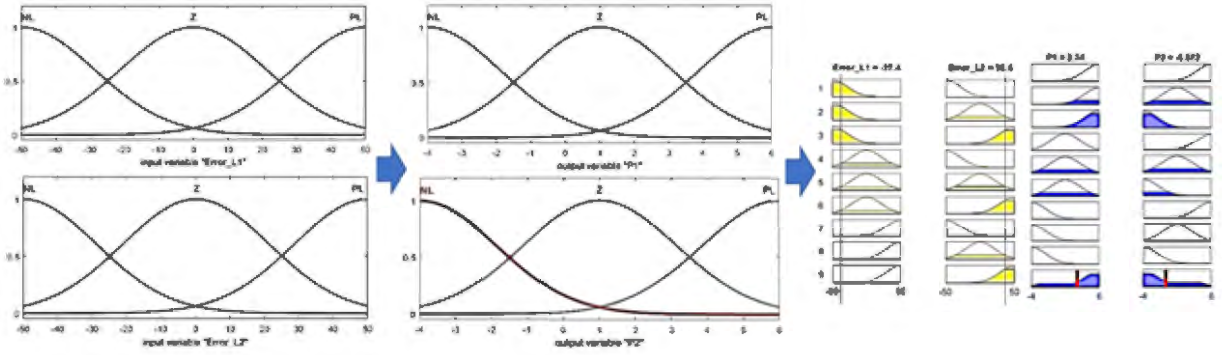

Figure 5–7. Fuzzy Controller Design Showing Fuzzy Variable and Fuzzy Rule-Based for Inferencing Output Pressure.

5.3 Robot Dynamic Modelling

The complexity of the dynamics model of the serial robotic manipulator increases significantly with the increase in degrees of freedom. The result is that although linearised models of parameters (such as mass, inertia, *etc.*) exist in theory, they are very difficult and complex in concrete operation or calculation [157].

For this designed prototype, the forced vibration damping model of a single degree of freedom system is chosen for analysis because the prototype is actuated by periodic forces [157].

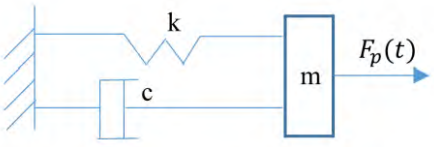

Figure 5–8. Schematic Drawings of Dynamic Model.

As shown in Figure 5–8, the basic forced vibration equation for a linear system with damper can be expressed as:

$$m\ddot{y} + c\dot{y} + ky = F_p(t) \tag{5.8}$$

Or

$$\ddot{y} + 2\xi\omega\dot{y} + \omega^2 y = \frac{F_p(t)}{m} \tag{5.9}$$

Where ξ is the damping ratio and ω is angular velocity.

This equation is a typical nonhomogeneous linear differential equation, so the general solution should be the sum of the general solution of the homogeneous equation (free vibration solution) and the particular solution of the inhomogeneous equation [157].

Three force equations are shown below:

$$F_1 = -m\ddot{y} = -k\mu y_{st} cos\omega t \tag{5.10}$$

$$F_S = -ky = -k\mu y_{st} cos\omega t \tag{5.11}$$

$$F_D = c\dot{y} = -Fsin\omega t \tag{5.12}$$

In this case, dynamic load is balanced with damping force. Also, the inertial and restorative forces are balanced [157]. The process of deriving equation 5.10 to 5.12 is provided in Appendix B.

5.4 Results and Discussion

Evaluation and the related results from the MANFIS-based inverse kinematics solver and the fuzzy controller are discussed in this section. First, in order to evaluate the inverse kinematics solver, a training database consisting of 60,000 sets of end effector positions is obtained using forward kinematics. Here the input angular positions are from the hip, knee and the ankle joints. During gait, the required ranges of motions at hip and knee joints are $\pm 20^0$ and -60^0 respectively, where extension is considered as a positive rotation. Similarly, during walking,

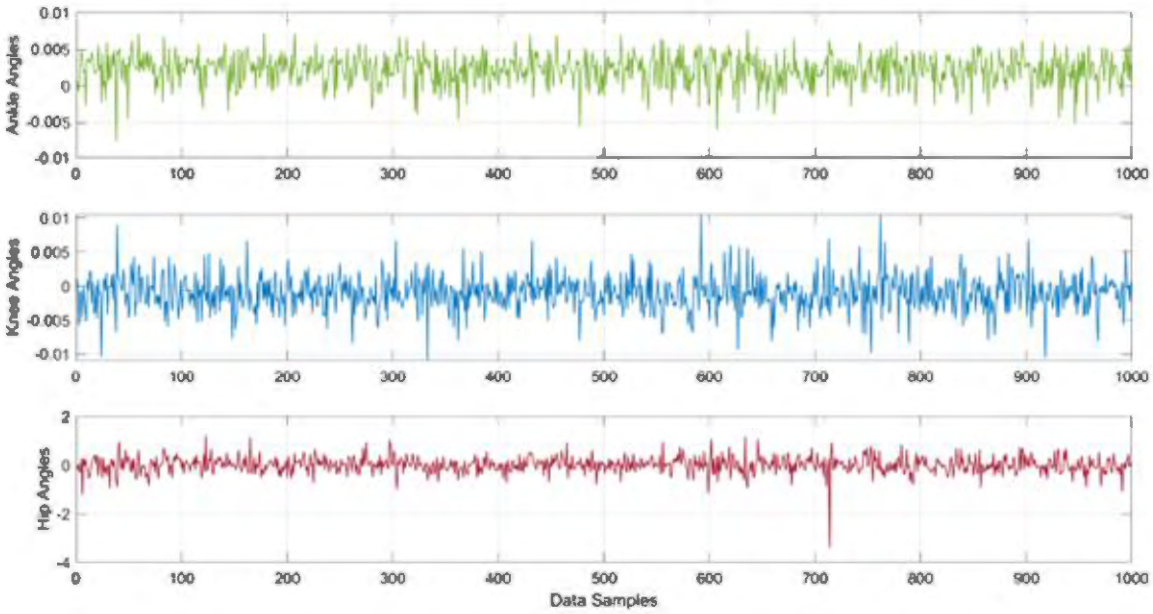

Figure 5–9. Estimated Joint Errors Using Inverse Kinematics Solver in ANFIS.

the ankle plantarflexion motion is about $+20^0$, whereas the dorsiflexion is normally -5^0 [158]. The database is created by incrementing the three rotations by one degree and so the database has $(25 \times 60 \times 40)$ rows with as many end effector positions which are found using the forward kinematics analysis. The database is further divided into training, testing and validation datasets with 70%, 15% and 15% of the data respectively. The sum of squared errors for the test data from the MANFIS model was found to be 9.24×10^{-3}, 7.92×10^{-3}, 117.3×10^{-3} degrees respectively for predicting ankle, knee and hip joints respectively. Since the robot link connected at the hip joint has larger rotational inertia, it is subjected to larger deflections compared to the robot links connected at the knee and ankle. This fact is apparent from the results in Figure 5–9 where errors in estimating hip angles are larger compared to the errors in the estimation of ankle and knee joint angles for given positions of the end effector.

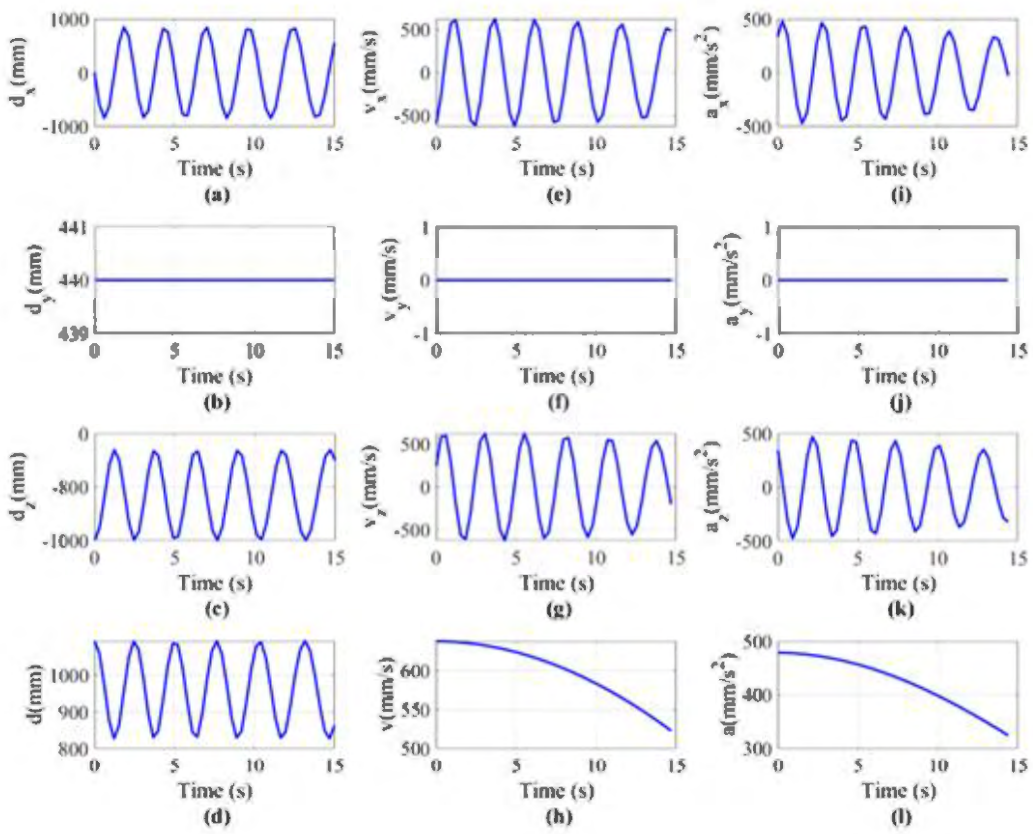

Figure 5–10. Displacement (a) along x-axis, (b) along y-axis, (c) along z-axis, (d) resultant displacement. Velocity (e) along x-axis, (f) along y-axis, (g) along z-axis, (h) resultant velocity. Acceleration (i) along x-axis, (j) along y-axis, (k) along z-axis, (l) resultant acceleration of the endpoint (ankle joint) with hip rotation only.

The Newton–Raphson method is a popular tool to solve inverse kinematics and in this research results from MANFIS are benchmarked against the results obtained from an iterative Newton–Raphson approach [159]. It is known that the N–R method, which is basically a numerical method, can be computationally intensive since multiple iterations are required to achieve convergence. Further, the selection of the initial solution is also critical for the convergence of this method. While it is possible to address the issue of initialising solutions from previous results, the computational efficiency can only be achieved using more powerful computing hardware. During simulation experiments in the thesis research, it was found that the N–R method takes 110 milliseconds for 100 IK computations. On the contrary, the MANIS-based IK solver took only 2.5 milliseconds for 100 IK computations.

Later, feasibility of the controller (Figure 5–7) is evaluated during experiments which are conducted with the gait robot and the interfacing dSPACE® hardware. The fuzzy logic

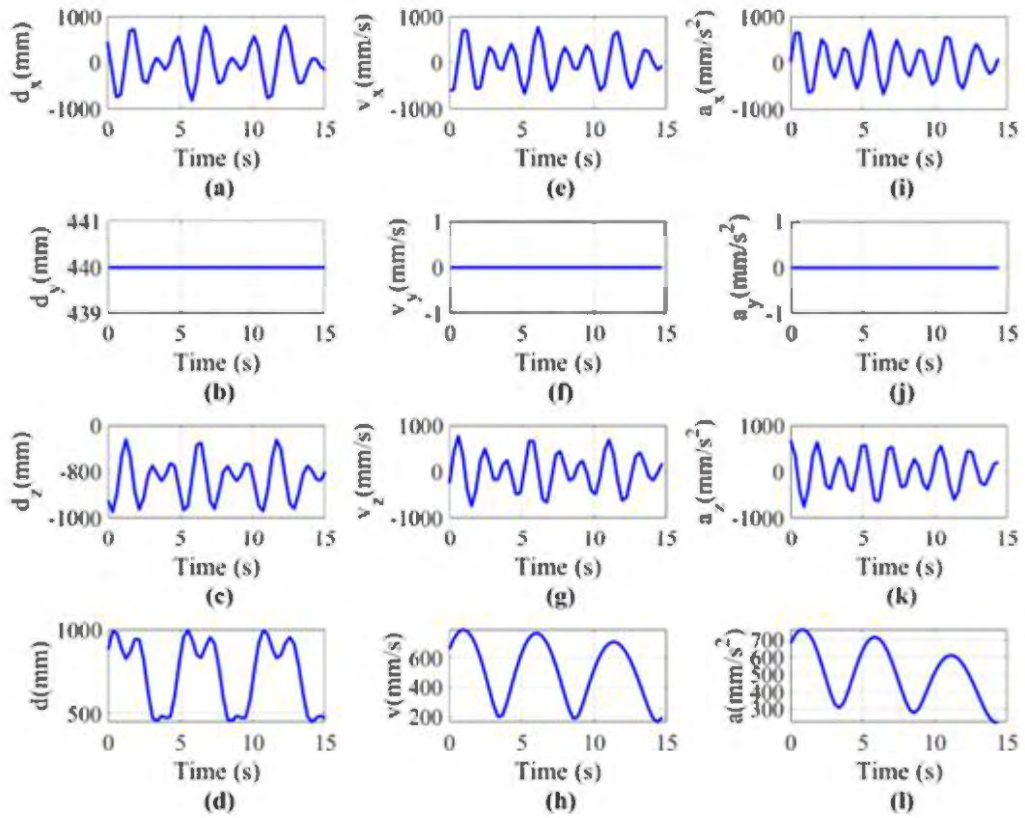

Figure 5–11. Displacement (a) along x-axis, (b) along y-axis, (c) along z-axis, (d) resultant displacement. Velocity (e) along x-axis, (f) along y-axis, (g) along z-axis, (h) resultant displacement. Acceleration (i) along x-axis, (j) along y-axis, (k) along z-axis, (l) resultant acceleration of the endpoint (forefoot) with hip, knee and ankle rotation.

controller is used to actuate the gait robot and for the first set of experiments, only hip rotations (in the sagittal plane) are given to the controller. Position coordinates of the end effector that are recorded during 'only hip rotations' are plotted together with the end effector velocity and acceleration (Figure 5–10). The input hip rotations in the sagittal plane ($x_0 - z_0$ plane) resulted in linear motion of the end effector in $x_0 - z_0$ plane, as seen in Figure 5–10 (a-c). Later, the controller is commanded with rotations at robot hip, knee and ankle joints simultaneously and the resulting end effector positions are plotted in Figure 5–11 together with related velocities and accelerations. Results obtained for the positions from experiments (Figures 5-10 and 5-11) are once again analysed from the forward and inverse kinematics modules and are found to be correct.

5.5 Chapter Summary

To evaluate the design of the gait robot, kinematic analysis was performed. Performing inverse kinematics was not possible following the analytical methods because the gait robot designed is an open chain mechanism. The multiple adaptive neuro-fuzzy inference system (MANFIS) developed during this research contains three fuzzy inferencing systems to provide joint angles at ankle, knee, and hip to achieve a target end effector position. This model takes position coordinates of the forefoot containing phalanges as inputs and produces three joint angles through three different ANFIS models. These outputs can be obtained either as three different outputs or as a single vector of three values. The MANFIS-based IK solver is found to be the faster method when benchmarked against the Newton–Raphson method.

Later, to move the robot on commended trajectories, a fuzzy logic controller is designed and implemented using appropriate hardware interface. Results from the controller were checked from similar results obtained through the kinematic analysis and found to be similar.

Chapter 6 – Control and Experimental Evaluation

A significant component of designing an effective rehabilitation robot involves the development of a suitable control strategy. By allowing the robot to adapt to the individual needs of each patient, gait rehabilitation robots can provide a more effective and efficient form of therapy, leading to improved outcomes for people who require gait rehabilitation [24, 160]. Although the mechanism designs and the compliant actuation provide a safe and secure platform for rehabilitation, they increase the complexity of system modelling and subsequently the design of the control system. Additionally, while the passive DOFs provided by the gait rehabilitation robot increase the flexibility of the robot, they also increase the intricacies of identification of system dynamics. Hence, during this research an autodidactic approach was developed for system dynamics identification based on the Koopman operator. The learned operator was integrated with the nonlinear model predictive controller (NMPC) to guide the robot along the predefined path while adapting to the nonlinear dynamics of the physical human–robot interaction. Finally, the rehabilitation robot and the control scheme were experimentally validated with healthy human subjects. The results demonstrated that the nonlinear model predictive controller could successfully manipulate the gait rehabilitation robot with the user to achieve the desired orientation during the entire gait cycle.

6.1 Introduction

During this research, the mechanism design of the gait rehabilitation robot was accentuated to include self-alignment and gravity-balancing. Moreover, the gait rehabilitation robot was designed to provide five passive DOFs in addition to three active DOFs. The actuation was provided by the pneumatic muscle actuators (PMA) to increase the compliance of the robot and provide a safe environment. However, in addition to improving the mechanism design, a rehabilitation robot should also adapt to the intrinsic nonlinearity of the physical human–robot interaction dynamics. Furthermore, as explained in the previous sections, a pair of PMAs were

required to actuate each joint, that is the hip, knee, and ankle joints. This implies that a coordinated and synchronised movement of six actuators was necessary to achieve the required target orientation. Therefore, the Koopman operator was applied in identifying the system dynamics and modelling. The Koopman operator [161] maps the nonlinear dynamics to a raised dimensional space where the dynamics are linearized. The Koopman Operator is a data-based learning approach that provides a novel perspective to analyse and identify systems with nonlinear dynamics. This phenomenon is demonstrated in [162], wherein the Koopman operator theory is applied to predict and control a nonlinear dynamical system. Additionally, [163] proves that a Koopman operator-based controller is highly effective for systems that do not rely on physics governing equations. Several attempts were therefore made to design the control system of nonlinear dynamical systems, such as wind farms [164], high-speed trains [165], hydraulic fracturing processes [166], chemical processes, fluid systems [167], vehicles [168], soft robotic systems [56, 169], wheeled mobile robots [170], and complaint wrist rehabilitation robot [171] using the Koopman operator. With the help of Koopman operator, a system identification model can be designed to understand the non-linearities of the compliant lower-limb robotic orthosis with self-aligning and gravity-balancing mechanisms. Based on this model, a controller can be designed to manipulate the robotic orthosis to guide the human subject along the predefined trajectory. Therefore, Koopman Operator based system identification model was devised to control the lower-limb robotic orthosis.

Further, a Nonlinear Model Predictive Controller (NMPC) based on the Koopman operator was developed. A trajectory tracking control problem for a nonlinear disturbance observer is solved in [172] for a single DOF orthosis for knee flexion/extension. An NMPC with a Koopman operator-based identification of the system dynamics for a multi-DOF gait rehabilitation robot with self-aligning and gravity-balancing mechanisms has not been reported in the literature, according to the authors' best knowledge.

6.2 System Identification using Koopman Operator

The Koopman operator is a mathematical tool for analysing and identifying nonlinear dynamic systems. It is a linear operator that transforms a function of the state of a dynamic system into a function of its future behaviour. The Koopman operator is a powerful tool for the analysis of nonlinear systems, as it provides a linear representation of the underlying dynamics of the system from the observed data, making it easier to study and understand.

The human-robot combined dynamics of the lower limb were modelled as equation (6.1) which represents a nonlinear dynamics system:

$$x(k+1) \;=\; d\big(x(k), u(k)\big) \tag{6.1}$$

Here, $x(k) \in \mathcal{X} \subset \mathbb{R}^n$ is system state at $k \geq 0$, $u(k) \in \mathbb{R}^n$ is input at k, $\mathcal{X}$ is a compact subset, and d is a continuously differentiable function. The solution of Equation (1) at time $k = 0$ with the initial condition is x_0, u_0 is referred as the flow map and is represented by $\phi_k(x_0, u_0)$.

Equation (6.1) can be lifted to an infinite-dimensional function space referred by $\mathcal{F}$ which composes of the continuous and real-valued functions. $K : \mathcal{F} \to \mathcal{F}$ is the Koopman operator that characterizes the flow of the system for each $k \geq 0$ according to:

$$(Kf)(x) \;=\; f\big(d\big(x(k), u(k)\big)\big) \tag{6.2}$$

Here, $f \in \mathcal{F}$ is the observable function, K has infinite dimensionality, and therefore a physical representation is not possible using a finite-dimensional matrix. The system dynamics evolve linearly in the space spanned by the observable function. Using the flow map, equation (6.2) can be rewritten as:

$$K\,f = f \circ \phi_k \tag{6.3}$$

Table 6–1. Algorithm for System Identification.

Algorithm: Pseudocode describing the Koopman Nonlinear System Identification	
Input:	λ and $\{a[k], b[k]\}$ for $k = 1, \ldots, K$
Step 1:	Lift data using basis function ψ
Step 2:	Koopman operator $(\bar{U}_{T_s})$ is approximated using (55)
Step 3:	Generator $(\bar{G})$ is identified using (53)
Step 4:	(54) is used to solve for vector field $(\bar{F})$
Output:	$\bar{F} : R^n \times R^m \rightarrow R^n$

Where $(\circ)$ is the function composition. By using linear regression to recorded data, an updated version of the Extended Dynamic Mode Decomposition can identify a finite-dimensional approximation for the Koopman operator.

$\bar{\mathcal{F}} \in \mathcal{F}$ is a finite-dimensional subspace spanned by $N > n$ (N=35 for this case) linearly independent basis function $\psi : \mathbb{R}^{n+m} \rightarrow \mathbb{R}^N$. With the basis function, any finite-dimensional space observable $\bar{f} \in \mathcal{F}$ can be expressed linearly as a combination of elements of the basis function:

$$\bar{f} = \theta_1 \psi_1 + \cdots + \theta_{N+m} \psi_{N+m} \tag{6.4}$$

Here $\theta_i \in \mathbb{R}$. The above Equation can be transformed using vectorization as:

$$\bar{f} = \theta^T \psi(x, u) \tag{6.5}$$

Using equation (6.5), the linear Koopman operator approximation on finite-dimensional subspace $\bar{\mathcal{F}}$ is given by:

$$\bar{K}\theta = \theta' \tag{6.6}$$

Here, θ and θ' are both vector representation of observables in $\bar{\mathcal{F}}$. According to equation (6.3),

$$\bar{K}\,\bar{f}(x,u) \;=\; \bar{f} \;\circ\; \phi_k(x,u) \tag{6.7}$$

$$(\bar{K}\,\theta^T)\,\psi(x,u) \;=\; \theta^T\psi \circ\; \phi_k(x,u) \tag{6.8}$$

$$\bar{K}^T\psi(x,u) \;=\; \psi \circ\; \phi_k(x,u) \tag{6.9}$$

Equation (6.8) is derived by substituting equation (6.5) in equation (6.7). The best approximation of K on $\bar{\mathcal{F}}$ is yielded by solving equation (6.9) in L^2 norm sense:

$$\bar{K} \;= \big(\psi^T(x,u)\big)^{\dagger}\big(\;\psi \circ\; \phi_k(x,u)\big) \tag{6.10}$$

The † superscript represents the Moore-Penrose pseudo-inverse [173]. For approximating the Koopman operator from a set of data, T discrete state measurement in the form of "snapshot pair" $(a[t], b[t])$ are taken for each $t \;\in\; \{1,\ldots,T\}$:

$$a[t] \;=\; \begin{bmatrix} x[t] \\ u[t] \end{bmatrix} \tag{6.11}$$

$$b[t] \;=\; \begin{bmatrix} \phi_{K_s}(x[t]) \;+\; \sigma[t] \\ u[t] \end{bmatrix} \tag{6.12}$$

Here, $\sigma[t]$ represents the noise measurement, which is unavoidable due to sensors, k_s is the sampling period, which is identical for every pair, $x[t]$ and $u[t]$ represent the measured system state and control input at t^{th} time step, respectively. The snapshot pairs are lifted and combined into the following $X \;\times\; (N \;+\; m)$ matrices:

$$\psi_a \;:=\; \begin{bmatrix} \psi(a[1])^T \\ . \\ . \\ . \\ \psi(a[T])^T \end{bmatrix} \tag{6.13}$$

$$\psi_b := \begin{bmatrix} \psi(b[1])^T \\ . \\ . \\ . \\ \psi(b[T])^T \end{bmatrix} \tag{6.14}$$

From equation (6.10), the $\overline{K}_{k_s}$ is given by:

$$\overline{K}_{k_s} := \psi_a{}^{\dagger}\psi_b \tag{6.15}$$

To build a model in the form of equation (6.1), we introduce an infinitesimal generator of the set of Koopman operators. The generator $G : \mathcal{F} \rightarrow \mathcal{F}$, that describes the dynamics of the observables along the trajectories. is given by:

$$G = F \cdot \nabla_s \tag{6.16}$$

The relationship between the Koopman operator and the generator is given by:

$$K = e^{Gk} \tag{6.17}$$

The generator can be calculated with the approximation of $\overline{K}_{k_s}$, by inverting Equation (6.17):

$$\bar{G} = \frac{1}{k_s} \log \overline{K}_{k_s} \tag{6.18}$$

Here, log represents the principal matrix logarithm, which is only defined for matrices with non-negative real parts of the eigenvalues. Therefore, this method would be invalid for insufficient data points.

The value of $\bar{F}$ can be regulated using (6.16) and (6.18). Considering it is applied to an observable $f \in \mathcal{F}$, G is equivalent to:

$$G\, f(x,u) = \frac{\partial f(x,u)}{\partial x}\, F(x,u) \tag{6.19}$$

Using θ to signify vector representation of observables f, and $a = [x^T, u^T]^T$ to represent an augmented state, equation (6.18) can be rewritten as:

$$(\bar{G}\theta)^T\psi(a) = \theta^T \frac{\partial\psi(a)}{\partial x} \bar{F}(x,u) \tag{6.20}$$

$$\bar{F}(x,u) = \begin{bmatrix} \frac{\partial\psi(a_1)}{\partial x} \\ \cdot \\ \cdot \\ \cdot \\ \frac{\partial\psi(a_t)}{\partial x} \end{bmatrix}^{\dagger} \begin{bmatrix} \bar{G}^T \\ \cdot \\ \cdot \\ \cdot \\ \bar{G}^T \end{bmatrix} \psi(a) \tag{6.21}$$

Data-driven models tend to overfit and lack predictive power. To make the model impervious to outliers, L^1 regularization method of Least Absolute Shrinkage and Selection Operator (LASSO) is used as represented by (6.22):

$$\vec{\bar{K}}_{k_s} = \underset{\bar{K}_{k_s}}{arg\,min} \left\| \vec{\psi}_a \vec{K}_{k_s} - \vec{\psi}_b \right\|_2^2 + \lambda \left\| \vec{K}_{k_s} \right\|_1 \tag{6.22}$$

Here, $\lambda \in R^+$ is the weight of the L^1 penalty term, and $\vec{\cdot}$ denotes the matrix in vectorized form with consistent dimensions.

The system dynamics identification procedure is recapped in Table 6–1.

6.3 Nonlinear Model Predictive Controller Design

Implementing a system identification model using the Koopman Operator allows a model-based controller to manipulate the gait robot that selects appropriate control inputs [174]. A popular model-based design technique is the model predictive controller (MPC) that continuously optimizes the control input over a finite period and applies it to every time step. Furthermore, an NMPC is used since the system has nonlinear dynamics. With the introduction of the Koopman operator for identification of system dynamics, the nonlinear MPC can be described as:

$$\underset{u \in L^2([t_0,t_f];R^m)}{minimize} \int_{t_0}^{t_f} \left(E(x)^T P E(x)\right) + u(t)^T Q u(t) dt$$
$$s.t. \qquad L\left(x(t), u(t)\right) \leq 0_q \ \forall t \in [t_0, t_f] \tag{6.23}$$

Here $E(x) = \left(x(t) - x_{ref}(t)\right)$ is the control error and $x_{ref}: [t_0, t_f] \rightarrow R^n$ is the predefined trajectory, where $0 \leq t_0 \leq t_f$, and the initial orientation $x_0 = x(t_0)$ is known, $L^2\left([t_0, t_f]; R^m\right)$ is the square-integrable function space from $[t_0, t_f]$ to R^m, $P \in R^{n \times n}$ and $Q \in R^{m \times m}$ are positive semidefinite matrices. P represents the deviation cost of the $'x'$ from the desired orientation whereas Q encapsulates control expenditure cost. The constraints are defined by $L: \mathbb{R}^n \times \mathbb{R}^m \rightarrow \mathbb{R}^q$ and 0_q is a zero-vector with $q-$elements. The solution to Equation (6.23) gives the open-loop control input. However, the control without feedback is not robust enough to prevail over model errors. As a result, the system's performance degrades over time. Therefore, a linear feedback controller based on the local linearization of the nonlinear model around the desired trajectory is added to this controller. The complete control scheme is depicted in Figure 6–1.

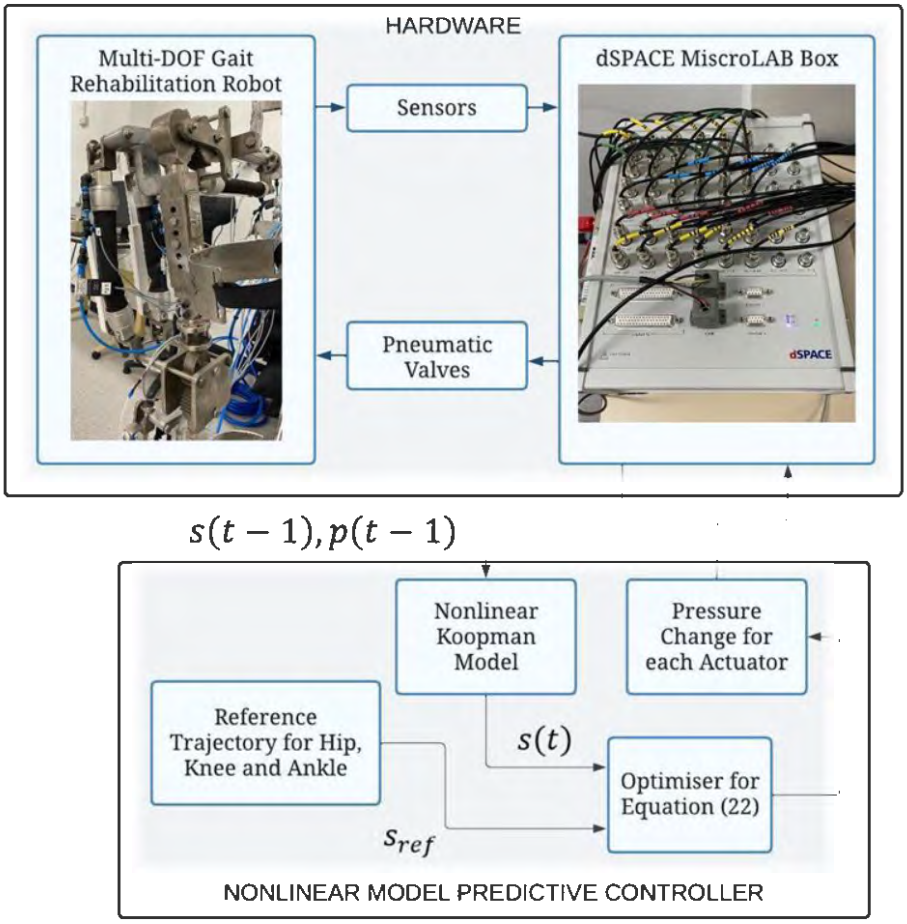

Figure 6–1. Schematic Diagram of the Gait Rehabilitation Robot with Nonlinear Model Predictive Controller based on Koopman Operator.

6.4 Experiment Setup

The efficiency of the developed mechanisms was established by equipping the prototype with the NMPC and testing with one healthy human subject as this research is the proof-of-concept in terms of the development of robotic orthosis. A single subject is sufficient to carry out such single case experimental design in the field of development of rehabilitation robotics [175]. The experimentation with healthy users was approved by the University of Canberra's Human Research Ethics Committee. The ethics approval is in Appendix B and participants' signed consent forms are in Appendix C. The prototype is actuated using pneumatic muscle actuators. The experimental setup is shown in Figure 6–2. As explained in earlier sections, two actuators

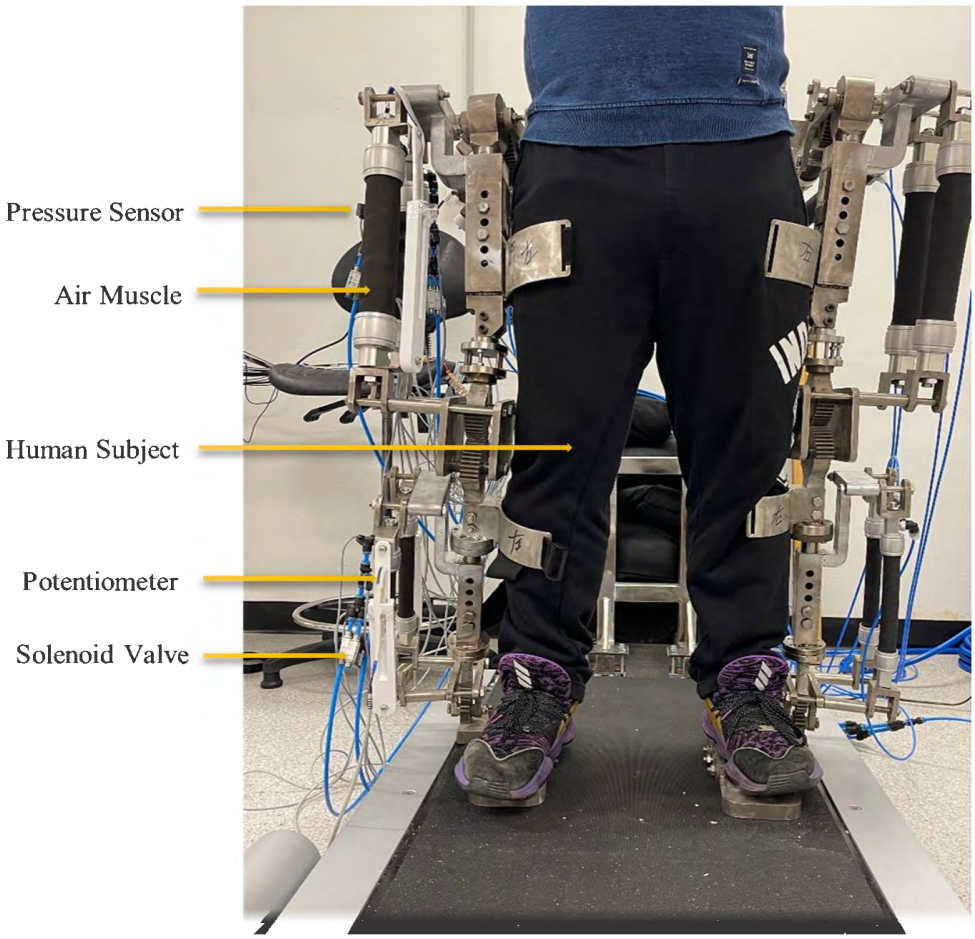

Figure 6–2. Experimental Setup for the Gait Rehabilitation Robot with a Healthy Human User.

are used to actuate the hip, knee and ankle joint each. Therefore, six PMAs of varying lengths are connected along each robotic limb. Two solenoid valves are attached to each actuator: one for inflating the actuator by letting the air in and the other for deflating the actuator. Each PMA is also appended with a pressure sensor and linear potentiometer to monitor the pressure and length of each PMA. Before experimenting with the human users, the Koopman operator was learned from the data collected from the forward kinematic analysis.

The robot was tested with one healthy human user with no previous lower limb or spinal cord injuries. The shank and thigh of the human user was secured with the robotic counterparts via braces. The robot was set up on top of a treadmill such that the bottom part of the footplate rested on the movable strip of the treadmill. The user was asked to remain passive and not exert any force for the entirety of the experiment. The treadmill was moved at 1 miles/s and the same

velocity was given to the controller. The reference trajectory, the actual trajectory followed by the robot, and any errors were recorded. The lengths of all six PMAs were also recorded.

6.5 Data Collection and Robot System Identification

The prototype developed here has an open chain mechanism. Hence, the forward kinematics has a closed-form solution since this is an Injective Function. For the present prototype with eight DOFs, forward kinematics can be mathematically explained as equation (5.2). MATLAB® was used to create the forward kinematics model and collect the data for system identification.

Identifying a system using the Koopman Operator is a data-driven process; hence, the model can be overfitted. Therefore, the data to train the Koopman operator was collected in abundance to avoid the issue of overfitting the model. During gait, the required ranges of motions at the hip and knee joints are $\pm 20^0$ and -60^0, respectively, where extension is considered as positive rotation. Similarly, during walking, the ankle plantarflexion motion is about $+20^0$, whereas the dorsiflexion is normally -5^0 [158]. The data was collected through simulations to obtain noise-free data. The successive joint position and velocity were recorded from the kinematic analysis and used to approximate the Koopman operator. The system state is eight-dimensional, representing the robot's eight DOFs. The control input is six-dimensional that represents the pressure across all six PMAs. The data was collected for each joint separately with an increment of 1^0 for each joint within their respective range of motion. Collecting datasets with this method lead to forty-eight thousand sets. In order to avoid overfitting, 30,000 sets were exhausted to train the Koopman operator, and 18,000 for validation. Later, the controller was built with this learned Koopman model. Equation (6.22) was solved with $\lambda = 0$, which signifies that least-square solutions were used.

6.6 Results

The trajectory tracked by the robot and the actual reference trajectories are presented in Figure 6–3. As can be concluded from the figure, the controller could satisfactorily aid the anatomical joints through the required orientations. The NMPC was constructed using the identified model for the system dynamics using the Koopman operator. The gait rehabilitation robot illustrated in Chapter 3 was interfaced with this controller to trace the predefined trajectory while guiding the subject's hip, knee, and ankle joints. The error for the rotational motion of each robotic joint was quantified using the average Euclidean error between the required orientation and the instantaneous orientation for every time step for the entire duration of the trial:

$$Error = \frac{\sum_{j=0}^{N_s} \sqrt{\left(x[j] - x_{ref}[j]\right)^T \left(x[j] - x_{ref}[j]\right)}}{N_s} \tag{6.24}$$

Here, N_s is the number of time steps in the experiment which is same for all three joints: $N_s = 250$. The bounded trajectory tracking errors are represented in Figure 6–4. The trajectory errors are bounded because the observables for the Koopman operator were learned by confirming them as eigenfunctions. The range of motion of the hip, knee, and ankle joints is

summarized in Table 6–2 along with the error calculated using equation (6.24).

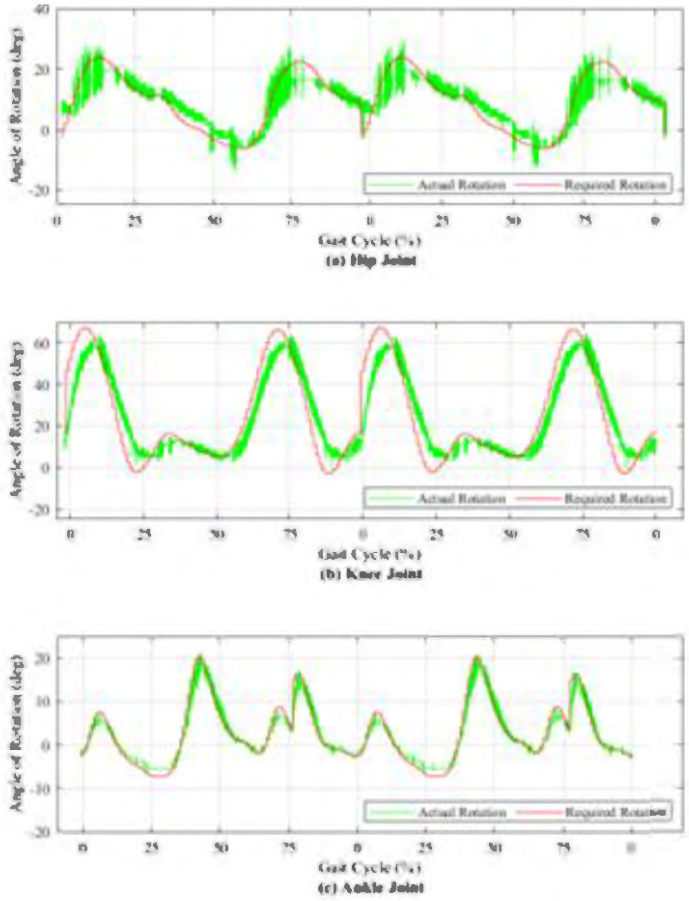

Figure 6–3. Required Orientation and the Actual Orientation attained by the a) Hip, b) Knee and c) Ankle Joints.

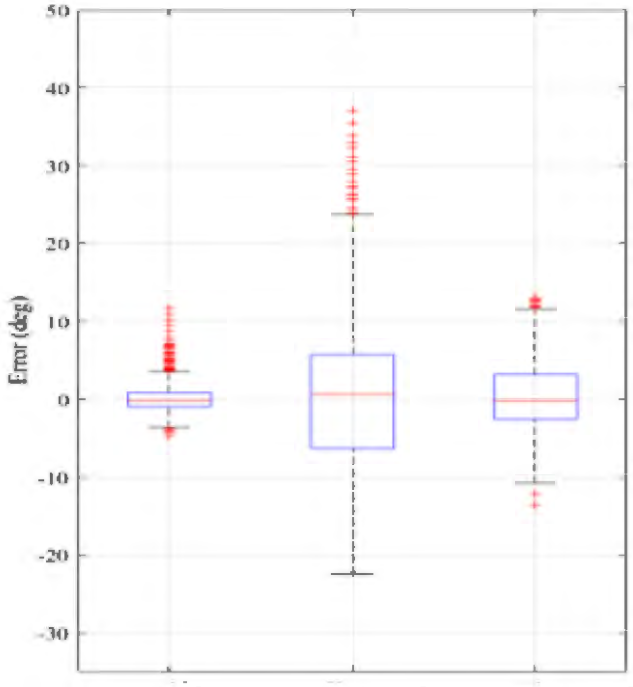

Figure 6–4. Errors between Required Orientation and Actual Orientation for the Ankle, Knee, and Hip Joints.

One of the main challenges with the development of the controller was the actuation of all six PMAs simultaneously. Thus, Figure 6–5 shows the length of the six pneumatic muscle actuators for one leg. The actuators have been divided into three groups of two actuators each based on the active degree of freedom dependent on them. From a safety point-of-view, the acceleration of each joint was also recorded. The results in Figure 6–6 show the acceleration transitions smoothly which implies that the controller can protect the human user against sudden jerks.

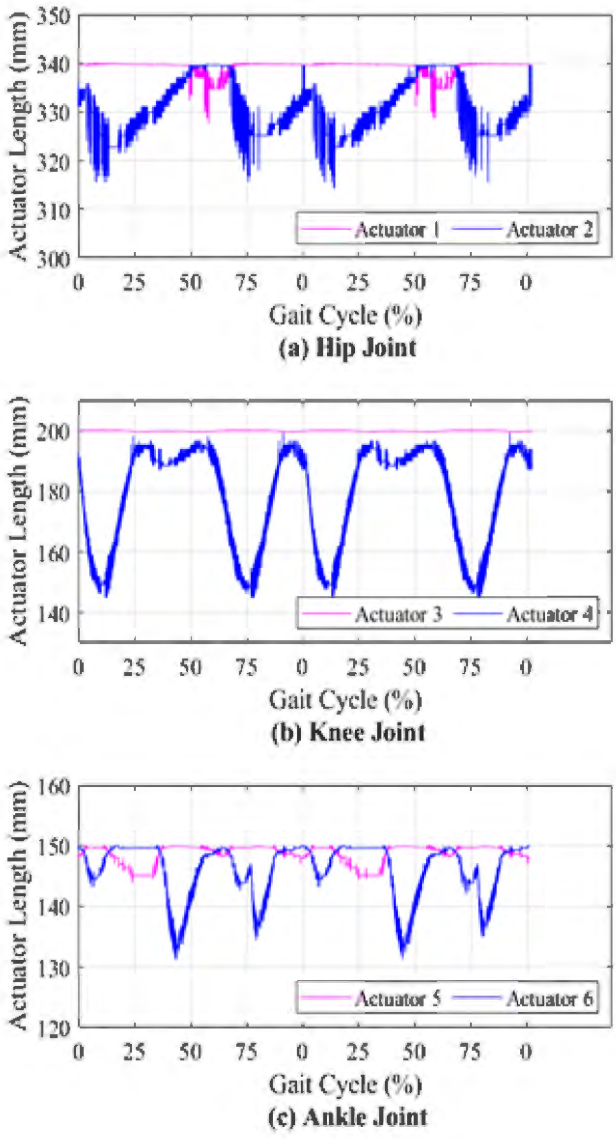

Figure 6–5. Actuator Lengths for attaining the Required Orientation of a) Hip, b) Knee and c) Ankle Joints.

The main purpose of this study was to identify robust design and actuation issues for ambulatory rehabilitation robots and to propose new designs that could potentially address these issues. To achieve this goal, this thesis proposes the first design of a multi-DOFs walking robot with three active degrees of freedom and five passive degrees of freedom to provide users with a natural walking experience. A walking robot prototype developed as part of this research can actuate the hip, knee and ankle joints and provide passive motion to the pelvis, hip and ankle joints. In addition, the proposed design allows for vertical movement at the pelvis, abduction–adduction and flexion–extension movements at the hip joints, and slight internal–external rotation and abduction–adduction movements at the knee and ankle joints. Accompanied flexion–extension is possible.

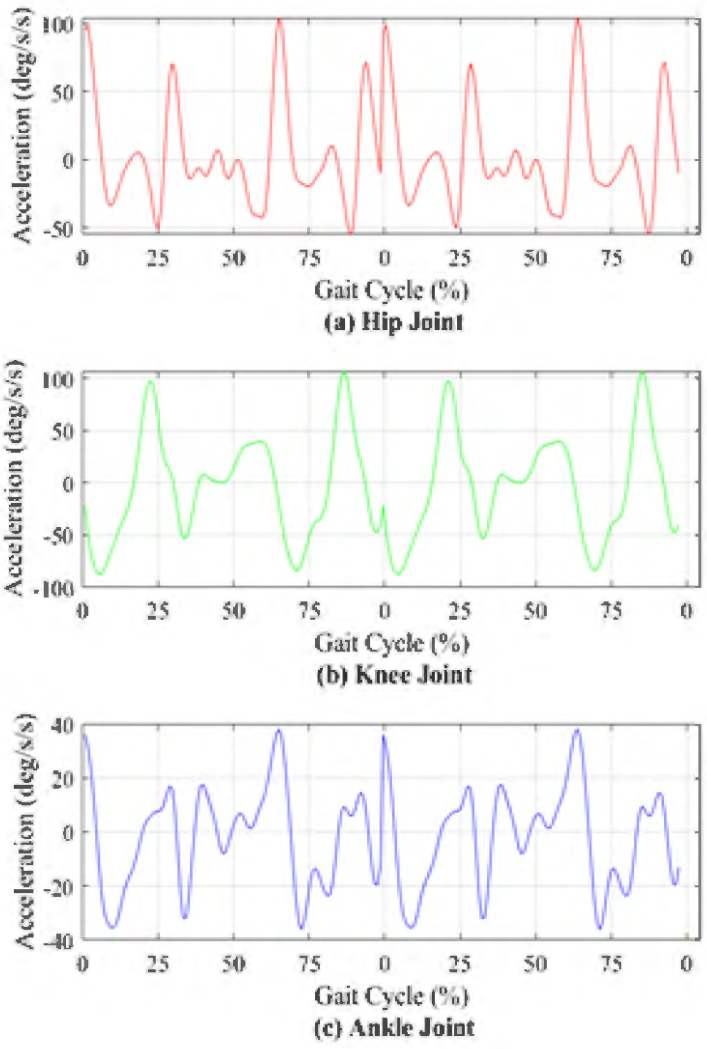

Figure 6–6. Acceleration of a) Hip, b) Knee and c) Ankle Joints.

The use of PMAs for actuators makes the proposed gait robot intrinsically compliant and therefore safe to be used by human users. Actuation amplification has been achieved using a novel mechanism for the gait robot powered by PMAs. This is an important contribution that overcomes the force output limitations for robotic orthoses powered by PMAs. A self-alignment mechanism for providing better alignment of robot joints with anatomical joints was also achieved using two approaches including the use of rubber bushes and dampers.

However, identifying system dynamics becomes complex with introducing PMAs and multiple active and passive DOFs. Hence, a system identification model was developed using the Koopman operator. The Koopman operator has a significant advantage in converting nonlinear and uncertain dynamics into linear dynamics. Koopman operators are learned using linear regression, which is a machine-learning-based approach. Such linear approximation, using Koopman operators, enables efficient system identification and control synthesis of the gait robot. Further, the system identification model was then used in conjunction with a nonlinear model predictive controller to guide the hip, knee, and ankle joints to attain the human gait rehabilitation objective. Figure 6–3 shows the orientations of the three joints with respect to the required orientations. The range of motion of the ankle and the hip joints is achieved properly. However, the robotic knee joint lags the reference orientation for the gait cycle. The knee joint has the highest range of motion and has the most complex structure. The mechanical amplification of the actuation might also account for the time delay. Nevertheless, the tracking errors are bounded as can be seen from Figure 6–5.

The identification of eigen functions while approximating the Koopman operator lends an innate stability to the algorithm. Each eigen function provides a mode and the corresponding eigenvalue determines whether the mode is stable or unstable. For asymptotic stability the norm of eigenvalues must be less than one. Therefore, the Koopman operator is approximated such that the norm of the eigenvalues for the operator is less than one. The rehabilitation robots work

Table 6–2 Range of Motion and Mean Trajectory Tracking Error for Hip, Knee, and Ankle Joints.

Joint	**Required Range of motion (degrees)** **Min/Max**	**Acquired Range of Motion (degrees)** **Min/Max**	**Error with Standard deviation (degrees)**
Hip	-6.2 / 24.1	-13.9 / 29.3	0.3 ± 4.0
Knee	-3 / 67.3	0 / 64.6	0.7 ± 9.9
Ankle	-6.9 / 20.5	-6.6 / 20.3	0.4 ± 1.6

closely with the human users and thus, the stability of the control scheme is crucial for the robot design. It can be concluded from Table 6–2 that the prototype along with the controller can successfully attain the required orientations. The gait rehabilitation robot has a higher maximum attainable orientation for the hip. The pair of PMAs used to actuate the hip joint are the longest and thus have the highest margin of error as they are more prone to buckling and bending [176]. The knee and ankle joints can safely attain the required ranges of motion. The maximum achievable orientation for the knee is considerably less than the required due to the lock mechanism introduced to increase the safety of the device. The table also proves the efficiency of the mechanism since the knee joint has only anti-clockwise motion. Another significant finding from the results is that the error is highest for the knee joint. This can be attributed to the fact that the knee has the highest range of motion.

The developed controller was able to guide the six pneumatic muscle actuators in a synchronised manner, as can be concluded from Figure 6–5. Further analysis of Figure 6–5 demonstrates that the actuation of the hip and the knee joints was provided predominantly by a single actuator. This fact is also corroborated by Figure 6–3 which shows that the hip and the knee joints have chiefly positive orientations for various stages of the gait cycle. The other

actuator is necessary to bring the said joints to their initial positions. On the other hand, for the ankle joint, coordinated movement of both the actuators is crucial since the ankle has plantarflexion as well as dorsiflexion.

6.7 Chapter Summary

To make the mechanisms practically feasible, a nonlinear model predictive controller appended with system identification based on the Koopman operator was developed. Such an approach for a gait rehabilitation robot has not been previously mentioned in the literature according to the author's best knowledge. Nonetheless, there are a few limitations that could be addressed in the future. The lag caused at the knee joint can be rectified by increasing the efficiency of the control design. Furthermore, the current controller scheme does not account for the user's difficulty level and intention. In future, this research aims to incorporate users' involvement by gauging their difficulty level and intention.

Chapter 7 – Conclusion

The principal goal of this research was to develop an intrinsically compliant robotic orthosis for gait rehabilitation capable of performing the major ranges of joint motion while providing joint alignment as well as gravity-balancing to patients during the training process. A multi-DOFs rehabilitation robotic orthosis was designed, developed and analysed. The rehabilitation robot can provide self-alignment and gravity-balancing during the training process with the actuation of pneumatic muscles (PMAs). Modelling and nonlinear model predictive control (NMPC) was developed for the robotic orthosis and evaluated with healthy users. The robotic orthosis and NMPC based control have achieved the intended performance. This chapter discusses the major outcomes and contributions of the research. Limitations of the designed prototype are presented along with suggestions for future work.

7.1 Major Outcomes and Contributions

The major outcomes and contributions of this research include the design and analysis of a novel multi-DOFs compliantly actuated gait rehabilitation robot, development of three new self-aligning mechanisms, application of a gravity-balancing mechanism, and precise control of the developed rehabilitation robot. The major outcomes and contributions are detailed as follows.

7.1.1 Robotic Orthosis Design and Analysis

A new wearable gait rehabilitation robot, with three actuated DOFs and five passive DOFs, was designed and developed as an outcome of the thesis research. The developed prototype has hip, knee and ankle joints that are actuated by using a pair of pneumatic muscle actuators (PMAs) for each joint. The hip joint has actuated flexion/extension in the sagittal plane, passive abduction/adduction in the frontal plane, and rotation in the transverse plane. The hip joint can therefore provide three DOFs. The knee joint of the robot has actuated flexion–extension in the

sagittal plane. Additionally, it has a small passive rotation in the transverse plane lending two degrees of freedom to the knee joint. The ankle joint is analogous to the hip joint and can provide actuated plantarflexion/dorsiflexion in the sagittal plane and passive abduction/adduction and inversion/eversion in the frontal and transverse plane, respectively. Screw theory and fuzzy logic based computational model were proposed to carry out forward kinematics analysis and inverse kinematics analysis of the designed wearable gait rehabilitation robot.

7.1.2 Application of a Self-aligning Mechanism

One of the major contributions of this research is the development of a novel self-aligning mechanism. The anatomical joints including hip, knee and ankle have predominant rotational motions. However, there is also a small transverse displacement during the rotational motion. The gait robot designed here not only provides rotation but offers a small transverse freedom to emulate the anatomical joints. The biggest challenge with delivering both rotation and transverse motion is the time delay. Since both movements happen at the same instant anatomically, the gait robot should supply the necessary actuation for both the motions to achieve self-alignment. To address this challenge, decoupling mechanisms have been developed during this research. The basic principle of decoupling assists in both rotation as well as transverse motion and delivers it at the same instant by separating them into different mechanisms. Hence, gear-couple mechanism, toothed cam-couple mechanism and four-bar linkage mechanism have been developed and tested in conjunction with the pneumatic muscle actuators to bring decoupling into effect. By simulation-based and motion capture system-based tests, the gear-couple mechanism is chosen to be applied in the final prototype. Additionally, the gears have been modelled in a way that aids in mechanical amplification of the actuation provided by the PMAs. The self-alignment mechanism is provided for all three joints – hip, knee and ankle.

7.1.3 Application of a Gravity-balancing Mechanism

A partial gravity-balancing mechanism, which is applied in the design of a wearable gait rehabilitation robot, presents another contribution of this research. In the presented prototype, the partial gravity-balancing mechanism has been applied to the hip and the knee joints. The gravity-balancing mechanism ensures that the system equilibrium at various configurations should be maintained without the application of actuator forces. However, partial gravity-balancing offers a wide range of gravity-balancing to the users based on their physiological capabilities. To achieve the stated goal, springs are placed appropriately after identifying the centre of mass of the robot elements. The trajectory of the centre of mass is calculated using the link dimensions. Further, the mass of the thigh and shank are considered as point masses at their centre of mass. Finally, the position and stiffness coefficients of the spring are decided in a manner that the total mechanical energy of the system remains constant at all configurations Additionally, in the developed prototype, the position of the spring can be changed according to the user's anthropometric measurements.

7.1.4 Application of Compliant Actuators

Application of pneumatic muscles as actuators in the design of a robotic gait rehabilitation orthosis involving self-aligning mechanisms to provide compliant actuation is a significant contribution of this research. This feature has not been reported in other robotic rehabilitation orthoses reported in the literature to the best knowledge of the author. This allows the robot to provide a more natural and comfortable form of assistance, which can improve patients' ability to perform therapy exercises and reduce the risk of injury. PMAs are lightweight and have a high power/weight ratio. Compliant actuation of rehabilitation robots is an emerging area of research, and this work adds a new dimension in this area of research.

7.1.5 Nonlinear Model Predictive Control

The control scheme of a robotic system plays a crucial role in its operation. The importance is increased multi-fold in the case of a rehabilitation robot as it needs to be efficient as well as safe. Additionally, with the intervention of multiple passive and active degrees of freedom and intrinsically compliant pneumatic actuators, the design of the control system becomes more complicated. Therefore, in this research, a model was created based on the Koopman operator to identify the system dynamics. The Koopman operator eliminates the nonlinearities associated with the system by lifting it to an infinitely dimensional space. Thus, the system dynamics identification issue is simplified, and this model can be used for the design of a nonlinear model predictive controller. Such a controller design for a lower limb robotic orthosis with multiple active and passive degrees of freedom has not been recorded in the literature prior to this work.

7.2 Limitations

In the mechanism design, due to the design space, the robotic orthosis pelvis section is only designed to achieve passive vertical and lateral translations. To simulate natural human gait, the forward/backward translation and rotations for the pelvis section should also be considered.

In the actuation, pneumatic muscles provided by Festo® can compliantly provide enough torque and force to actuate the rehabilitation robot. However, the contractile length is not sufficient to achieve a larger range of motion. It may cause a decrease in the workspace of the rehabilitation robot.

In the controller, the lag caused at the knee joint can be rectified by increasing the efficiency of the control design. However, the current controller scheme does not account for the user's difficulty level and intention.

For the motion capture system used in experiment, it is only used to evaluate three self-aligning mechanisms and it cannot be used for verifying the gait or correlate the results.

7.3 Future Work

This research developed an intrinsically compliant robotic orthosis for gait rehabilitation capable of performing the major ranges of joint motion while providing joint alignment with gravity-balancing to users. As this research is a multi-disciplinary project that involves fields of mechanical engineering, biomechanics, computer science and physical therapy, there are immense possibilities of improvements in the mechanism design and control aspects of this research. Following are some suggestions for future works.

In the mechanism aspect, toothed cam-couple mechanism and four-bar linkage mechanism can be analysed and improved to be applied in future prototype. Developing other novel designs to achieve better self-alignment with the anatomical joints can be also considered, and the pelvis part can be made in a better bio-inspired way. The limitation in the contractile length of pneumatic muscles could be solved by using different mechanisms to achieve a larger range of motion. In the actuation aspect, a new type of pneumatic muscles with longer contractile length could be considered as a research objective. Development of other compliant actuators could also be an interesting future direction of research. In the control aspect, more efficient controllers can be developed which can provide a better estimate of a user's impairment level and can customise the robot-provided assistance according to the impairment level of each patient. In addition, a better motion capture system could be used for verifying gait or correlate the results to provide better evidence of performance in designed mechanisms. The experimental results could also be obtained from more test subjects with different characteristics to show the reliability of the proposed design. As the ultimate end users will be stroke patients, the laboratory environment and venue will be gradually transformed into a

place suitable for them. At the same time, the safety of experimental equipment and robotic orthosis will also be further tested and improved to ensure the safety of future stroke subjects.

Appendix A – Solution of Forward Kinematics

This section describes the position analysis of the robot from the kinematics perspective. The gait robot discussed here is an open chain mechanism or a serial robot consisting of the hip, knee and ankle joints. The overall positioning system used for robot joints is shown in Figure 5–1 with reference positions on a natural vertical attitude. Point O is referred to as the left-top corner of the pelvis part with the $x - y - z$ directions of the reference coordinate system shown in Figure 5–1. L_1 is referred to as the vertical dimension between Point O and the left hip joint in the design, while L_2 is represented as the width of the gait robot (distance between two hip joints). L_3 is the length of the thigh segment on the robot (distance between hip and knee joints) and L_4 is the shank length (distance between knee and ankle joints). S_1 to S_8 represent the motion of joints depending on the degrees of freedom on designed joints. S_3, S_5 and S_8 are translation motions facilitating the self-aligning of robot and human joints in the designed prototype.

Screw theory is used to derive forward and inverse kinematics. Table 5–1 shows the parameters used in the current positional analysis. Three coordinates in S_i column represented by S_x, S_y and S_z respectively refer to the type of motions each joint can achieve (Figure 5–1). Further, S_{ox}, S_{oy} and S_{oz} describe the positions of joints relative to the global coordinate system. These parameters are used in equations of screw theory to obtain transformation matrices.

The elements described in Table 5–2 are used to calculate each element in eight homogenous transformation matrices to be used for the eight joints. Here, $C\Theta$ stands for cosΘ and SΘ is used in place of SinΘ. Parameters in Table 5–1 are substituted into relations provided in Table 5–2 to derive transformation matrices. While calculating

$a_{14}, a_{24}, and\ a_{34}$, the value of t is considered to be zero. The homogenous transformation matrices A_1 to A_8 are expressed as $(A1 - A8)$.

$$A_1 = \begin{bmatrix} C\Theta_1 & 0 & S\Theta_1 & L_1 S\Theta_1 \\ 0 & 1 & 0 & 0 \\ -S\Theta_1 & 0 & C\Theta_1 & L_1 C\Theta_1 - L_1 \\ 0 & 0 & 0 & 1 \end{bmatrix}$$

$$A_2 = \begin{bmatrix} 1 & 0 & 0 & 0 \\ 0 & C\Theta_2 & -S\Theta_2 & L_2 - L_2 C\Theta_2 - L_1 S\Theta_2 \\ 0 & S\Theta_2 & C\Theta_2 & -L_2 S\Theta_2 + L_1 C\Theta_2 - L_1 \\ 0 & 0 & 0 & 1 \end{bmatrix}$$

$$A_3 = \begin{bmatrix} 1 & 0 & 0 & 0 \\ 0 & 1 & 0 & 0 \\ 0 & 0 & 1 & d_3 \\ 0 & 0 & 0 & 1 \end{bmatrix}$$

$$A_4 = \begin{bmatrix} C\Theta_4 & 0 & S\Theta_4 & L_1 S\Theta_4 + L_3 S\Theta_4 \\ 0 & 1 & 0 & 0 \\ -S\Theta_4 & 0 & C\Theta_4 & L_1 C\Theta_4 + L_3 C\Theta_4 - L_1 - L_3 \\ 0 & 0 & 0 & 1 \end{bmatrix}$$

$$A_5 = \begin{bmatrix} 1 & 0 & 0 & 0 \\ 0 & 1 & 0 & 0 \\ 0 & 0 & 1 & d_5 \\ 0 & 0 & 0 & 1 \end{bmatrix}$$

$$A_6 = \begin{bmatrix} C\Theta_6 & -S\Theta_6 & 0 & L_2 S\Theta_6 \\ S\Theta_6 & C\Theta_6 & 0 & L_2 - L_2 C\Theta_6 \\ 0 & 0 & 1 & 0 \\ 0 & 0 & 0 & 1 \end{bmatrix}$$

$$A_7 = \begin{bmatrix} C\Theta_7 & 0 & S\Theta_7 & L_1 S\Theta_7 + L_3 S\Theta_7 + L_4 S\Theta_7 \\ 0 & 1 & 0 & 0 \\ -S\Theta_7 & 0 & C\Theta_7 & (L_1 + L_3 + L_4) C\Theta_7 - L_1 - L_3 - L_4 \\ 0 & 0 & 0 & 1 \end{bmatrix}$$

$$A_8 = \begin{bmatrix} 1 & 0 & 0 & 0 \\ 0 & 1 & 0 & 0 \\ 0 & 0 & 1 & d_8 \\ 0 & 0 & 0 & 1 \end{bmatrix}$$

Table A–1. Elements of the Homogeneous Transformation Matrix.

a_{11}	$-S(\theta_7)*(C(\theta_6)*(C(\theta_1)*C(\theta_4)-C(\theta_2)*S(\theta_1)*S(\theta_4))+S(\theta_1)*S(\theta_2)*S(\theta_6))-C(\theta_7)*(C(\theta_1)*S(\theta_4)+C(\theta_2)*C(\theta_4)*S(\theta_1))$
a_{12}	$C(\theta_6)*S(\theta_1)*S(\theta_2)-S(\theta_6)*(C(\theta_1)*C(\theta_4)-C(\theta_2)*S(\theta_1)*S(\theta_4))$
a_{13}	$C(\theta_7)*(C(\theta_6)*C(\theta_1)*C(\theta_4)-C(\theta_2)*S(\theta_1)*S(\theta_4))+S(\theta_1)*S(\theta_2)*S(\theta_6))-S(\theta_7)*(C(\theta_1)*S(\theta_4)+C(\theta_2)*C(\theta_4)*S(\theta_1))$
a_{14}	$d_3*C(\theta_2)*S(\theta_1)-L_4*C(\theta_1)*S(\theta_4)-L_3*C(\theta_2)*S(\theta_1)+d_5*C(\theta_1)*S(\theta_4)-L_4*C(\theta_2)*C(\theta_4)*S(\theta_1)+d_5*C(\theta_2)*C(\theta_4)*S(\theta_1)+d_8*C(\theta_1)*C(\theta_7)*S(\theta_4)+d_8*C(\theta_2)*C(\theta_4)*C(\theta_7)*S(\theta_1)+d_8*C(\theta_1)*C(\theta_4)*C(\theta_6)*S(\theta_7)+d_8*S(\theta_1)*S(\theta_2)*S(\theta_6)*S(\theta_7)-d_8*C(\theta_2)*C(\theta_6)*S(\theta_1)*S(\theta_4)*S(\theta_7)$
a_{21}	$C(\theta_4)*C(\theta_7)*S(\theta_2)-S(\theta_7)*(C(\theta_2)*S(\theta_6)+C(\theta_6)*S(\theta_2)*S(\theta_4))$
a_{22}	$C(\theta_2)*C(\theta_6)-S(\theta_2)*S(\theta_4)*S(\theta_6)$
a_{23}	$C(\theta_7)*(C(\theta_2)*S(\theta_6)+C(\theta_6)*S(\theta_2)*S(\theta_4))+C(\theta_4)*S(\theta_2)*S(\theta_7)$
a_{24}	$L_2+L_3*S(\theta_2)-d_3*S(\theta_2)+L_4*C(\theta_4)*S(\theta_2)-d_5*C(\theta_4)*S(\theta_2)-d_8*C(\theta_4)*C(\theta_7)*S(\theta_2)+d_8*C(\theta_2)*S(\theta_6)*S(\theta_7)+d_8*C(\theta_6)*S(\theta_2)*S(\theta_4)*S(\theta_7)$
a_{31}	$S(\theta_7)*(C(\theta_6)*(C(\theta_4)*S(\theta_1)+C(\theta_1)*C(\theta_2)*S(\theta_4))-C(\theta_1)*S(\theta_2)*S(\theta_6))+C(\theta_7)*(S(\theta_1)*S(\theta_4)-C(\theta_1)*C(\theta_2)*C(\theta_4))$
a_{32}	$S(\theta_6)*(C(\theta_4)*S(\theta_1)+C(\theta_1)*C(\theta_2)*S(\theta_4))+C(\theta_1)*C(\theta_6)*S(\theta_2)$
a_{33}	$S(\theta_7)*(S(\theta_1)*S(\theta_4)-C(\theta_1)*C(\theta_2)*C(\theta_4))-C(\theta_7)*(C(\theta_6)*(C(\theta_4)*S(\theta_1)+C(\theta_1)*C(\theta_2)*S(\theta_4))-C(\theta_1)*S(\theta_2)*S(\theta_6))$
a_{34}	$d_3*C(\theta_1)*C(\theta_2)-L_3*C(\theta_1)*C(\theta_2)-L_1+L_4*S(\theta_1)*S(\theta_4)-d_5*S(\theta_1)*S(\theta_4)-L_4*C(\theta_1)*C(\theta_2)*C(\theta_4)+d_5*C(\theta_1)*C(\theta_2)*C(\theta_4)-d_8*C(\theta_7)*S(\theta_1)*S(\theta_4)+d_8*C(\theta_1)*C(\theta_2)*C(\theta_4)*C(\theta_7)-d_8*C(\theta_4)*C(\theta_6)*S(\theta_1)*S(\theta_7)+d_8*C(\theta_1)*S(\theta_2)*S(\theta_6)*S(\theta_7)-d_8*C(\theta_1)*C(\theta_2)*C(\theta_6)*S(\theta_4)*S(\theta_7)$

Appendix B – Dynamic Modelling

Differential response of equations (5.8) and (5.9) can be derived as:

$$dy(t) = \frac{F_p(\tau)d\tau}{m\omega_d} e^{-\xi\omega(t-\tau)} sin\omega_d(t-\tau) \qquad (B.1)$$

Where τ represents torque.

And displacement response can be derived as:

$$y(t) = \frac{1}{m\omega_d}\int_0^t F_p(\tau)\, e^{-\xi\omega(t-\tau)} sin\omega_d(t-\tau)d\boldsymbol{\tau} \qquad (B.2)$$

Initial conditions are determined as $y(0) = y_0$ and $v(0) = v_0$. So, the solution can be derived as:

$$y(t) = e^{-\xi\omega(t-\tau)}(y_0 cos\omega_d t + \frac{v_0 + \xi w_d y_0}{\omega_d} sin\omega_d t + \frac{1}{m\omega_d}\int_0^t F_p(\tau)\, e^{-\xi\omega(t-\tau)} sin\omega_d(t-\tau) \qquad (B.3)$$

Equation (5.9) shows that damping has little effect on the maximum displacement response under impact load.

Damping displacement response under suddenly applied load can also be derived by applying the Duhamel integral which is shown as equation (B.4):

$$y(t) = \frac{1}{m\omega_d}\int_0^t F_{p0}\, e^{-\xi\omega(t-\tau)} sin\omega_d(t-\tau)d\boldsymbol{\tau} \qquad (B.4)$$

Under this condition, the displacement response will be:

$$y(t) = \frac{F_{p0}}{m\omega^2}[1 - e^{-\xi\omega t}\left(cos\omega_d t + \frac{\xi\omega}{\omega_d} sin\omega_d t\right] = y_{st}\left[1 - e^{-\xi\omega t}\left(cos\omega_d t + \frac{\xi\omega}{\omega_d} sin\omega_d t\right)\right] \qquad (B.5)$$

When $t = \frac{\pi}{\omega_d}$, displacement will be in maximum value as:

$$y_{max} = y_{st}\left(1 + e^{-\frac{\xi\omega t}{\omega_d}}\right) \tag{B.6}$$

The dynamic coefficient can be expressed as:

$$\mu = \frac{y_{max}}{y_{st}}\left(1 + e^{-\frac{\xi\omega t}{\omega_d}}\right) \tag{B.7}$$

And it can be approximately calculated as:

$$\mu \approx 1 + e^{-\xi\pi} \tag{B.8}$$

The damping displacement response under harmonic load can be expressed as:

$$\ddot{y} + 2\xi\omega\dot{y} + \omega^2 y = \frac{F}{m}sin\Theta t \tag{B.9}$$

The general solution of equation (B.9) can be derived as:

$$y(t) = e^{-\xi\omega t}(C_1 cos\omega_d t + C_2 sin\omega_d t) + (A_1 sin\Theta_t + A_2 cos\Theta_t) \tag{B.10}$$

In this case, the steady state response can be simply expressed as:

$$y(t) = Asin(\Theta_t - \alpha) \tag{B.11}$$

Where $A = \frac{F}{m\omega^2}\frac{1}{\sqrt{\left(1-\frac{\Theta^2}{\omega^2}\right)+4\xi^2\frac{\Theta^2}{\omega^2}}} = y_{st}\mu$ and $\alpha = tan^{-1}(\frac{2\xi\frac{\Theta}{\omega}}{1-\frac{\Theta^2}{\omega^2}})$. Thus, the dynamic coefficient for the steady state response can be derived as:

$$\mu = \frac{1}{\sqrt{\left(1 - \frac{\Theta^2}{\omega^2}\right) + 4\xi^2\frac{\Theta^2}{\omega^2}}} \tag{B.12}$$

Depending on the equation (B.12), it is easy to find that μ is relevant to the frequency ratio $\frac{\Theta}{\omega}$ and damping ratio $\boldsymbol{\xi}$. Dynamic coefficient μ rapidly decreases when the damping ratio

increases. When the frequency ratio $\frac{\theta}{\omega}$ is close to 1, the peak value of μ decreases significantly. If the damping ratio $\frac{\theta}{\omega}$ is exactly 1, $\mu = \frac{1}{2\xi}$ and $\mu_{max} \frac{1}{2\xi\sqrt{1-\xi^2}}$. The dynamic displacement will be delayed by one phase angle compared to the dynamic load.

When the $\frac{\theta}{\omega}$ tends to be zero, y(t) and $F_p(t)$ tends to be in same direction, in other words, dynamic load is mainly balanced by restoring force itself (similar to static effect).

When the $\frac{\theta}{\omega}$ tends to be infinite, $\boldsymbol{\alpha}$ tends to be π, so the y(t) and $F_p(t)$ tend to be in reverse. In this case, dynamic loads are mainly balanced by inertial forces.

When the $\frac{\theta}{\omega}$ tends to be 1, $\boldsymbol{\alpha}$ tends to be $tan^{-1}(2\xi)$ which is approximately equal to π/2. Thus, equation 5.10 to 5.12 can be expressed as section 5.3 shows.

Appendix C – Ethics Approval

UNIVERSITY OF CANBERRA

DISTINCTIVE BY DESIGN

Participant Information Form

Project Title

Development of a Gait Rehabilitation Robot for Stroke Patients

Researcher

Name: Yinan Jin
Faculty: Faculty of Science and Technology
Email: u3208626@uni.canberra.edu.au

Supervisor

Name: A/Prof. Shahid Hussain
Phone: +61 2 62068408
Email: shahid.hussain@canberra.edu.au

Co-Supervisor

Name: Prof. Roland Goecke
Phone: +61 2 62012114
Email: roland.goecke@canberra.edu.au

Project Aim

This research mainly aims to develop an intrinsically compliant robotic orthosis for gait rehabilitation capable of performing the major ranges of joint motion while providing joint alignment with gravity balancing to the patients in the training process.

General Outline of the Project

Participant will only be required to take part in one experimental trial. The duration of the trial is expected to span approximately 45 minutes. The experimental trial will be carried out in the HDR Technology Library in the University of Canberra.

Before the experimental trials begin, participant will be explained the operation of the robotic devices, the safety measures put in place to allow termination of the robot operation should an emergency arise. A brief demonstration of the prototype will also be given. Participant's age, gender and body weight will also be collected so that the results can be normalized with respect to the body weight and related to the corresponding demographic groups. Participant's range of motion of the lower limbs will be measured to ensure participant has normal range of motion. After the briefing and collection of information, participant's lower limbs will be strapped in place on the prototype device, and participant will be asked to start walking on the treadmill. The experimental trials consist of two parts, the first involves the passive movement of the lower limb by the robotic

device. During this part of the trial, participant should relax lower limb on the robotic device and allow the robot to move the limbs passively along a predefined motion path. During this time, information regarding the orientation of the lower limbs and the forces applied on the robot will be logged and analysed.

In the second part of the trial, participant will be asked to walk in a direction directed by the user interface. Using the treadmill armrests, participant is required to walk by himself/herself. The robot will provide a resistance against the motion during this part of the trial. Again, sensor information on the robotic device will be logged and analysed.

As discussed before, data collected will be in the form of sensor readings which are used to compute the motion and force/moment observed during the experimental trial. This information will also be used to identify properties of the participant's lower limbs. Additionally, participant's age, gender and body weight will also be recorded.

Funding has been obtained for the research. Faculty of Science and Technology, University of Canberra has provided the required funding of A$14,554 for this research in 2020.

Participant Involvement

Participant are invited to participate in this research by carrying a series of exercises using a prototype of designed gait rehabilitation device. Potential participant in this research is chosen from colleagues of the researcher who are healthy individuals over the age of 18 and have no existing neurological impairment caused by stroke. It is preferred that participant are familiar or comfortable with the operation of robotic devices. Participant will be shown the experimental setup and briefed about the operation of the prototype prior to Participant's commitment to participation in this research. Participant's identity will be kept anonymous from third parties.

Participation in the research is completely voluntary and participant may, without any penalty, decline to take part or withdraw at any time without providing an explanation or refuse to answer a question.

Benefits of Participation

There is a small chance where anomaly may be found in the data collected regarding the characteristics of participant's lower limb. Should this occur, participant will be informed and should consult a qualified health professional to verify such findings.

Risks of Participation

Participant may experience a small level of physical discomfort during a normal trial. However, should the level of discomfort exceed that of the participant's liking, participant can terminate the experimental trial by either indicating to the researcher or by using the emergency stop button provided. Since the actuators used in the prototype can produce significant forces, there is a possibility of injury should the hardware or software of the prototype malfunctions. This will be very unlikely as the prototype would have been tested extensively before the commencement of the experimental trial. In addition to that, the researcher will be present to provide aid if

required. Along with the researcher, Mr. Jamie Plowman, the Laboratory engineer will be present during the experiment procedure. He is also a certified first aid officer. To ensure that prompt medical attention is available during emergencies, the trials will be conducted during the operating hours of the University of Canberra clinic.

Confidentiality & Anonymity

Participant's identity will be kept anonymous from all third parties. If the data collected is used in publications, participant will be referred to using a generic identifier such as "subject A".

Participation in this research is entirely voluntary. Assurance from the head of department has been obtained such that neither participant's grades nor relations with the university will be affected by agreement/refusal to participate in this research.

Data Storage

All data will be stored electronically on a computer hard drive kept in a secure location. The data will be stored in such a way that a third party will not be able to identify the participant through the information stored on the data file. The information collected will be kept for a period of up to five years as reference for current and possibly future research. The data can be used for future projects. When no longer required, such data files will be destroyed through permanent deletion. If participant is interested, participant can also arrange with the researcher a suitable time to discuss any information derived from offline analysis of the collected data.

With participant's permission, a photograph/video of the experimental trial may also be taken using an electronic device. The photograph/video of the trial will also be stored electronically on a hard drive kept in a secure location. The video will be taken in such a way that it will provide minimal features which can be used to reveal participant's identity.

Future Research

If participant agree, the information collected during the conduct of this research may be used in future research projects on related research areas. Any future use of data will comply with any conditions imposed by the Human Research Ethics Committee of the University of Canberra

Ethics Committee Clearance

The project has been approved by the Human Research Ethics Committee of the University of Canberra (HREC – 10399).

Queries and Concerns

Queries or concerns regarding the research can be directed to the researcher and/or supervisor.
Contact details are at the top of this form.
If you have any complaints or reservations about the ethical conduct of this research, you may contact the University of Canberra's Research Ethics & Integrity Unit team via telephone 02 6206 3916 or email humanethicscommittee@canberra.edu.au or researchethicsandintegrity@canberra.edu.au

If you would like some guidance on the questions you could ask about your participation please refer to the Participant's Guide located at http://www.canberra.edu.au/ucresearch/attachments/pdf/a-m/Agreeing-to-participate-in-research.pdf

Appendix D – Consent Forms

UNIVERSITY OF CANBERRA
Faculty of Science & Technology
University of Canberra
Bruce, ACT – 2617
Australia

CONSENT FORM

(Participants)

THIS FORM WILL BE HELD FOR A PERIOD OF 5 YEARS

Project title: Development of a Gait Rehabilitation Robot for Stroke Patients
Name(s) of Researchers(s): Yinan Jin, A/Prof. Shahid Hussain, Prof. Roland Goecke

I have read the Participant Information Sheet; have understood the nature of the research and why I have been selected. I have had the opportunity to ask questions and have them answered to my satisfaction. I have chosen to participate in this research on a voluntary basis.

- I agree to take part in this research
- I understand that participation in this research will require physical interaction with a prototype robotic device. I will be guided to walk on a treadmill by the device which has been explained to me.
- I understand that there is a slight possibility of injury should the prototype device malfunction, and I accept this risk. I can press the emergency button to stop the device whenever necessary.
- The emergency button has been shown to me.
- I understand that my identity will not be revealed in publications derived from this research.
- I understand that the information related to the experimental trial which I am involved in will be recorded using sensors on the prototype device and stored electronically with secure access.
- I understand that I am free to withdraw my participation at any time.
- I understand that participation in this research will not affect my grades or my relations with the university (where applicable).
- I agree/do not agree to be videotaped.
- I understand that the data will be kept for five years, after which they will be destroyed permanently.
- I understand that I am only required to attend one experimental trial.
- I agree to be informed of any incidental findings that arise from this research.

Name YINAN JIN

Signature 金燚男 Date 18/04/2022

UNIVERSITY OF CANBERRA
Faculty of Science & Technology
University of Canberra
Bruce, ACT – 2617
Australia

CONSENT FORM

(Participants)

THIS FORM WILL BE HELD FOR A PERIOD OF 5 YEARS

Project title: Development of a Gait Rehabilitation Robot for Stroke Patients
Name(s) of Researchers(s): Yinan Jin, A/Prof. Shahid Hussain, Prof. Roland Goecke

I have read the Participant Information Sheet; have understood the nature of the research and why I have been selected. I have had the opportunity to ask questions and have them answered to my satisfaction. I have chosen to participate in this research on a voluntary basis.

- I agree to take part in this research
- I understand that participation in this research will require physical interaction with a prototype robotic device. I will be guided to walk on a treadmill by the device which has been explained to me.
- I understand that there is a slight possibility of injury should the prototype device malfunction, and I accept this risk. I can press the emergency button to stop the device whenever necessary.
- The emergency button has been shown to me.
- I understand that my identity will not be revealed in publications derived from this research.
- I understand that the information related to the experimental trial which I am involved in will be recorded using sensors on the prototype device and stored electronically with secure access.
- I understand that I am free to withdraw my participation at any time.
- I understand that participation in this research will not affect my grades or my relations with the university (where applicable).
- I agree/do not agree to be videotaped.
- I understand that the data will be kept for five years, after which they will be destroyed permanently.
- I understand that I am only required to attend one experimental trial.
- I agree to be informed of any incidental findings that arise from this research.

Name TANISHKA GOYAL

Signature Tanishka Date 16 Aug 2022

UNIVERSITY OF CANBERRA
Faculty of Science & Technology
University of Canberra
Bruce, ACT – 2617
Australia

CONSENT FORM

(Participants)

THIS FORM WILL BE HELD FOR A PERIOD OF 5 YEARS

Project title: Development of a Gait Rehabilitation Robot for Stroke Patients
Name(s) of Researchers(s): Yinan Jin, A/Prof. Shahid Hussain, Prof. Roland Goecke

I have read the Participant Information Sheet; have understood the nature of the research and why I have been selected. I have had the opportunity to ask questions and have them answered to my satisfaction. I have chosen to participate in this research on a voluntary basis.

- I agree to take part in this research
- I understand that participation in this research will require physical interaction with a prototype robotic device. I will be guided to walk on a treadmill by the device which has been explained to me.
- I understand that there is a slight possibility of injury should the prototype device malfunction, and I accept this risk. I can press the emergency button to stop the device whenever necessary.
- The emergency button has been shown to me.
- I understand that my identity will not be revealed in publications derived from this research.
- I understand that the information related to the experimental trial which I am involved in will be recorded using sensors on the prototype device and stored electronically with secure access.
- I understand that I am free to withdraw my participation at any time.
- I understand that participation in this research will not affect my grades or my relations with the university (where applicable).
- I agree/do not agree to be videotaped.
- I understand that the data will be kept for five years, after which they will be destroyed permanently.
- I understand that I am only required to attend one experimental trial.
- I agree to be informed of any incidental findings that arise from this research.

Name Fahad Hussain

Signature Fahad Date 10/10/2022

UNIVERSITY OF CANBERRA
Faculty of Science & Technology
University of Canberra
Bruce, ACT – 2617
Australia

CONSENT FORM

(Participants)

THIS FORM WILL BE HELD FOR A PERIOD OF 5 YEARS

Project title: Development of a Gait Rehabilitation Robot for Stroke Patients
Name(s) of Researchers(s): Yinan Jin, A/Prof. Shahid Hussain, Prof. Roland Goecke

I have read the Participant Information Sheet; have understood the nature of the research and why I have been selected. I have had the opportunity to ask questions and have them answered to my satisfaction. I have chosen to participate in this research on a voluntary basis.

- I agree to take part in this research
- I understand that participation in this research will require physical interaction with a prototype robotic device. I will be guided to walk on a treadmill by the device which has been explained to me.
- I understand that there is a slight possibility of injury should the prototype device malfunction, and I accept this risk. I can press the emergency button to stop the device whenever necessary.
- The emergency button has been shown to me.
- I understand that my identity will not be revealed in publications derived from this research.
- I understand that the information related to the experimental trial which I am involved in will be recorded using sensors on the prototype device and stored electronically with secure access.
- I understand that I am free to withdraw my participation at any time.
- I understand that participation in this research will not affect my grades or my relations with the university (where applicable).
- I agree/do not agree to be videotaped.
- I understand that the data will be kept for five years, after which they will be destroyed permanently.
- I understand that I am only required to attend one experimental trial.
- I agree to be informed of any incidental findings that arise from this research.

Name [illegible]

Signature [illegible] Date 03 05 2022

Appendix E – Publications and Submissions

1. A research paper entitled *'Design and Analysis of a Multi-DOF Compliant Gait Rehabilitation Robot'* is published in Mechanics Based Design of Structure and Machines, An International Journal.

Authors: Yinan Jin, Prashant K. Jamwal, Roland Goecke, Mergen H. Ghayesh, and Shahid Hussain

DOI: 10.1080/15397734.2023.2215855

The content of this research paper is used in Chapter 3 and Chapter 5.

2. A research paper entitled *'Non-Linear MPC Design for a Self-Aligning Compliant Gait Rehabilitation Robot'* is submitted to IEEE/ASME Transactions on Mechatronics.

Authors: Yinan Jin, Tanishka Goyal, Prashant K. Jamwal, Roland Goecke, Mergen H. Ghayesh, and Shahid Hussain.

The content of this research paper is used in Chapter 6.

References

1. Vitiello, N., et al., *NEUROExos: A Powered Elbow Exoskeleton for Physical Rehabilitation.* IEEE Transactions on Robotics, 2013. **29**: p. 220-235.
2. WHO, *World Health Statistics 2022*. 2022: https://www.who.int/data/gho/publications/world-health-statistics.
3. Ingall, T., *Stroke-incidence, mortality, morbidity and risk.* Journal of insurance medicine (New York, N.Y.), 2004. **36**: p. 143-52.
4. Tsao, C., et al., *Heart Disease and Stroke Statistics-2023 Update: A Report From the American Heart Association.* Circulation, 2023. **147**.
5. Di Carlo, A., *Human and economic burden of stroke.* Age and ageing, 2009. **38**: p. 4-5.
6. Hussain, S., S. Xie, and G. Liu, *Robot assisted treadmill training: Mechanisms and training strategies.* Medical engineering & physics, 2011. **33**: p. 527-33.
7. Reinkensmeyer, D., J. Emken, and S. Cramer, *Robotics, Motor Learning, and Neurologic Recovery.* Annual review of biomedical engineering, 2004. **6**: p. 497-525.
8. Ackermann, M. and A. van den Bogert, *Predictive simulation of gait at low gravity reveals skipping as the preferred locomotion strategy.* Journal of biomechanics, 2012. **45**: p. 1293-8.
9. Tattersall, T., et al., *Imagined gait modulates neuronal network dynamics in the human pedunculopontine nucleus.* Nature neuroscience, 2014. **17**.
10. Hussain, S. *Design and Assist-as-Needed Control of an Intrinsically Compliant Robotic Orthosis for Gait Rehabilitation*. 2012.
11. Umberger, B., *Stance and swing phase costs in human walking.* Journal of the Royal Society, Interface / the Royal Society, 2010. **7**: p. 1329-40.
12. Zinn, M., et al., *A new actuation approach for human friendly robot design.* International Journal of Robotics Research, 2004. **23**(4-5): p. 379-398.

13. WALSH, C.J., *Biomimetic Design of an Under-Actuated Leg Exoskeleton For Load-Carrying Augmentation.* 2006.

14. Colombo, G., et al., *Treadmill training of paraplegic patients using a robotic orthosis.* Journal of rehabilitation research and development, 2000. **37**: p. 693-700.

15. Behrman, A. and S. Harkema, *Locomotor Training After Human Spinal Cord Injury: A Series of Case Studies.* Physical therapy, 2000. **80**: p. 688-700.

16. Finch, L., H. Barbeau, and B. Arsenault, *Influence of Body Weight Support on Normal Human Gait: Development of a Gait Retraining Strategy.* Physical therapy, 1991. **71**: p. 842-55; discussion 855.

17. Roy, A., et al., *Robot-Aided Neurorehabilitation: A Novel Robot for Ankle Rehabilitation.* IEEE Transactions on Robotics, 2009. **25**: p. 569-582.

18. Hussain, S., S.Q. Xie, and G. Liu, *Robot assisted treadmill training: Mechanisms and training strategies.* Medical Engineering & Physics, 2011. **33**(5): p. 527-533.

19. Hussain, S., *"State-of-the-Art Robotic Gait Rehabilitation Orthoses: Design and Control Aspects,"* NeuroRehabilitatin, 2014. **35**: p. 701-709.

20. McCrory, B., A. Harlow, and J. Burnfield, *Musculoskeletal Risk to Physical Therapists during Overground Gait Training: A Case Report.* Proceedings of the Human Factors and Ergonomics Society Annual Meeting, 2014. **58**: p. 1219-1223.

21. Falavigna, A., et al., *Increased prevalence of low back pain among physiotherapy students compared to medical students.* European spine journal : official publication of the European Spine Society, the European Spinal Deformity Society, and the European Section of the Cervical Spine Research Society, 2010. **20**: p. 500-5.

22. Jamwal, P.K., S. Hussain, and M. Ghayesh, *Robotic orthoses for gait rehabilitation: An overview of mechanical design and control strategies.* Proceedings of the Institution of

Mechanical Engineers, Part H: Journal of Engineering in Medicine, 2020. **234**: p. 095441191989829.

23. Carlo, A., *Human and Economic Burden of Stroke* Age and Aging, 2009. **38**: p. 4-5.
24. Young, A.J. and D.P. Ferris, *State of the Art and Future Directions for Lower Limb Robotic Exoskeletons.* IEEE Trans Neural Syst Rehabil Eng, 2017. **25**(2): p. 171-182.
25. Marchal-Crespo, L., *Review of control strategies for robotic movement training after neurologic injury.* J. Neuroeng. Rehabil., 2007. **14**: p. 22-44.
26. Ramirez-Bautista, J.A., et al., *Review on plantar data analysis for disease diagnosis.* Biocybernetics and Biomedical Engineering, 2018. **38**(2): p. 342-361.
27. Ramirez-Bautista, J.A., et al., *A Review in Detection and Monitoring Gait Disorders Using In-Shoe Plantar Measurement Systems.* IEEE Reviews in Biomedical Engineering, 2017. **10**: p. 299-309.
28. Reinkensmeyer, D.J., J.L. Emken, and S.C. Cramer, *Robotics, motor learning, and neurologic recovery.* Annual Review of Biomedical Engineering, 2004. **6**: p. 497-525.
29. Hogan, N., et al., *Motions or muscles? Some behavioral factors underlying robotic assistance of motor recovery.* Journal of rehabilitation research and development, 2006. **43**: p. 605-18.
30. Huang, J., X. Tu, and J. He, *Design and Evaluation of the RUPERT Wearable Upper Extremity Exoskeleton Robot for Clinical and In-Home Therapies.* IEEE Transactions on Systems, Man, and Cybernetics: Systems, 2016. **46**(7): p. 926-935.
31. Jamwal, P.K. and S. Hussain, *Multicriteria Design Optimization of a Parallel Ankle Rehabilitation Robot: Fuzzy Dominated Sorting Evolutionary Algorithm Approach.* IEEE Transactions on Systems, Man, and Cybernetics: Systems, 2016. **46**(5): p. 589-597.

32. Jamwal, P.K., et al., *Impedance Control of an Intrinsically Compliant Parallel Ankle Rehabilitation Robot.* IEEE Transactions on Industrial Electronics, 2016. **63**(6): p. 3638-3647.

33. Chaparro-Cárdenas, S.L., et al., *A review in gait rehabilitation devices and applied control techniques.* Disability and Rehabilitation: Assistive Technology, 2018. **13**(8): p. 819-834.

34. Vallery, H., et al., *Compliant actuation of rehabilitation robots.* Robotics & Automation Magazine, IEEE, 2008. **15**: p. 60-69.

35. Zoss, A.B., H. Kazerooni, and A. Chu, *Biomechanical design of the Berkeley lower extremity exoskeleton (BLEEX).* IEEE/ASME Transactions on Mechatronics, 2006. **11**(2): p. 128-138.

36. Cempini, M., et al., *Self-alignment mechanisms for assistive wearable robots: A kinetostatic compatibility method.* IEEE Transactions on Robotics, 2013. **29**(1): p. 236-250.

37. Schiele, A. and F.C.T. Van Der Helm, *Kinematic design to improve ergonomics in human machine interaction.* IEEE Transactions on Neural Systems and Rehabilitation Engineering, 2006. **14**(4): p. 456-469.

38. Wang, D., et al., *Adaptive knee joint exoskeleton based on biological geometries.* IEEE/ASME Transactions on Mechatronics, 2014. **19**(4): p. 1268-1278.

39. Giovacchini, F., et al., *A light-weight active orthosis for hip movement assistance.* Robotics and Autonomous Systems, 2015. **73**: p. 123-134.

40. Hyun, D.J., et al., *Biomechanical design of an agile, electricity-powered lower-limb exoskeleton for weight-bearing assistance.* Robotics and Autonomous Systems, 2017. **95**: p. 181-195.

41. Junius, K., et al., *Bilateral, Misalignment-Compensating, Full-DOF Hip Exoskeleton: Design and Kinematic Validation.* Applied Bionics and Biomechanics, 2017. **2017**.

42. Saccares, L., I. Sarakoglou, and N.G. Tsagarakis. *It-knee: An exoskeleton with ideal torque transmission interface for ergonomic power augmentation*. in *IEEE International Conference on Intelligent Robots and Systems*. 2016.

43. Cempini, M., M. Cortese, and N. Vitiello, *A powered finger-thumb wearable hand exoskeleton with self-aligning joint axes.* IEEE/ASME Transactions on Mechatronics, 2015. **20**(2): p. 705-716.

44. Perry, J.C., J. Rosen, and S. Burns, *Upper-limb powered exoskeleton design.* IEEE/ASME Transactions on Mechatronics, 2007. **12**(4): p. 408-417.

45. Stienen, A.H.A., et al., *Self-Aligning Exoskeleton Axes Through Decoupling of Joint Rotations and Translations.* IEEE Transactions on Robotics, 2009. **25**(3): p. 628-633.

46. Stienen, A.H.A., et al., *Self-Aligning Exoskeleton Axes Through Decoupling of Joint Rotations and Translations.* IEEE Transactions on Robotics, 2009. **25**(3): p. 628-633.

47. Otten, A., et al., *LIMPACT:A Hydraulically Powered Self-Aligning Upper Limb Exoskeleton.* IEEE/ASME Transactions on Mechatronics, 2015. **20**(5): p. 2285-2298.

48. Zanotto, D., et al., *Knee Joint Misalignment in Exoskeletons for the Lower Extremities: Effects on User's Gait.* IEEE Transactions on Robotics, 2015. **31**(4): p. 978-987.

49. Cao, J., S.Q. Xie, and R. Das, *MIMO Sliding Mode Controller for Gait Exoskeleton Driven by Pneumatic Muscles.* IEEE Transactions on Control Systems Technology, 2018. **26**(1): p. 274-281.

50. Winter, D.A., *Biomechanics and Motor Control of Human Movement*. 2009: Wiley Online Library.

51. Chang, M.K., *An adaptive self-organizing fuzzy sliding mode controller for a 2-DOF rehabilitation robot actuated by pneumatic muscle actuators.* Control Engineering Practice, 2010. **18**(1): p. 13-22.

52. Festo_Corporation. *Fluidic Muscle DMSP*. 2022; Available from: https://www.festo.com/us/en/p/fluidic-muscle-id_DMSP/.

53. Beyl, P., et al., *Design and control of a lower limb exoskeleton for robot-assisted gait training.* Applied Bionics and Biomechanics, 2009. **6**(2): p. 229-243.

54. Huang, M., et al., *An online gain tuning proxy-based sliding mode control using neural network for a gait training robotic orthosis.* Cluster Computing, 2016. **19**(4): p. 1987-2000.

55. Bruder, D., et al., *Modeling and Control of Soft Robots Using the Koopman Operator and Model Predictive Control*. 2019.

56. Bruder, D., et al., *Data-Driven Control of Soft Robots Using Koopman Operator Theory.* IEEE Transactions on Robotics, 2021. **37**(3): p. 948-961.

57. Bruder, D., et al., *Koopman-Based Control of a Soft Continuum Manipulator Under Variable Loading Conditions.* IEEE Robotics and Automation Letters, 2021. **PP**: p. 1-1.

58. Bruder, D., C. Remy, and R. Vasudevan, *Nonlinear System Identification of Soft Robot Dynamics Using Koopman Operator Theory*. 2018.

59. EksoBionics, *How Exoskeletons Are Changing The Construction Industry*. 2021.

60. Aoyagi, D., et al., *A Robot and Control Algorithm That Can Synchronously Assist in Naturalistic Motion During Body-Weight-Supported Gait Training Following Neurologic Injury.* IEEE Transactions on Neural Systems and Rehabilitation Engineering, 2007. **15**(3): p. 387-400.

61. Zanotto, D., P. Stegall, and S.K. Agrawal. *ALEX III: A novel robotic platform with 12 DOFs for human gait training*. in *2013 IEEE International Conference on Robotics and Automation*. 2013.

62. Zitzewitz, J.v., M. Bernhardt, and R. Riener, *A Novel Method for Automatic Treadmill Speed Adaptation.* IEEE Transactions on Neural Systems and Rehabilitation Engineering, 2007. **15**(3): p. 401-409.

63. Frey, M., et al., *A Novel Mechatronic Body Weight Support System.* IEEE Transactions on Neural Systems and Rehabilitation Engineering, 2006. **14**(3): p. 311-321.

64. Colombo, G., et al., *Treadmill training of paraplegic patients using a robotic orthosis.* Journal of Rehabilitation Research and Development, 2000. **37**(6): p. 693-700.

65. Schmidt, H., et al., *Gait rehabilitation machines based on programmable footplates.* Journal of NeuroEngineering and Rehabilitation, 2007. **4**(1): p. 2.

66. Bogey, R. and T.G. Hornby, *Gait Training Strategies Utilized in Poststroke Rehabilitation: Are We Really Making a Difference?* Topics in stroke rehabilitation, 2007. **14**: p. 1-8.

67. Fisher, S., L. Lucas, and T. Thrasher, *Robot-Assisted Gait Training for Patients with Hemiparesis Due to Stroke.* Topics in stroke rehabilitation, 2011. **18**: p. 269-76.

68. D.B Reynolds, D.W.R., C. A. Phillips and G. Bandry, *Modeling the Dynamic Characteristics of Pneumatic Muscle.* Annals of Biomedical Engineering, 2003. **31**: p. 310-317.

69. Banala, S.K., et al., *Gravity-Balancing Leg Orthosis and Its Performance Evaluation.* IEEE Transactions on Robotics, 2006. **22**(6): p. 1228-1239.

70. Agrawal, S.K., et al., *Assessment of Motion of a Swing Leg and Gait Rehabilitation With a Gravity Balancing Exoskeleton.* IEEE Transactions on Neural Systems and Rehabilitation Engineering, 2007. **15**(3): p. 410-420.

71. Banala, S.K., et al., *Robot Assisted Gait Training With Active Leg Exoskeleton (ALEX).* IEEE Transactions on Neural Systems and Rehabilitation Engineering, 2009. **17**(1): p. 2-8.

72. Agrawal, S., et al., *Assessment of Motion of a Swing Leg and Gait Rehabilitation With a Gravity Balancing Exoskeleton.* IEEE transactions on neural systems and rehabilitation engineering : a publication of the IEEE Engineering in Medicine and Biology Society, 2007. **15**: p. 410-20.

73. Banala, S., et al., *Robot assisted gait training with active leg exoskeleton (ALEX). IEEE Trans Neural Syst Rehabil Eng.* IEEE transactions on neural systems and rehabilitation engineering : a publication of the IEEE Engineering in Medicine and Biology Society, 2009. **17**: p. 2-8.

74. Banala, S., et al., *Gravity-Balancing Leg Orthosis and Its Performance Evaluation.* Robotics, IEEE Transactions on, 2007. **22**: p. 1228-1239.

75. Zanotto, D., et al., *Knee Joint Misalignment in Exoskeletons for the Lower Extremities: Effects on User's Gait.* IEEE Transactions on Robotics, 2015. **31**: p. 978-987.

76. Stegall, P., et al., *Rehabilitation Exoskeleton Design: Exploring the Effect of the Anterior Lunge Degree of Freedom.* IEEE Transactions on Robotics, 2013. **29**(4): p. 838-846.

77. Farris, R., et al., *A Preliminary Assessment of Legged Mobility Provided by a Lower Limb Exoskeleton for Persons With Paraplegia.* IEEE transactions on neural systems and rehabilitation engineering : a publication of the IEEE Engineering in Medicine and Biology Society, 2013. **22**.

78. Farris, R., H. Quintero, and M. Goldfarb, *Preliminary Evaluation of a Powered Lower Limb Orthosis to Aid Walking in Paraplegic Individuals.* IEEE transactions on neural

systems and rehabilitation engineering : a publication of the IEEE Engineering in Medicine and Biology Society, 2011. **19**: p. 652-9.

79. Lu, R., et al., *Development and Learning Control of a Human Limb With a Rehabilitation Exoskeleton.* Industrial Electronics, IEEE Transactions on, 2014. **61**: p. 3776-3785.
80. Tanabe, S., S. Hirano, and E. Saitoh, *Wearable Power-Assist Locomotor (WPAL) for supporting upright walking in persons with paraplegia.* NeuroRehabilitation, 2013. **33**.
81. Kagawa, T., et al., *Optimization-Based Motion Planning in Joint Space for Walking Assistance With Wearable Robot.* IEEE Transactions on Robotics, 2015. **31**(2): p. 415-424.
82. Tsukahara, A., et al., *Restoration of Gait for Spinal Cord Injury Patients Using HAL With Intention Estimator for Preferable Swing Speed.* IEEE Transactions on Neural Systems and Rehabilitation Engineering, 2014. **23**.
83. Suzuki, K., et al., *Intention-Based Walking Support for Paraplegia Patients with Robot Suit HAL.* Advanced Robotics, 2007. **21**: p. 1441-1469.
84. Guo, Z., H. Yu, and Y.H. Yin, *Developing a Mobile Lower Limb Robotic Exoskeleton for Gait Rehabilitation.* Journal of Medical Devices, 2014. **8**(4).
85. Veneman, J.F., et al., *A series elastic- and bowden-cable-based actuation system for use as torque actuator in exoskeleton-type robots.* International Journal of Robotics Research, 2006. **25**(3): p. 261-281.
86. Asseldonk, E.H.F.v., et al., *The Effects on Kinematics and Muscle Activity of Walking in a Robotic Gait Trainer During Zero-Force Control.* IEEE Transactions on Neural Systems and Rehabilitation Engineering, 2008. **16**(4): p. 360-370.

87. Veneman, J., et al., *Design and Evaluation of the LOPES Exoskeleton Robot for Interactive Gait Rehabilitation.* Neural Systems and Rehabilitation Engineering, IEEE Transactions on, 2007. **15**: p. 379-386.

88. Meuleman, J., et al., *LOPES II—Design and Evaluation of an Admittance Controlled Gait Training Robot With Shadow-Leg Approach.* IEEE Transactions on Neural Systems and Rehabilitation Engineering, 2016. **24**(3): p. 352-363.

89. Díaz, I., J.J. Gil, and E. Sánchez, *Lower-Limb Robotic Rehabilitation: Literature Review and Challenges.* Journal of Robotics, 2011. **2011**.

90. Schmidt, H., et al., *HapticWalker - a novel haptic foot device.* TAP, 2005. **2**: p. 166-180.

91. Morris, A., et al. *A robotic walker that provides guidance*. in *2003 IEEE International Conference on Robotics and Automation (Cat. No.03CH37422)*. 2003.

92. Yu, H., et al., *Control design of a novel compliant actuator for rehabilitation robots.* Mechatronics, 2013. **23**: p. 1072–1083.

93. Yu, H., et al., *Human–Robot Interaction Control of Rehabilitation Robots With Series Elastic Actuators.* IEEE Transactions on Robotics, 2015. **31**(5): p. 1089-1100.

94. Hussain, S., et al., *An intrinsically compliant robotic orthosis for treadmill training.* Medical engineering & physics, 2012. **34**.

95. Sawicki, G. and D. Ferris, *A pneumatically powered knee-ankle-foot orthosis (KAFO) with myoelectric activation and inhibition.* Journal of neuroengineering and rehabilitation, 2009. **6**: p. 23.

96. Caldwell, D., et al., *"Soft" Exoskeletons for Upper and Lower Body Rehabilitation - Design, Control and Testing.* I. J. Humanoid Robotics, 2007. **4**: p. 549-573.

97. Costa, N. and D.G. Caldwell, *Control of a Biomimetic Soft-actuated 10DoF Lower Body Exoskeleton*. Vol. 8. 0001. 495-501.

98. Awad, L., et al., *A soft robotic exosuit improves walking in patients after stroke.* Science Translational Medicine, 2017. **9**: p. eaai9084.

99. Park, Y.-L., et al., *Design and control of a bio-inspired soft wearable robotic device for ankle-foot rehabilitation.* Bioinspiration & biomimetics, 2014. **9**: p. 016007.

100. Leal Junior, A., R. Andrade, and A. Bento Filho, *Series Elastic Actuator: Design, Analysis and Comparison*. 2016.

101. Mat Dzahir, M.A. and S.-i. Yamamoto, *Recent Trends in Lower-Limb Robotic Rehabilitation Orthosis: Control Scheme and Strategy for Pneumatic Muscle Actuated Gait Trainers.* Robotics, 2014. **3**: p. 120-148.

102. Klein, J., et al. *Biomimetic orthosis for the neurorehabilitation of the elbow and shoulder (BONES)*. in *2008 2nd IEEE RAS & EMBS International Conference on Biomedical Robotics and Biomechatronics*. 2008.

103. Agrawal, S.K. and A. Fattah, *Theory and design of an orthotic device for full or partial gravity-balancing of a human leg during motion.* IEEE Trans Neural Syst Rehabil Eng, 2004. **12**(2): p. 157-65.

104. Tschiersky, M., et al., *Gravity Balancing Flexure Springs for an Assistive Elbow Orthosis.* IEEE Transactions on Medical Robotics and Bionics, 2019. **1**(3): p. 177-188.

105. Riener, R., et al., *Patient-cooperative strategies for robot-aided treadmill training: first experimental results.* IEEE Trans Neural Syst Rehabil Eng, 2005. **13**(3): p. 380-94.

106. Colombo, G., et al., *Treadmill training of paraplegic patients using a robotic orthosis.* J Rehabil Res Dev, 2000. **37**(6): p. 693-700.

107. Almaghout, K., et al., *Design and control of a lower limb rehabilitation robot considering undesirable torques of the patient's limb.* Proceedings of the Institution of Mechanical Engineers, Part H: Journal of Engineering in Medicine, 2020. **234**(12): p. 1457-1471.

108. Hussain, S., S. Xie, and P.K. Jamwal, *Robust Nonlinear Control of an Intrinsically Compliant Robotic Gait Training Orthosis.* Systems, Man, and Cybernetics: Systems, IEEE Transactions on, 2013. **43**: p. 655-665.

109. Jezernik, S., et al., *Adaptive robotic rehabilitation of locomotion: a clinical study in spinally injured individuals.* Spinal Cord, 2003. **41**(12): p. 657-666.

110. Hogan, N., *Impedance Control: An Approach to Manipulation: Part I—Theory.* Journal of Dynamic Systems Measurement and Control-transactions of The Asme, 1985. **107**: p. 1-7.

111. Koopman, B., E.H.F. van Asseldonk, and H. van der Kooij, *Selective control of gait subtasks in robotic gait training: foot clearance support in stroke survivors with a powered exoskeleton.* Journal of NeuroEngineering and Rehabilitation, 2013. **10**(1): p. 3.

112. Hussain, S., S.Q. Xie, and P.K. Jamwal, *Adaptive Impedance Control of a Robotic Orthosis for Gait Rehabilitation.* IEEE Transactions on Cybernetics, 2013. **43**(3): p. 1025-1034.

113. Heuillet, A., F. Couthouis, and N. Díaz-Rodríguez, *Explainability in deep reinforcement learning.* Knowledge-Based Systems, 2021. **214**: p. 106685.

114. Mauroy, A. and J. Goncalves, *Koopman-Based Lifting Techniques for Nonlinear Systems Identification.* IEEE Transactions on Automatic Control, 2017. **PP**.

115. Bemporad, A., et al., *The explicit linear quadratic regulator for constrained systems.* Automatica, 2002. **38**(1): p. 3-20.

116. Mamakoukas, G., et al., *Derivative-based koopman operators for real-time control of robotic systems.* IEEE Transactions on Robotics, 2021. **37**(6): p. 2173-2192.

117. Camacho, E.F. and C.B. Alba, *Model predictive control*. 2013: Springer science & business media.

118. Korda, M. and I. Mezić, *Linear predictors for nonlinear dynamical systems: Koopman operator meets model predictive control.* Automatica, 2018. **93**: p. 149-160.

119. Castaño, M.L., et al. *Control-oriented Modeling of Soft Robotic Swimmer with Koopman Operators*. in *2020 IEEE/ASME International Conference on Advanced Intelligent Mechatronics (AIM)*. 2020.

120. Kim, T., M. Jeong, and K. Kong, *Bioinspired Knee Joint of a Lower-Limb Exoskeleton for Misalignment Reduction.* IEEE/ASME Transactions on Mechatronics, 2022. **27**(3): p. 1223-1232.

121. Ching-Ping, C. and B. Hannaford, *Measurement and modeling of McKibben pneumatic artificial muscles.* IEEE Transactions on Robotics and Automation, 1996. **12**(1): p. 90-102.

122. Chou, C.-P. and B. Hannaford. *Static and dynamic characteristics of McKibben pneumatic artificial muscles*. in *Proceedings - IEEE International Conference on Robotics and Automation*. 1994.

123. Sarkisian, S.V., et al., *Design, Development, and Validation of a Self-Aligning Mechanism for High-Torque Powered Knee Exoskeletons.* IEEE Transactions on Medical Robotics and Bionics, 2020. **2**(2): p. 248-259.

124. Brockett, C.L. and G.J. Chapman, *Biomechanics of the ankle.* Orthop Trauma, 2016. **30**(3): p. 232-238.

125. Gray, H.A., et al., *Three-dimensional motion of the knee-joint complex during normal walking revealed by mobile biplane x-ray imaging.* Journal of Orthopaedic Research, 2019. **37**(3): p. 615-630.

126. Zhou, L., et al., *Design of a passive lower limb exoskeleton for walking assistance with gravity compensation.* Mechanism and Machine Theory, 2020. **150**.

127. Qian, K., et al., *Robust Iterative Learning Control for Pneumatic Muscle With Uncertainties and State Constraints.* IEEE Transactions on Industrial Electronics, 2023. **70**(2): p. 1802-1810.

128. Reynolds, D., et al., *Modeling the Dynamic Characteristics of Pneumatic Muscle.* Annals of biomedical engineering, 2003. **31**: p. 310-7.

129. Zhang, J., et al., *Robotic Artificial Muscles: Current Progress and Future Perspectives.* IEEE Transactions on Robotics, 2019. **35**(3): p. 761-781.

130. Colbrunn R. W., Nelson G. M., and Quinn R. D., *Modeling of Braided Pneumatic Actuators for Robotic Control.* Proceedings of the International Conference on Intelligent Robots and Systems, 2001. **Oct 29th - Nov.03rd ,2001.**

131. Tondu, B. and P. Lopez, *Theory of an artificial pneumatic muscle and application to the modelling of McKibben artificial muscle.* Theorie d'un muscle artificiel pneumatique et application a la modelisation du muscle artificiel de McKibben, 1995. **320**(3): p. 105-114.

132. Tsagarakis, N. and D.G. Caldwell. *Improved modelling and assessment of pneumatic muscle actuators*. in *Proceedings - IEEE International Conference on Robotics and Automation*. 2000.

133. Reynolds, D.B., et al., *Modeling the dynamic characteristics of pneumatic muscle.* Annals of Biomedical Engineering, 2003. **31**(3): p. 310-317.

134. Repperger, D.W., et al., *Actuator design using biomimicry methods and a pneumatic muscle system.* Control Engineering Practice, 2006. **14**(9): p. 999-1009.

135. FESTO. *https://www.festo.com/au/en/*. 2023.

136. Vincent, J.F.V., et al., *Biomimetics: its practice and theory.* Journal of the Royal Society, Interface, 2006. **3**(9): p. 471-482.

137. Roth, R.R., *The foundation of bionics.* Perspect Biol Med, 1983. **26**(2): p. 229-42.

138. Dickinson, M.H., *Bionics: Biological insight into mechanical design.* Proceedings of the National Academy of Sciences, 1999. **96**(25): p. 14208-14209.

139. Cumming, J., S. Barr, and T. Howe, *Prosthetic rehabilitation for older dysvascular people following a unilateral transfemoral amputation.* Cochrane database of systematic reviews (Online), 2006. **1**: p. CD005260.

140. Shigley, J. and J. Uicker, *Theory of Machines and Mechanisms.* 2011.

141. Rider, M., *Introduction to Mechanisms*. 2015. p. 1-15.

142. Flandry, F. and G. Hommel, *Normal Anatomy and Biomechanics of the Knee.* Sports medicine and arthroscopy review, 2011. **19**: p. 82-92.

143. Abulhasan, J. and M. Grey, *Anatomy and Physiology of Knee Stability.* Journal of Functional Morphology and Kinesiology, 2017. **2**: p. 34.

144. Heath, C., *The Effects of Physical Forces on Cartilage Tissue Engineering.* Biotechnology & genetic engineering reviews, 2000. **17**: p. 533-51.

145. Wang, M. and Z. Peng, *Wear in human knees.* Biosurface and Biotribology, 2015. **50**.

146. Kennedy, F., *Biomechanics of the hip and knee: Implant wear*. 2013. p. 56-92.

147. Pickard, J.K., J.A. Carretero, and J.-P. Merlet, *Appropriate analysis of the four-bar linkage.* Mechanism and Machine Theory, 2019. **139**: p. 237-250.

148. Roetenberg, D., H. Luinge, and P. Slycke, *Xsens MVN: Full 6DOF human motion tracking using miniature inertial sensors.* Xsens Motion Technol. BV Tech. Rep., 2009. **3**.

149. Ausejo, S. and X. Wang, *Motion Capture and Reconstruction*. 2008.

150. Menolotto, M., et al., *Motion Capture Technology in Industrial Applications: A Systematic Review.* Sensors, 2020. **20**: p. 5687.

151. Bodenheimer, B. and C. Rose, *The Process of Motion Capture: Dealing with the Data.* 1997.

152. Lloyd, S., R.A. Irani, and M. Ahmadi, *Fast and Robust Inverse Kinematics of Serial Robots Using Halley's Method.* IEEE Transactions on Robotics, 2022. **38**(5): p. 2768-2780.

153. Zhong, G., B. Peng, and W. Dou, *Kinematics analysis and trajectory planning of a continuum manipulator.* International Journal of Mechanical Sciences, 2022. **222**.

154. Kashyap, A.K., D.R. Parhi, and A. Pandey, *Multi-objective optimization technique for trajectory planning of multi-humanoid robots in cluttered terrain.* ISA Transactions, 2022. **125**: p. 591-613.

155. Refaai, M.R.A., *An Improved Inverse Kinematics Solution for a Robot Arm Trajectory Using Multiple Adaptive Neuro-Fuzzy Inference Systems.* Advances in Materials Science and Engineering, 2022. **2022**.

156. Jamwal, P.K., et al., *Forward kinematics modelling of a parallel ankle rehabilitation robot using modified fuzzy inference.* Mechanism and Machine Theory, 2010. **45**(11): p. 1537-1554.

157. Kachapi, S. and D. Ganji, *Dynamics and Vibrations*. Vol. 202. 2014.

158. Mena, D., J.M. Mansour, and S.R. Simon, *Analysis and synthesis of human swing leg motion during gait and its clinical applications.* Journal of Biomechanics, 1981. **14**(12): p. 823-832.

159. Xu, J., W. Wang, and Y. Sun, *Two optimization algorithms for solving robotics inverse kinematics with redundancy*. Journal of Control Theory and Applications, 2010. **8**(2): p. 166-175.

160. Hussain, S., Jamwal, P. K., M.H. Ghayesh, and S.Q. Xie, *Assist-as-needed control of an intrinsically compliant robotic gait training orthosis.* IEEE Transactions on Industrial Electronics, 2017. **64**(2): p. 1675-1685.

161. Koopman, B.O., *Hamiltonian Systems and Transformation in Hilbert Space.* Proceedings of the National Academy of Sciences, 1931. **17**(5): p. 315-318.

162. Mezić, I. and A. Banaszuk, *Comparison of systems with complex behavior.* Physica D: Nonlinear Phenomena, 2004. **197**(1): p. 101-133.

163. Proctor, J.L., S.L. Brunton, and J.N. Kutz, *Including inputs and control within equation-free architectures for complex systems.* The European Physical Journal Special Topics, 2016. **225**(13): p. 2413-2434.

164. Cassamo, N. and J.-W. van Wingerden, *On the Potential of Reduced Order Models for Wind Farm Control: A Koopman Dynamic Mode Decomposition Approach.* Energies, 2020. **13**(24).

165. Chen, B., et al., *Data-Driven Koopman Model Predictive Control for Optimal Operation of High-Speed Trains.* IEEE Access, 2021. **9**: p. 82233-82248.

166. Narasingam, A. and J.S.-I. Kwon, *Application of Koopman operator for model-based control of fracture propagation and proppant transport in hydraulic fracturing operation.* Journal of Process Control, 2020. **91**: p. 25-36.

167. Narasingam, A. and J.S.-I. Kwon, *Koopman Lyapunov-based model predictive control of nonlinear chemical process systems.* AIChE Journal, 2019. **65**(11): p. e16743.

168. Cibulka, V., et al., *Model Predictive Control of a Vehicle using Koopman Operator*. IFAC-PapersOnLine, 2020. **53**(2): p. 4228-4233.

169. Kamenar, E., et al. *Prediction of the behavior of a pneumatic soft robot based on Koopman operator theory*. in *2020 43rd International Convention on Information, Communication and Electronic Technology (MIPRO)*. 2020.

170. Ren, C., et al., *Koopman-Operator-Based Robust Data-Driven Control for Wheeled Mobile Robots.* IEEE/ASME Transactions on Mechatronics, 2023. **28**(1): p. 461-472.

171. Goyal, T., et al., *Learning Koopman Embedding Subspaces for System Identification and Optimal Control of a Wrist Rehabilitation Robot.* IEEE Transactions on Industrial Electronics, 2022: p. 1-9.

172. Jammeli, I., et al., *An Assistive Explicit Model Predictive Control Framework for a Knee Rehabilitation Exoskeleton.* IEEE/ASME Transactions on Mechatronics, 2022. **27**(5): p. 3636-3647.

173. MacAusland, R., *The Moore-Penrose inverse and least squares.* Math 420: Advanced Topics in Linear Algebra, 2014: p. 1-10.

174. Dong, L., et al., *Functional Nonlinear Model Predictive Control Based on Adaptive Dynamic Programming.* IEEE Transactions on Cybernetics, 2019. **49**(12): p. 4206-4218.

175. Yang, L., S. Armijo-Olivo, and D. Gross, *Single-Case Experimental Design in Rehabilitation: Basic Concepts, Advantages, and Challenges.* American journal of physical medicine & rehabilitation, 2023. **Publish Ahead of Print**.

176. Spong, M.W., S. Hutchinson, and M. Vidyasagar, *Robot modeling and control*. 2005: jon wiley & sons.

177. Barad, J. AutoAmbulator: Robotic Rehab for Neuro-Disease Patients. 2006.

178. Srivastava, S., et al., *Assist-as-Needed Robot-Aided Gait Training Improves Walking Function in Individuals Following Stroke.* IEEE Transactions on Neural Systems and Rehabilitation Engineering, 2014.

179. Sargsyan, S., V. Arakelian, and S. Briot, *Robotic Rehabilitation Devices of Human Extremities: Design Concepts and Functional Particularities*. Vol. 3. 2012.

180. Chen, G., P. Qi, and H. Yu, *Mechanical design and evaluation of a compact portable knee–ankle–foot robot for gait rehabilitation.* Mechanism and Machine Theory, 2016. **103**: p. 51–64.